

Tab 1

# LAUNCH CANADA

# 2025 CHALLENGE



Metropolitan Aerospace & Combustion Hub

***LC2025 Design Report***  
Chimera Liquid Rocket Engine

Competing Team [3]

### **REVISION HISTORY**

REVISION	DESCRIPTION	DATE
R0	Initial Release	1/31/2025

## **AUTHORS**

The following team members of Competing Team 3 of the Launch Canada 2025 Challenge have all taken part as authors or editors of this report:

William Pirie - Team Captain

Shivesh Maraj - Chief Engineer

Ben Kubica - Propulsion Lead

Juliano Sciabbarrasi - Propulsion General Member

Julia Puszynska - Propulsion General Member

Alexandre Beaudoin - Propulsion General Member

Dmitriy Leminov - Propulsion and Transfer & Control General Member

Alexandru Lungu - Propulsion General Member

Tristan Stanford - Transfer & Control General Member

Adam Oudeh - Structures Lead

Leandro Tomarchio - Structures Lead

## **ABSTRACT**

This report details the design, analysis, and testing plan for Chimera, a pressure-fed liquid bipropellant rocket engine utilizing ethanol and nitrous oxide propellants, developed by the Metropolitan Aerospace and Combustion Hub (MACH). The engine is designed to produce 1500 lbf of initial thrust with a 9.2-second burn duration. Key subsystems include a regulated pressurant feed system, student-researched ablative thrust chamber, like-like impinging injector, and thrust vector control (TVC) capable of  $\pm 10^\circ$  gimbal angles. The propellant feed system employs a 6.8L composite overwrapped pressure vessel for pressurant storage, maintaining fuel tank pressure through a dome-loaded regulator system. Self-pressurizing nitrous oxide was selected for oxidizer delivery to minimize system complexity while maintaining adequate performance. Comprehensive analysis of transient engine performance predicts thrust decay from 1420 lbf to 817 lbf over the burn duration, with an initial specific impulse 189s seconds. The thrust chamber incorporates a silica-phenolic ablative liner with a graphite throat insert, designed to withstand the thermal and mechanical loads of combustion while maintaining structural integrity. Testing validation includes hydrostatic proof testing, cold flow characterization, and incremental hot fire testing, culminating in full-duration static and TVC-enabled test firings. This development represents advancement in student-led liquid propulsion research, with particular focus on performance characterization, operational safety, and system reliability.

## TABLE OF CONTENTS

1.0 INTRODUCTION	14
2.0 PROJECT BACKGROUND & JUSTIFICATION	16
3.0 CONCEPT OF OPERATIONS (CONOPS)	17
3.1 OVERVIEW	17
3.2 ARRIVAL & SITE SETUP	18
3.3 SYSTEM VERIFICATION & LEAK TESTING	18
3.4 PROPELLANT HANDLING & FILLING	18
3.5 TANK PRESSURIZATION & HOTFIRE TEST EXECUTION	19
3.6 PURGE AND DEPRESSURIZATION	19
3.7 TEARDOWN & SITE RESTORATION	19
4.0 REQUIREMENTS	20
5.1 PROPULSION SUBTEAM	45
5.1.4.1 TORCH INJECTOR	78
5.1.4.2 TORCH COMBUSTION CHAMBER	80
5.1.5 THRUST VECTOR CONTROL	81
5.2.2.1. INTRODUCTION	90
5.2.2.2. SYSTEM ARCHITECTURE	90
5.2.2.3. DATA FLOW & EXECUTION PROCESS	90
5.2.2.4. COMMUNICATION & CONTROL MECHANISMS	90
5.3 STRUCTURES SUBTEAM	92
5.3.1 PLUMBING AND PROPULSION SYSTEM INTEGRATION	92
5.3.2 LEVER ARM	92
5.3.3 WINCH EXTENSION	93
5.3.4 SUPPORT TOWER	93
6.0 PLANNED TESTING	94
6.1 TANK HYDROSTATIC TESTING	96
6.2 CONTROL & ACTUATION TESTS	98
6.3 INTEGRATED STRUCTURE LIFT TEST	99
6.4 SUB-SCALE COLDFLOW TEST	99
6.5 FULL SCALE INJECTOR COLDFLOW TEST	99
6.6 IGNITOR TEST (PUCK)	100
6.7 FULL DURATION STATIC HOTFIRE TEST	100
6.8 FULL DURATION TVC HOTFIRE TEST	100
7.0 PROJECT TIMELINE	102
8.0 PROJECT RISKS	103
8.1 SAFETY AND OPERATIONAL RISKS	103
8.1.1 PROPULSION SYSTEM RISKS	103

8.1.1.1 NITROUS OXIDE THERMAL DECOMPOSITION	103
8.1.1.1.1 CURRENT MITIGATION STRATEGIES	104
8.1.1.1.2 ADDITIONAL RECOMMENDATIONS	104
8.1.1.2 PRESSURE VESSEL FAILURE	104
8.1.1.3 PREMATURE IGNITION	105
8.1.1.4 VALVE SEQUENCING ERRORS	105
8.1.1.5 FLOW CONTROL ISSUES	105
8.1.2 STRUCTURAL RISKS	106
8.1.2.1 SUPPORT TOWER FAILURE	106
8.1.2.2 LIFT SYSTEM MALFUNCTION	106
8.1.2.3 ENGINE MOUNT FAILURE	107
8.1.2.4 TVC SYSTEM STRUCTURAL ISSUES	107
8.1.3 PERSONNEL SAFETY RISKS	107
8.1.3.1 CHEMICAL EXPOSURE	108
8.1.3.2 HIGH PRESSURE SYSTEMS	108
8.2 TECHNICAL PERFORMANCE RISKS	108
8.2.1 COMBUSTION SYSTEM RISKS	109
8.2.1.1 INJECTOR PERFORMANCE	109
8.2.1.2 CHAMBER LINER DEGRADATION	110
8.2.1.3 COMBUSTION INSTABILITY	110
8.2.1.4 IGNITION RELIABILITY	110
8.2.2 CONTROL SYSTEM RISKS	111
8.2.2.1 SENSOR FAILURES	111
8.2.2.2 DATA ACQUISITION ISSUES	111
8.2.2.3 COMMUNICATION LOSS	111
8.2.2.4 SOFTWARE MALFUNCTIONS	111
8.2.3 TVC SYSTEM RISKS	112
8.2.3.1 ACTUATOR PERFORMANCE	112
8.2.3.2 GIMBAL MECHANISM ISSUES	112
8.2.3.3 CONTROL ALGORITHM FAILURES	112
8.2.3.4 POSITION FEEDBACK ERRORS	112
8.3 SCHEDULE AND RESOURCE RISKS	112
8.3.1 MANUFACTURING RISKS	113
8.3.1.1 COMPONENT PROCUREMENT DELAYS	113
8.3.1.2 MACHINE SHOP AVAILABILITY	113
8.3.1.3 QUALITY CONTROL ISSUES	113
8.3.2 TESTING PROGRAM RISKS	114
8.3.2.1 TEST SITE AVAILABILITY	114
8.3.2.2 WEATHER CONSTRAINTS	114

8.3.2.3 EQUIPMENT AVAILABILITY	114
8.3.2.4 TEST SCHEDULE DELAYS	114
8.3.3 COMPETITION TIMELINE RISKS	115
8.3.3.1 REGULATORY APPROVAL DELAYS	115
8.3.3.2 DOCUMENTATION REQUIREMENTS	115
8.3.3.3 TRANSPORTATION LOGISTICS	115
8.3.3.4 Resource Allocation Issues	115
8.4 RISK ASSESSMENT MATRIX	115
8.4.1 RISK EVALUATION CRITERIA	116
8.4.1.1 PROBABILITY RATINGS	116
8.4.1.2 SEVERITY RATINGS	116
8.4.1.3 RISK CATEGORIES	117
8.5.1.4 MITIGATION EFFECTIVENESS	117
8.4.2 RISK PRIORITIZATION	117
8.4.2.1 HIGH-PRIORITY RISKS	117
8.4.2.2 MEDIUM-PRIORITY RISKS	118
8.4.2.3 LOW-PRIORITY RISKS	118
8.4.2.4 MONITORING REQUIREMENTS	118
8.5 RISK MATRICES	119
REFERENCES	122
APPENDIX A - FLUID SYSTEM CALCULATIONS AND SIZING	125
APPENDIX B - THRUST VECTOR CONTROL ACTUATOR SIZING	137
APPENDIX B.2 - GRAVITATIONAL FORCE ACTING ON TVC	138
APPENDIX C - INJECTOR STRESS ANALYSIS	138

## LIST OF FIGURES

Figure 1.1: Chimera Engine Cross-Section	14
Figure 1.2: GAR-E hotfire.	15
Figure 3.1: ConOps for Chimera Liquid Engine Hotfire at Launch Canada	18
Figure 4.1. Logical decomposition of the Chimera rocket engine system.	21
Figure 5.1.1.1: Transient nitrous oxide tank pressure	47
Figure 5.1.1.2: Transient nitrous oxide flow rate	47
Figure 5.1.1.3: Predicted thrust curve for Chimera 9.2s burn	48
Figure 5.1.2.1: Complete P&ID of Day-Glo Propellant Feed System	49
Figure 5.1.2.2: Vertically stacked propulsion system layout	50
Figure 5.1.2.1.1: Pressurant tank pressure vs. time	52
Figure 5.1.2.1.2: Dome regulator (R1) volumetric flow rate vs. time	53
Figure 5.1.1.1.3: Completed pressurant bay plumbing	54
Figure 5.1.2.2.1: Run bay with installed MOV and MFV assemblies.	60
Figure 5.1.2.2.2: SRAD Cavitating Venturis Used for Previous Engine.	61
Figure 5.1.1.3.1: GSE Plumbing CAD.	62
Figure 5.1.1.3.2: GSE plumbing panel in currently assembled state.	63
Figure 5.1.3.1.1: Broad functional decomposition of the injector with major considerations.	67
Figure 5.1.3.1.2: Cross-section of injector geometry.	68
Figure 5.1.3.1.3: External view of the injector assembly.	68
Figure 5.1.3.1.4: View of the injector face.	69
Figure 5.1.3.1.5: Wireframe view of the injector face, showing fuel feed passages.	69
Figure 5.1.3.1.6: Close-up of element geometry.	70
Figure 5.1.3.2.1: Ablative Mixtures To Date	73
Figure 5.1.3.2.2: Sample undergoing tensile testing ahead of ablative testing.	74
Figure 5.1.3.3.1: Puck igniter used in MACH's first successful hot fire	75
Figure 5.1.4.1 Preliminary P&ID.	76
Figure 5.1.4.2: Propellant System Layout.	78
Figure 5.1.4.1.1: Torch injector section view.	79
Figure 5.1.4.1.2: Torch injector side view.	79
Figure 5.1.4.5: Torch injector face view.	80
Figure 5.1.4.6: Full assembly of torch ignitor.	81
Figure 5.1.5.1 CAD of the TVC system on the engine	82
Figure 5.1.5.2 Linear Actuator used in TVC	84
Figure 5.1.5.3 CAD of the engine gimbal	84

Figure 5.2.1.1 Overall System Architecture	86
Figure 5.2.1.2 Mission Control Architecture	87
Figure 5.2.1.3 GSE Architecture	88
Figure 5.2.1.4 Avionics Stack Architecture	89
Figure 5.2.2.1 Chimera Control Program flow chart diagram	91
Figure 6.1.1: Ethanol tank hydrostatic test	97
Figure 6.1.2: Nitrous tank hydrostatic test	98
Figure 7.1: Project timeline for Chimera liquid engine project	102
Figure A.1.1: Pressure (psi) vs. Time for Custom and Flownex Models	126
Figure A.2.1: Flownex model constrained for initial steady-state solution	131
Figure A.2.2: Predicted pressurant tank pressure vs. time (Custom MATLAB model)	132
Figure A.2.3: Predicted regulator volumetric flow rate vs. time (Custom MATLAB model)	132

## LIST OF TABLES

Table 4.1: Chimera Liquid Engine Subsystem Requirements	22
Table 4.2: Chimera Liquid Engine Verification Matrix	30
Table 5.1.1: Propulsion System Specifications	45
Table 5.2.7.1: CEA Results for End of Burn	48
Table 5.1.2.2.1.1: Ethanol Tank FOS	56
Table 5.1.2.2.1.2: Nitrous Tank FOS	56
Table 5.1.3.2.1: Ablative Mixtures To Date	72
Table 5.1.4.1: Propellant System BOM	77
Table 6.1: Testing Plan Summary	94
Table 8.1: Summary of Key Safety and Operational Risks	103
Table 8.2: Summary of Key Technical Performance Risks	109
Table 8.3: Summary of Key Schedule and Resource Risks.	113
Table 8.4.1: Risk matrix probability standardization.	116
Table 8.4.2: Risk rating severity system description.	116
Table 8.5.3: Mitigation Effectiveness Matrix	117
Table 8.5.1: Safety Risk Matrix	119
Table 8.5.2: Technical Risk Matrix	119
Table 8.5.3: Schedule Risk Matrix	120
Table A.1.1: Custom Model & Flownex Model Results	127
Table C.1.1: Variables for rule-of-thumb head calculations according to [A]	139
Table E.1: CEA Results	144
Table E.2: Summary of Chamber Dimensions	145

## ABBREVIATIONS & NOMENCLATURE

BB	Beaglebone Black	BPVC	Boiler and Pressure Vessel Code
CEA	Chemical Equilibrium with Applications	CONOPS	Concept of Operations
COTS	Commercial Off-The-Shelf	CD	Combustion Dynamics
Cv	Valve Flow Coefficient	DIO	Digital Input Output
DAQ	Data Acquisition Unit	EthaNOS	Ethanol & Nitrous Oxide
FEA	Finite Element Analysis	GAR-E	Garolite Ablative Rocket-Engine
GNSS	Global Navigation Satellite System	GSE	Ground Support Equipment
GUI	Graphical User Interface	Isp	Specific Impulse
Li-Po	Lithium Polymer (Battery)	LOV	Loss of Vehicle
LRE	Liquid Rocket Engine	MACH	Metropolitan Aerospace Combustion Hub
MCU	Microcontroller Unit	MEWP	Maximum Expected Working Pressure
MEOP	Maximum Expected Operating Pressure	MFV	Main Fuel Valve
MOV	Main Oxidizer Valve	MPV	Main Pressurant Valve
N <sub>2</sub>	Nitrogen	N <sub>2</sub> O	Nitrous Oxide
OS	Operating System	P&ID	Piping & Instrumentation Diagram
PM	Propellant Management	PCB	Printed Circuit Board
PPE	Personal Protective Equipment	PRA	Probabilistic Risk Assessment
PSR	Probable Severity Rating	PSU	Power Supply Unit
R#	Revision # (of this report)	RF	Radio Frequency

RMS	Risk Management System	SBC	Single Board Computer
SERM	Safety & Emergency Response Manual	SOP	Standard Operating Procedure
SRAD	Student Researched And Developed	SSR	Solid State Relay
T&C	Transfer & Control	TMU	Toronto Metropolitan University
UTS	Ultimate Tensile Strength		

## **UNITS**

<i>ft</i>	Feet
<i>kg</i>	Kilograms
<i>lbm</i>	Pounds (mass)
<i>m</i>	Meters
<i>N</i>	Newton
<i>lbf</i>	Pounds (force)
<i>s</i>	Seconds

## 1.0 INTRODUCTION

MACH is a student organization working out of Toronto Metropolitan University. MACH's mission is to design, build, and test liquid bipropellant rocket engines. Through focusing on the development of liquid propulsion systems, MACH hopes to provide its members with hands-on experience with high pressure fluid systems, engineering design, and experimental rocketry.

The Chimera engine project is MACH's latest endeavor, aimed at advancing student-led research in liquid rocket propulsion. The project encompasses the complete design, fabrication, and testing of a pressure-fed bipropellant engine, integrating critical subsystems such as combustion chambers, propellant feed lines, ignition systems, and thrust vector control (TVC) mechanisms. By leveraging industry-standard methodologies and rigorous testing protocols, MACH ensures that its members gain practical skills directly applicable to the aerospace sector. The Chimera engine is intended to be the highest thrust and burn duration engine that the team has created to date.

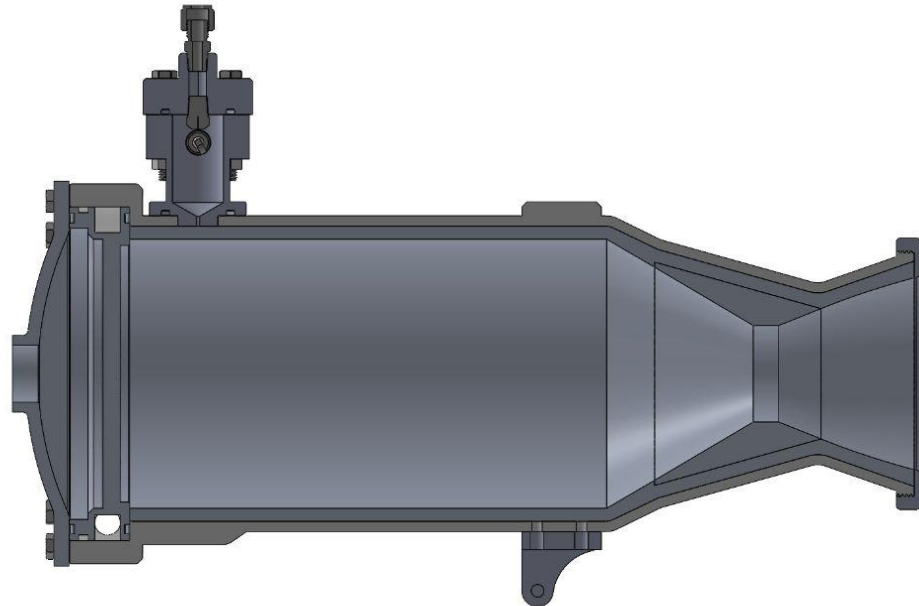


Figure 1.1: Chimera Engine Cross-Section

Through this initiative, MACH not only advances its technical capabilities but also contributes to the broader rocketry community. The knowledge and experience gained from Chimera will

inform future projects, laying the groundwork for increasingly sophisticated propulsion systems. As MACH continues to grow, its commitment to innovation and experiential learning remains at the core of its mission, equipping students with the expertise to drive advancements in aerospace technology.

Over the past seven years, the team has steadily honed its expertise in liquid rocket engine development, culminating in a significant milestone at the Launch Canada 2024 competition. At this event, the team successfully tested its first liquid engine—the GAR-E—a 300 lbf liquid nitrous ethanol engine featuring a Garolite ablative thrust chamber. This test validated critical aspects of our design approach, including propellant systems, thrust chambers, and ignition systems. Despite encountering numerous setbacks and failures along the way, the successful demonstration of the GAR-E underscored our commitment to iterative improvement and innovation, laying a strong foundation for future advancements.



Figure 1.2: GAR-E hotfire.

## **2.0 PROJECT BACKGROUND & JUSTIFICATION**

Liquid propulsion systems have contributed to fundamental advancements in rocketry since the early 20th century, first making appearances in military contexts and then further advancing and powering legendary systems like Saturn V, Space shuttle, and modern reusable rockets like Falcon 9 and Starship. A major advantage of liquid propellant systems is the feasibility of throttle vector control, allowing for precise steering, and including shutdown and restarting capabilities. Liquid propellants enhance cost-effectiveness through precise fuel management, optimized efficiency, and advancements in manufacturing, such as 3D printing and improved cryogenic storage, which have further reduced production and operational costs. Having these benefits, student teams have the opportunity to expand their horizons in the field of rocketry while building their knowledge on the very machines and mechanisms that apply in and around our world today. Moreover, by engaging in liquid propulsion projects, student teams are not only subjected to preparing for their careers in advanced aerospace engineering, but also laying the foundation for a future where Canada plays a larger role in launch vehicle development and propulsion research.

Chimera, our team's liquid propellant engine, will use ethanol and nitrous oxide for the engines' propellant, allowing safer and more cost-efficient alternatives to cryogenic fuels. The engine cycle will be pressure fed (yielding a thrust of approximately 1500 lbf), have a torch ignition system, and will be able to do multiple restarts, allowing for flexible mission profiles.

In addition to the team's compassion and hard work towards the Chimera engine, significant sponsors and industry partners that help bring this project to life and support our team include TMU, Pratt & Whitney, Ansys, Solidworks, and Swagelok, alongside specialized engineering and manufacturing firms such as Dishon Limited, Stein Industries, Aqua Environment, and JAKŠA Solenoid Valves. These organizations play a crucial role in providing the essential resources for the testing and development of the liquid propulsion system. With the aid of funding, software, high-performance components, and technical expertise, the team is able to excel in the field of student-led rocketry innovation.

The team does not intend to bring the Chimera engine to market, as the primary goal is research, education, and technical development rather than commercialization. This project serves to bridge the gap between theoretical coursework and real-world problem engineering, and for students to gain practical and hands-on experience with liquid propulsion, a field with limited opportunities in Canada. However, the skills and knowledge we gain and refine from this project will be taken under our belts as we move forward into the industry.

## 3.0 CONCEPT OF OPERATIONS (CONOPS)

### 3.1 OVERVIEW

The Concept of Operations (CONOPS) for the Chimera engine test campaign outlines the specific steps required for a successful test day. This structured approach ensures safety, efficiency, and consistency in test execution. The operational workflow is divided into key phases, from the arrival of personnel and equipment at the test site to test execution and post-test activities. The system ConOps has been presented in Figure 3.1.

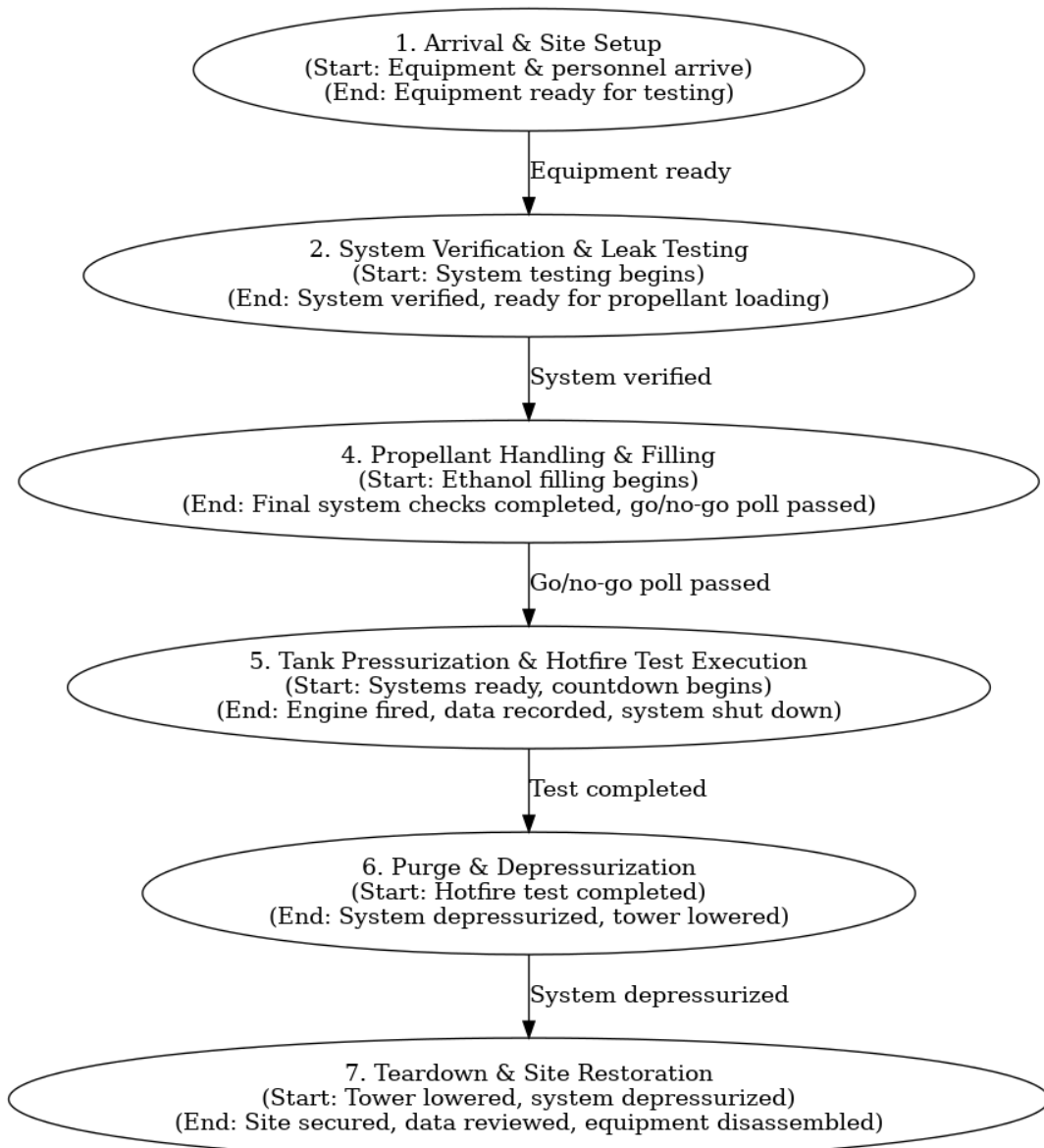


Figure 3.1: ConOps for Chimera Liquid Engine Hotfire at Launch Canada

### 3.2 ARRIVAL & SITE SETUP

**Start:** Equipment and personnel arrive at the test site.

**End:** All equipment is fully assembled and ready for testing.

- Conduct an initial site inspection and assess environmental conditions.
- Unload all equipment and transport it to designated areas.
- Establish mission control, power distribution, telemetry, and communications systems.
- Secure the thrust stand in compacted dirt, ensuring stability.
- Prepare the test site by setting up flame trench protection and clearing any debris.
- Assemble the propellant stand, engine, thrust assembly, and all electronics.
- Integrate subsystems into the test stand and perform initial mechanical and electrical system checks.

### 3.3 SYSTEM VERIFICATION & LEAK TESTING

**Start:** System testing begins.

**End:** All tests passed, system verified, and ready for propellant loading.

- Connect the test computer and the Telemetry & Control (TNC) system.
- Perform communication checks, control verification, and valve actuation tests.
- Set dome regulators to pre-defined operating pressures.
- Conduct pneumatic leak testing on all high-pressure components.
- Perform an inert nitrogen ( $N_2$ ) flush and depressurization of the system upon passing leak checks.
- Disarm main pressurant and propellant valves prior to fueling operations.
- Raise the test tower into its vertical position and secure it to the pad.

### 3.4 PROPELLANT HANDLING & FILLING

**Start:** Ethanol filling begins.

**End:** Final system checks completed, and go/no-go poll passed.

- Perform ethanol fill procedure, ensuring correct quantity and system integrity.
- Switch Red Team personnel to execute the nitrous oxide ( $N_2O$ ) connection procedure.
- Arm the main pressurant, propellant, and fill valves.
- Connect ignitor power and arm the ignitor circuit.
- Evacuate the pad and declare "Evacuation" status to restrict personnel access.
- Remotely initiate  $N_2O$  loading and pressurization procedures.

- Conduct a final system check and execute a go/no-go poll before proceeding.

### **3.5 TANK PRESSURIZATION & HOTFIRE TEST EXECUTION**

**Start:** All systems are ready, and test countdown begins.

**End:** Engine successfully fired, data recorded, and system safely shut down.

- Perform a final verification of sensor data, telemetry connections, and actuator status.
- Initiate tank pressurization sequence, ensuring proper pressure ramp-up.
- Arm the ignition system and confirm adherence to safety protocols.
- Initiate countdown sequence and execute the automated hotfire test sequence.
- Monitor real-time data streams, ensuring parameters remain within acceptable ranges.
- Log key performance metrics such as thrust, chamber pressure, injector performance, and temperature.
- Upon test completion, initiate engine shutdown sequence and confirm flame-out.

### **3.6 PURGE AND DEPRESSURIZATION**

**Start:** Hotfire test completed.

**End:** System safely depressurized, and tower lowered.

- Initiate controlled depressurization of all propellant and pressurant lines.
- Engage purge procedures to remove residual oxidizer and fuel from system components.
- Perform post-test inspections of the engine, injector, and thrust stand for anomalies.
- Collect final telemetry data and confirm all valves have returned to a safe state.
- Lower the test tower to its stowed position and secure it.

### **3.7 TEARDOWN & SITE RESTORATION**

**Start:** Tower is lowered, and system is fully depressurized.

**End:** Site secured, data reviewed, and equipment disassembled.

- Begin systematic disassembly of the test stand and associated infrastructure.
- Perform a detailed inspection of all components for signs of wear, damage, or needed modifications.
- Transport test equipment and materials back to storage locations.
- Clean up the test site, ensuring environmental and safety compliance.
- Conduct a post-test debrief with personnel to review findings and process improvements.
- Compile collected data for further analysis and documentation in the final test report.

## **4.0 REQUIREMENTS**

Based on the mission requirements of performing a 10 second static engine test with a 1500 lbf thrust on startup, logical decomposition of the subsystems was performed. Identification of the subsystems served as an important step for deriving subsequent subsystem requirements. The results of the logical decomposition process have been provided in Figure 4.1.

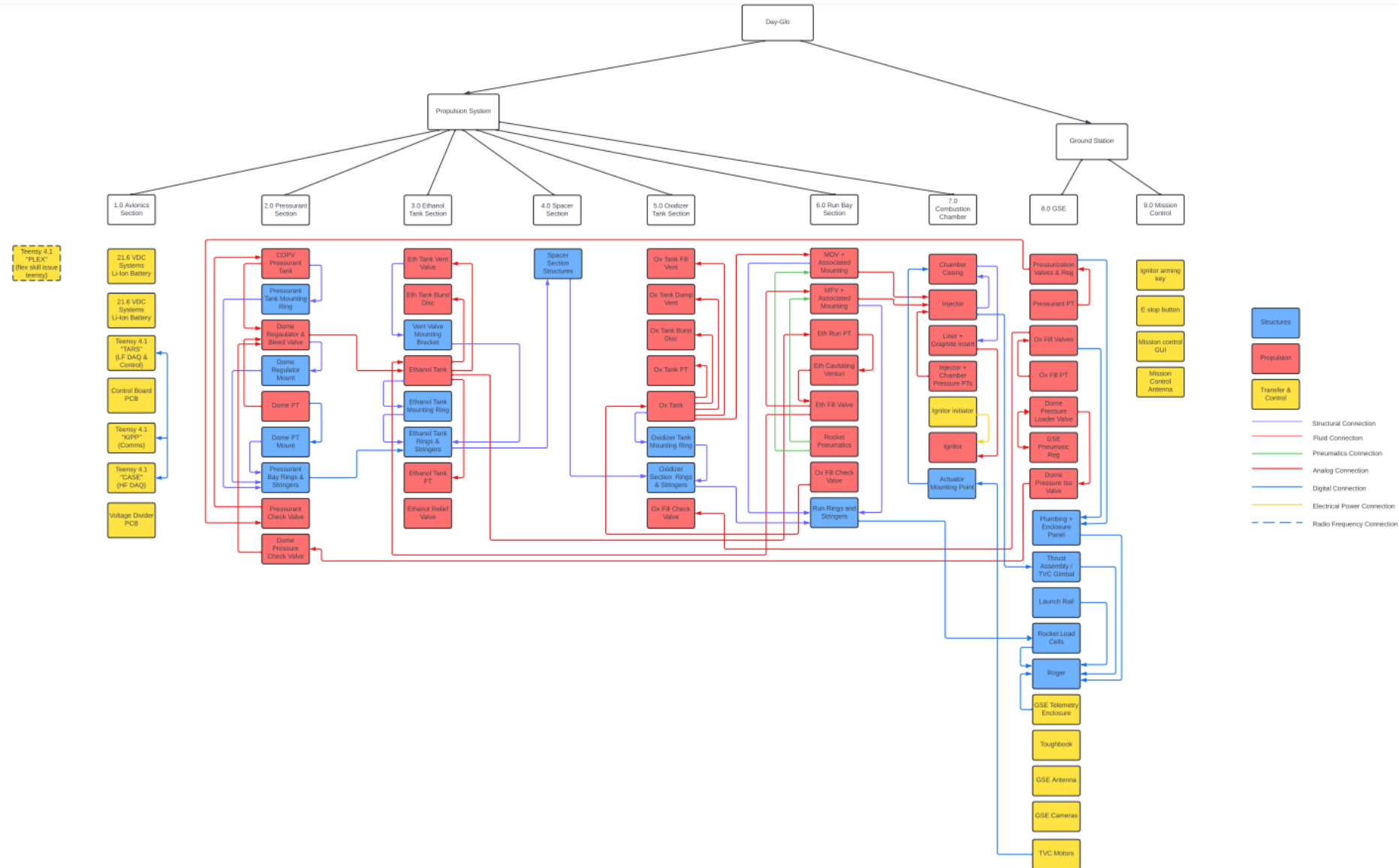


Figure 4.1. Logical decomposition of the Chimera rocket engine system.

Based on the subsystem decomposition in the preceding figure, subsystem requirements were derived. Each subsystem requirement was carefully revised to ensure that it was verifiable. From this, a verification plan was developed to ensure that nothing would be missed in the verification & validation process. A summary of the verification processes, current status and important notes from the process have been presented in the verification matrix provided in Table 4.2.

Table 4.1: Chimera Liquid Engine Subsystem Requirements

Req. #	Requirement
<b>2.1 Pressurant Tank</b>	
2.1.1	COPV pressurant tank shall have a pressure rating equal to or above its maximum expected operating pressure (MEOP).
2.1.2	COPV pressurant tank shall be hydrotested to a pressure greater than 1.1x the MEOP.
2.1.3	Volume of the COPV pressurant tank shall be sufficiently large to ensure that the working pressure never exceeds 4000 psi due to supply bottle restrictions.
2.1.4	COPV pressurant tank shall have pressure relief device(s) to ensure that the pressure remains below the MEOP.
2.1.5	Pressurization rate of the COPV pressurant tank shall be less than 1000 psi/minute at all phases of the pressurization process.
2.1.6	Pressurant tank shall be capable of being relieved manually in the event of premature regulator closure and failure of additional relief mechanisms.
<b>2.2 Pressurant Tank Mounting Ring</b>	
2.2.1	COPV mounting ring shall restrict lateral and vertical motion of the tank.
2.2.2	COPV mounting ring shall dampen vibration of the tank during transportation.
<b>2.3 Dome Regulator</b>	
2.3.1	Dome loaded pressure regulator shall be sized to handle the nominal volumetric flowrate of pressurant at all phases of engine operation (Excluding purge).
2.3.2	Dome loaded pressure regulator shall have inlet and outlet pressure ratings that are within the expected operating conditions.

2.3.3	Dome loaded pressure regulator shall have a temperature rating that is within the expected conditions for the testing environment.
<b>2.4 Dome Regulator Mount</b>	
2.4.1	Regulator mount shall provide a direct structural connection between the pressure regulator and structural frame.
<b>3.1 Ethanol Tank Vent Valve</b>	
3.1.1	The ethanol tank shall be connected to a normally open valve that allows for passive venting in the event of control loss.
3.1.2	The ethanol tank vent valve shall have a pressure rating that exceeds the MEOP of the ethanol tank.
<b>3.2 Ethanol Tank Burst Disc</b>	
3.2.1	The ethanol tank burst disc shall be capable of handling the volumetric flowrate corresponding to the worst-case unexpected failure mode of the pressurant system.
3.2.2	The ethanol tank burst disc shall open at a pressure that ensures the maximum pressure excursion above the tank's working pressure does not exceed the proof pressure of the tank (1300 psi).
<b>3.3 Vent Valve Mounting Bracket</b>	
3.3.1	Vent valve mount shall provide a direct structural connection between the vent valve and structural frame.
<b>3.4 Ethanol Tank</b>	
3.4.1	The ethanol tank volume shall be sufficient to accommodate the expected liquid fuel volume and gas ullage, ensuring that pressure during a fully open regulator failure does not exceed the tank's proof pressure.
3.4.2	The ethanol tank shall be capable of withstanding a pressure that is between 1.1–1.5× the MEOP without yielding).
3.4.3	The ethanol tank shall have a burst factor of safety of at least 2 at the MEOP.

<b>3.5 Ethanol Tank Relief Valve</b>	
3.5.1	The ethanol tank relief valve shall open at a pressure above the tank's working pressure and below the MEOP.
3.5.2	The tank pressure at the fully open relief valve position shall be used to define the tank's MEOP.
3.5.3	The ethanol tank relief valve shall be capable of handling the volumetric flowrate of expected pressure excursions above the tank's working pressure.
<b>5.1 Ox Tank Fill Vent</b>	
5.1.1	The oxidizer tank fill vent shall have an orifice size of between 0.3 and 2mm.
5.1.2	The oxidizer tank fill vent shall be capable of operating in low temperature environments with no impact of valve operation and performance.
5.1.3	The oxidizer tank fill vent shall be a normally closed valve.
5.1.4	The oxidizer tank fill vent shall be capable of being operated remotely.
<b>5.2 Oxidizer Tank Dump Valve</b>	
5.2.1	The oxidizer tank dump valve shall be positioned below the tank to ensure it drains liquid nitrous rather than gas.
5.2.2	The oxidizer tank dump valve shall have an orifice size that is sufficiently large to allow a fully loaded oxidizer tank to be emptied in 30 minutes.
5.2.3	The oxidizer tank dump valve shall fail in the open position to ensure that the oxidizer tank contents are dumped if communication is lost with the test stand.
<b>5.3 Oxidizer Tank Burst Disc</b>	
5.3.1	The oxidizer tank burst disc shall open at a pressure between the MEOP and proof pressure of the tank.
5.3.2	The oxidizer tank burst disc shall be capable of handling the volumetric flowrate corresponding to the worst-case unexpected failure mode without exceeding the tank's proof pressure.

<b>5.4 Oxidizer Tank</b>	
5.4.1	The oxidizer tank volume shall be sufficient to accommodate the expected liquid volume and gas ullage according to filling ratios defined in standards for safe handling of nitrous oxide.
5.4.2	The oxidizer tank shall be capable of withstanding a pressure that is between 1.1–1.5× the MEOP without yielding.
5.4.3	The oxidizer tank shall have a burst factor of safety of at least 2 of the MEOP.
<b>6.1 Main Oxidizer Valve</b>	
6.1.1	The main oxidizer valve, mounting hardware and actuation mechanism shall be capable of fitting within the 6.5 inch cylindrical volume allocated for run line hardware.
6.1.2	The main oxidizer valve orifice size shall be large enough to ensure that the flow is not cavitated and choked at the main valve.
6.1.3	The main oxidizer valve shall be actuated to the fully open position in less than 0.2s at the MEWP.
6.1.4	The wetted materials in the main oxidizer valve shall be compatible with nitrous oxide.
6.1.5	The main oxidizer valve shall be actuated remotely.
<b>6.2 Main Fuel Valve</b>	
6.2.1	The main fuel valve, mounting hardware and actuation mechanism shall be capable of fitting within the 6.5 inch cylindrical volume allocated for the run line hardware.
6.2.2	The main fuel valve orifice size shall be large enough to ensure that the flow is not cavitated and choked at the main valve.
6.2.3	The main fuel valve shall be actuated to the fully open position in less than 0.2s at the MEWP.
6.2.4	The wetted materials in the main fuel valve shall be compatible with ethanol.
6.2.5	The main fuel valve shall be actuated remotely.
<b>6.3 Ethanol Cavitating Venturi</b>	
6.3.1	The ethanol cavitating venturi shall be capable of interfacing with a standard 37 degree JIC

	fitting.
6.3.2	The ethanol cavitating venturi shall have an internal profile that chokes the fuel flow rate to within 0.05 kg/s of the theoretical flow rate.
6.3.3	The ethanol cavitating venturi shall not yield or fracture when subjected to the full fuel flow rate at the maximum expected working pressure.

#### 6.4 Ethanol Tank Fill Valve

6.4.1	The ethanol tank fill valve shall have a pressure rating that exceeds the MEOP of the ethanol tank.
6.4.2	The ethanol tank fill valve shall be opened and closed manually during fill.
6.4.3	The ethanol tank fill valve shall be located below the fuel tank..

#### 7.1 Chamber Casing

7.1.1	The combustion chamber casing shall have a yield FOS of greater than 1.5 at the maximum expected operating pressure.
7.1.2	The combustion chamber casing shall be capable of being connected to the TVC linear actuators.

#### 7.2 Injector

7.2.1	The injector shall have no interpropellant seals between the nitrous and fuel volutes.
7.2.2	The injector orifices shall be sized such that a minimum stiffness of 10% is achieved for the entirety of the burn duration.
7.2.3	The injector material shall be compatible with both ethanol and nitrous oxide.
7.2.4	The injector material shall retain its structural integrity at the maximum expected operating temperature during the burn.

#### 7.3 Liner + Graphite Insert

7.3.1	The combustion chamber liner shall not completely ablate away by the end of the burn.
7.3.2	The combustion chamber liner shall possess sufficient strength to prevent cracking or failure throughout the duration of the hotfire test.

7.3.3	The graphite insert shall not crack or become dislodged at any point during the hotfire test.
-------	---

#### 7.4 Ignition System

7.4.1	The ignition system shall be capable of being activated remotely at mission control.
7.4.2	The ignitor shall remain fixed inside the combustion chamber until stable self-sustained combustion is attained.
7.4.3	The ignition system shall provide sufficient activation energy to vaporize and combust the mixed propellants during startup.
7.4.4	The ignitor burn duration shall be at least 7s.
7.4.5	The ignitor shall produce thick, visible smoke that can be seen using the camera system.

#### 8.1.1 GSE Pressurization Control Valves

8.1.1.1	The pressurization control valves shall be remotely actuated.
8.1.1.2	The control valves for the GSE pressurant panel shall be configured to ensure that the N2 cylinder contents are NOT passively vented.
8.1.1.3	The GSE pressurant control valves shall have a pressure rating that exceeds the MEOP of the pressurant tank.
8.1.1.4	The GSE pressurant control panel shall contain a relief valve that passively vents pressurant in the event of pressure excursions above the maximum expected working pressure.

#### 8.1.2 GSE Pressurization Control Regulator

8.1.2.1	The pressurization regulator shall be hand-loaded.
8.1.2.2	The GSE pressurization control regulator shall have an inlet pressure rating that exceeds the supply pressure from a 6K nitrogen supply cylinder.
8.1.2.3	The GSE pressurization control regulator shall have an outlet pressure range that encompasses the MEWP of the pressurant tank.

#### 8.1.3 GSE Pressurization Vent Valve

8.1.3.1	The pressurization panel on the GSE subassembly shall passively vent pressurant contained within isolated portions of plumbing if control is lost.
---------	--

<b>8.2.1 Oxidizer Fill Valve</b>	
8.2.1.1	The oxidizer fill valve shall have a pressure rating that exceeds the MEOP of the nitrous supply cylinder.
8.2.1.2	The oxidizer fill valve shall be actuated remotely to allow for remote fill capabilities.
8.2.1.3	The wetted components of the oxidizer fill valve shall be compatible with nitrous oxide.
8.2.1.4	The oxidizer fill valve shall be actuated pneumatically.
<b>8.3.1 Dome Pressure Loader Valve</b>	
8.3.1.1	The dome pressure loader valve shall have an inlet pressure rating that exceeds the expected supply pressure from a T nitrogen supply cylinder.
8.3.1.2	The dome pressure loader valve shall be hand-loaded.
8.3.1.3	The dome pressure loader valve shall allow for precise control of the outlet pressure, ensuring that the dome pressure is achieved within +/- 20 psi of the target value.
<b>8.3.2 GSE Pneumatic Regulator</b>	
8.3.2.1	The GSE pneumatic regulator shall allow for precise control of the outlet pressure, ensuring that the pneumatic pressure is maintained to 100 psi +/- 5 psi.
8.3.2.2	The GSE pneumatic regulator shall have an inlet pressure rating that exceeds the expected supply pressure range from a T nitrogen supply cylinder.
<b>8.4.1 Thrust Mount (Rodger)</b>	
8.4.1.1	The thrust assembly shall be capable of both static and thrust-vectorized operation of the engine.
8.4.1.2	The thrust assembly shall be capable of withstanding the maximum expected thrust (1500 lbf) with a yield safety factor of at least 3.
8.4.1.3	The thrust assembly shall be capable of measuring engine thrust in the static engine configuration.
8.4.1.4	The thrust mount gimbal shall not yield when subjected to the maximum expected thrust (1500 lbf) at all deflection angles permitted by the thrust vectoring system.

8.4.1.5	The thrust mount gimbal during thrust vectored operation shall permit the engine to rotate by +/- 10 degrees about both the x and y axis simultaneously.
<b>8.4.2 GSE Structure (Roger)</b>	
8.4.2.1	The GSE structure shall provide support for the GSE plumbing, support rails, and thrust mount.
8.4.2.2	The GSE structure shall be anchored to the ground such that no movement is possible at any point during the hotfire test of the engine.
8.4.2.3	The GSE structure shall have a winch that allows for raising and lowering of the support rail.
8.4.2.4	The GSE structure shall have load cells for measuring the propellant feed system during fill.
<b>8.4.3 Support Rail</b>	
8.4.3.1	The support rail shall be capable of being raised, lowered and disassembled into 10ft segments for transportation.
8.4.3.2	The support rail shall be supporting the propellant system as it is raised and lowered without structural failure.
8.4.3.3	The support rail shall be rigidly supported in its upright position to minimize movement and oscillation of the propellant system during testing.
8.4.3.4	The support tail shall contain scaffolding to minimize the impact of wind on the load cell measurements.
<b>8.4.4 TVC Actuators</b>	
8.4.4.1	The actuators used during thrust-vectored operation shall provide an actuation force that is sufficient to overcome the inertial, static friction, and dynamic friction forces experienced during all points of the test.
8.4.4.2	The actuators used during thrust-vectored operation shall have a travel rate that permits at least one full circular sweep of the engine during the 9.2s burn.
8.4.4.3	The actuators used during thrust-vectored operation shall be capable of interfacing with COTS ball joints.

Table 4.2: Chimera Liquid Engine Verification Matrix

Req. #	Requirement Description	Method of Verification	Status	Remarks
2.1.1	COPV pressurant tank shall have a pressure rating equal to or above its maximum expected operating pressure (MEOP).	<ul style="list-style-type: none"> <li>Analysis of manufacturer documentation</li> <li>Comparison of tank rating (4500 psi) to 3200 psi MEOP</li> </ul>	Complete	The manufacturer's rating of 4500 psi exceeds the 3200 psi MEOP, satisfying the requirement.
2.1.2	COPV pressurant tank shall be hydrotested to at least 1.1x MEOP.	<ul style="list-style-type: none"> <li>Review of manufacturer hydrostatic test certificate</li> <li>Confirmation that test pressure exceeded required value</li> </ul>	Complete	The manufacturer performed a hydrostatic test above the minimum requirement, as indicated by their certificate.
2.1.3	Volume of the COPV pressurant tank shall be sufficiently large to ensure the working pressure never exceeds 4000 psi due to supply bottle restrictions.	<ul style="list-style-type: none"> <li>Simulation in Flownex for worst-case discharge</li> <li>Verification of pressure remaining below 4000 psi</li> </ul>	Complete	Flownex simulations show that the selected 6.8 L tank volume keeps the pressure below 4000 psi under supply constraints.
2.1.4	COPV pressurant tank shall have pressure relief device(s) to ensure that the pressure remains below the MEOP.	<ul style="list-style-type: none"> <li>Inspection of relief valve installation</li> <li>Verification of set point at 4000 psi and orifice sizing</li> </ul>	Complete	The relief valve set at 4000 psi, combined with a flow restriction orifice, prevents exceeding the 4500 psi tank rating.
2.1.5	Pressurization rate of the COPV pressurant tank shall be less than 1000 psi/minute at all phases of the pressurization process.	<ul style="list-style-type: none"> <li>Flownex flow rate simulation</li> <li>Orifice sizing calculations</li> </ul>	Complete	The flow restriction orifice was sized so that the pressurization rate remains below 1000 psi/minute in all phases.
2.1.6	Pressurant tank shall be capable of being relieved manually in the event of premature regulator closure and failure of additional relief mechanisms.	<ul style="list-style-type: none"> <li>Inspection of manual bleed valve placement</li> <li>Functional test of manual depressurization</li> </ul>	In Progress	A manual bleed valve is installed upstream of the regulator. The final integrated test will confirm effective manual relief.

2.2.1	COPV mounting ring shall restrict lateral and vertical motion of the tank.	<ul style="list-style-type: none"> <li>Physical inspection of assembled mount</li> <li>Observation of tank movement in situ</li> </ul>	Complete	The tank is placed in a pass-through hole that restricts both lateral and vertical motion, confirmed through inspection.
2.2.2	COPV mounting ring shall dampen vibration of the tank during transportation.	<ul style="list-style-type: none"> <li>Transport trial observation</li> <li>Check for excessive vibration in assembled configuration</li> </ul>	In Progress	Preliminary transport tests showed limited vibration. A final test will be conducted with the integrated setup.
2.3.1	Dome loaded pressure regulator shall handle the nominal volumetric flowrate of pressurant at all phases (excluding purge).	<ul style="list-style-type: none"> <li>Flownex simulation of up to 150 SCFM</li> <li>Comparison to supplier flow-capacity curves</li> </ul>	Complete	Simulations and supplier data indicate the regulator can accommodate more than 150 SCFM.
2.3.2	Dome loaded pressure regulator shall have inlet and outlet pressure ratings that are within the expected operating conditions.	<ul style="list-style-type: none"> <li>Datasheet review (0–5000 psi rating)</li> <li>Comparison with 3200 psi inlet and 900 psi outlet</li> </ul>	Complete	The regulator is rated up to 5000 psi, exceeding the 3200 psi inlet and 900 psi outlet requirements.
2.3.3	Dome loaded pressure regulator shall have a temperature rating that is within the expected conditions for the testing environment.	<ul style="list-style-type: none"> <li>Datasheet review of temperature limits</li> <li>Confirmation that test temperatures remain above -50 °C</li> </ul>	Complete	The regulator is rated to -50 °C, which covers all planned test conditions (above 0 °C).
2.4.1	Regulator mount shall provide a direct structural connection between the pressure regulator and structural frame.	<ul style="list-style-type: none"> <li>Inspection of COTS bracket installation</li> <li>Verification that regulator is secured to the frame</li> </ul>	Complete	The selected bracket provides a rigid connection between the regulator and the frame with minimal movement.
3.1.1	The ethanol tank shall be connected to a normally open valve that allows for passive venting in the event of control loss.	<ul style="list-style-type: none"> <li>Identification of normally open valve type</li> <li>Inspection of plumbing to confirm direct vent path</li> </ul>	Complete	A Jaksa D22NNO normally open valve is attached, ensuring passive venting if power is lost or controls fail.

3.1.2	The ethanol tank vent valve shall have a pressure rating that exceeds the MEOP of the ethanol tank.	<ul style="list-style-type: none"> <li>Datasheet pressure rating check</li> <li>Comparison to 1030 psi MEOP</li> </ul>	Complete	The valve is rated at 250 bar (~3625 psi), surpassing the 1030 psi MEOP requirement.
3.2.1	The ethanol tank burst disc shall be capable of handling the volumetric flowrate corresponding to the worst-case unexpected failure mode of the pressurant system.	<ul style="list-style-type: none"> <li>Flownex simulation of fully open dome regulator</li> <li>Verification that disc flow prevents exceeding tank proof</li> </ul>	Complete	The 1200 psi burst disc limits the pressure below the 1300 psi tank proof rating in a fully open regulator failure scenario.
3.2.2	The ethanol tank burst disc shall open at a pressure that ensures the maximum pressure excursion above the tank's working pressure does not exceed the proof pressure of the tank (1300 psi).	<ul style="list-style-type: none"> <li>Datasheet for 1200 psi burst</li> <li>Flownex check of transient overshoot</li> </ul>	Complete	The disc opens at 1200 psi, leading to a maximum of about 1260 psi, which is below the 1300 psi proof pressure.
3.3.1	Vent valve mount shall provide a direct structural connection between the vent valve and structural frame.	<ul style="list-style-type: none"> <li>CAD bracket inspection</li> <li>Physical assembly verification</li> </ul>	Complete	The bracket directly attaches the vent valve to the structural member, as confirmed in CAD and assembly.
3.4.1	The ethanol tank volume shall be sufficient to accommodate the expected liquid fuel volume and gas ullage, ensuring that pressure during a fully open regulator failure does not exceed the tank's proof pressure.	<ul style="list-style-type: none"> <li>Flownex simulation of worst-case regulator failure</li> <li>Consideration of 1200 psi burst disc interaction</li> </ul>	Complete	The tank volume and disc set point keep the pressure below 1300 psi proof in a fully open regulator event.
3.4.2	The ethanol tank shall be capable of withstanding a pressure that is between 1.1–1.5× the MEOP without yielding.	<ul style="list-style-type: none"> <li>Hydrostatic proof test at 1.26× MEOP</li> <li>Observation for permanent deformation</li> </ul>	Complete	A 15-minute hydrostatic test at 1.26× the 1030 psi MEOP showed no permanent deformation or yield.

3.4.3	The ethanol tank shall have a burst factor of safety of at least 2 at the MEOP.	<ul style="list-style-type: none"> <li>• Pin shear design analysis</li> <li>• Acceptance by LC judges for metal vessel standard</li> </ul>	Complete	The pin shear design yields about 1.94 safety factor at 2000 psi, which the LC judges accepted as sufficient.
3.5.1	The ethanol tank relief valve shall open at a pressure above the tank's working pressure and below the MEOP.	<ul style="list-style-type: none"> <li>• Supplier datasheet for set pressure</li> <li>• Comparison to 900 psi WP and 1030 psi MEOP</li> </ul>	Complete	The relief valve opens near 950 psi, falling between 900 psi (WP) and 1030 psi (MEOP).
3.5.2	The tank pressure at the fully open relief valve position shall be used to define the tank's MEOP.	<ul style="list-style-type: none"> <li>• Flownex flow simulation at full valve capacity</li> <li>• Steady-state pressure check</li> </ul>	In Progress	Simulations show ~1030 psi at full valve flow, which defines MEOP. A final integrated test will confirm it.
3.5.3	The ethanol tank relief valve shall be capable of handling the volumetric flowrate of expected pressure excursions above the tank's working pressure.	<ul style="list-style-type: none"> <li>• Flownex transient simulation</li> <li>• Valve capacity rating review</li> </ul>	Complete	The valve is sized for 130 SCFM, exceeding potential regulator leakage or transient flows.
5.1.1	The oxidizer tank fill vent shall have an orifice size of between 0.3 and 2 mm.	<ul style="list-style-type: none"> <li>• Inspection of orifice diameter (0.6 mm)</li> <li>• Confirmation from supplier data</li> </ul>	Complete	The selected fill vent has a 0.6 mm orifice, which lies within the specified 0.3–2 mm range.
5.1.2	The oxidizer tank fill vent shall be capable of operating in low temperature environments with no impact on valve operation and performance.	<ul style="list-style-type: none"> <li>• Historical usage review for freezing incidents</li> <li>• Planned cold fill checks</li> </ul>	In Progress	Prior use demonstrated no freezing. A dedicated cold fill test will formally confirm reliable performance.
5.1.3	The oxidizer tank fill vent shall be a normally closed valve.	<ul style="list-style-type: none"> <li>• Verification of valve type</li> <li>• Datasheet confirmation</li> </ul>	Complete	The solenoid valve is a normally closed variant, satisfying the requirement.
5.1.4	The oxidizer tank fill vent shall be capable of being operated remotely.	<ul style="list-style-type: none"> <li>• Review of electrical solenoid design</li> </ul>	In Progress	The valve can be actuated via the electronics

		<ul style="list-style-type: none"> <li>• GSE control integration test</li> </ul>		subsystem. The final GSE test is pending.
5.2.1	The oxidizer tank dump valve shall be positioned below the tank to ensure it drains liquid nitrous rather than gas.	<ul style="list-style-type: none"> <li>• Plumbing schematic check</li> <li>• Physical observation of tee placement below the run tank</li> </ul>	Complete	The dump line originates from a fitting below the tank, ensuring that liquid is removed first.
5.2.2	The oxidizer tank dump valve shall have an orifice size sufficiently large to allow a fully loaded oxidizer tank to be emptied in 30 minutes.	<ul style="list-style-type: none"> <li>• Flownex tank dump simulation</li> <li>• Potential inert abort test for empirical check</li> </ul>	In Progress	Simulations predict an empty time under 10 minutes. An optional live test may be conducted if resources permit.
5.2.3	The oxidizer tank dump valve shall fail in the open position to ensure that the oxidizer tank contents are dumped if communication is lost with the test stand.	<ul style="list-style-type: none"> <li>• Review of valve design (normally closed poppet with pilot solenoid)</li> <li>• Power-loss functional test</li> </ul>	In Progress	Although the valve is NC, the pilot solenoid ensures it opens when power is removed, provided pneumatic supply is present. A final integrated test remains.
5.3.1	The oxidizer tank burst disc shall open at a pressure between the MEOP and proof pressure of the tank.	<ul style="list-style-type: none"> <li>• Datasheet rating (1200 psi disc)</li> <li>• Comparison to 1030 psi MEOP and 1300 psi proof</li> </ul>	Complete	The disc rating of 1200 psi sits between the MEOP (1030 psi) and proof (1300 psi).
5.3.2	The oxidizer tank burst disc shall be capable of handling the volumetric flowrate corresponding to the worst-case unexpected failure mode without exceeding the tank's proof pressure.	<ul style="list-style-type: none"> <li>• Flownex simulation for a fully open regulator</li> <li>• Supplier disc flow capacity data</li> </ul>	In Progress	Additional analysis is ongoing to confirm the disc can handle enough flow to keep pressure below 1300 psi proof.
5.4.1	The oxidizer tank volume shall be sufficient to accommodate the expected liquid volume and gas ullage according to filling ratios defined in standards for safe handling of nitrous oxide.	<ul style="list-style-type: none"> <li>• Calculation per AIGA fill ratio (0.68 kg/L)</li> <li>• Comparison to 34 L tank volume</li> </ul>	Complete	The 34 L tank, at 0.68 kg/L, can safely hold 23 kg of nitrous for the 9.2 s burn.

5.4.2	The oxidizer tank shall be capable of withstanding a pressure that is between $1.1\text{--}1.5 \times$ the MEOP without yielding.	<ul style="list-style-type: none"> <li>• Hydrostatic test at <math>1.26 \times</math> MEOP</li> <li>• Check for permanent deformation</li> </ul>	Complete	The tank withstood $1.26 \times$ its MEOP with no permanent deformation, the same as the ethanol tank procedure.
5.4.3	The oxidizer tank shall have a burst factor of safety of at least 2 of the MEOP.	<ul style="list-style-type: none"> <li>• Design analysis of pin shear at 2000 psi</li> <li>• Acceptance by LC judges for metal vessel</li> </ul>	Complete	Similar to the ethanol tank, the factor of safety is near 1.94, which was accepted by judges.
6.1.1	The main oxidizer valve, mounting hardware and actuation mechanism shall be capable of fitting within the 6.5 inch cylindrical volume allocated for run line hardware.	<ul style="list-style-type: none"> <li>• Dimensional check in CAD</li> <li>• Inspection of as-assembled MOV unit</li> </ul>	Complete	All components fit within the 6.5 inch envelope, as verified by CAD and physical measurement.
6.1.2	The main oxidizer valve orifice size shall be large enough to ensure that the flow is not cavitated and choked at the main valve.	<ul style="list-style-type: none"> <li>• Calculation of valve Cv (47)</li> <li>• Comparison with feed line diameter</li> </ul>	Complete	A Cv of 47 corresponds to an effective orifice larger than the line diameter, ensuring no choking at the valve.
6.1.3	The main oxidizer valve shall be actuated to the fully open position in less than 0.2 s at the MEWP.	<ul style="list-style-type: none"> <li>• Bench test for actuation time</li> <li>• Planned integrated system test</li> </ul>	In Progress	Isolated tests showed 0.12 s actuation. A final test in the full system is forthcoming.
6.1.4	The wetted materials in the main oxidizer valve shall be compatible with nitrous oxide.	<ul style="list-style-type: none"> <li>• Datasheet review of 316 SS and PTFE</li> <li>• Reference to compatibility data</li> </ul>	Complete	Both 316 stainless steel and PTFE are accepted as compatible with nitrous oxide.
6.1.5	The main oxidizer valve shall be actuated remotely.	<ul style="list-style-type: none"> <li>• Examination of pneumatic pilot solenoid</li> <li>• System-level demonstration</li> </ul>	In Progress	The valve is driven by a pneumatic actuator controlled by a solenoid. A final integrated demonstration is planned.

6.2.1	The main fuel valve, mounting hardware and actuation mechanism shall be capable of fitting within the 6.5 inch cylindrical volume allocated for the run line hardware.	<ul style="list-style-type: none"> <li>CAD dimensional review</li> <li>Physical inspection of the MFV assembly</li> </ul>	Complete	The assembly, including bracket and actuator, fits inside the 6.5 inch space as confirmed by CAD.
6.2.2	The main fuel valve orifice size shall be large enough to ensure that the flow is not cavitated and choked at the main valve.	<ul style="list-style-type: none"> <li>Calculation of valve Cv (5.5)</li> <li>Comparison to downstream venturi size</li> </ul>	Complete	A Cv of 5.5 (~0.55" orifice) is larger than the venturi throat, so the valve is not the limiting component.
6.2.3	The main fuel valve shall be actuated to the fully open position in less than 0.2 s at the MEWP.	<ul style="list-style-type: none"> <li>Isolated timing test</li> <li>Planned integrated verification</li> </ul>	In Progress	A bench test showed 0.09 s to open fully. The integrated system test is not yet complete.
6.2.4	The wetted materials in the main fuel valve shall be compatible with ethanol.	<ul style="list-style-type: none"> <li>Datasheet review of materials</li> <li>Industry references on ethanol compatibility</li> </ul>	Complete	All wetted parts (316 stainless steel and PTFE) are suitable for ethanol service.
6.2.5	The main fuel valve shall be actuated remotely.	<ul style="list-style-type: none"> <li>Pneumatic solenoid inspection</li> <li>Confirmation of remote activation interface</li> </ul>	In Progress	The fuel valve includes a pneumatic actuator driven by a solenoid. Full system testing is pending.
6.3.1	The ethanol cavitating venturi shall be capable of interfacing with a standard 37 degree JIC fitting.	<ul style="list-style-type: none"> <li>Visual inspection of flared surface</li> <li>Reference to previous successful usage</li> </ul>	Complete	The venturi has a 37° flare, proven compatible with standard JIC connections in prior systems.
6.3.2	The ethanol cavitating venturi shall have an internal profile that chokes the fuel flow rate to within 0.05 kg/s of the theoretical flow rate.	<ul style="list-style-type: none"> <li>Planned cold flow test</li> <li>Comparison of measured mass flow to theoretical model</li> </ul>	Pending	A dedicated cold flow test will be run to confirm the actual mass flow is within ±0.05 kg/s of design.
6.3.3	The ethanol cavitating venturi shall not yield or fracture when	<ul style="list-style-type: none"> <li>Structural review of venturi design</li> </ul>	In Progress	This configuration has been used before without

	subjected to the full fuel flow rate at the maximum expected working pressure.	<ul style="list-style-type: none"> <li>• Inspection after prior usage</li> </ul>		failure. A final acceptance test will verify continued integrity.
6.4.1	The ethanol tank fill valve shall have a pressure rating that exceeds the MEOP of the ethanol tank.	<ul style="list-style-type: none"> <li>• Datasheet rating (1500 psi)</li> <li>• Comparison to 1030 psi MEOP</li> </ul>	Complete	The fill valve's 1500 psi rating meets the requirement above the 1030 psi MEOP.
6.4.2	The ethanol tank fill valve shall be opened and closed manually during fill.	<ul style="list-style-type: none"> <li>• Inspection of manual ball valve</li> <li>• Demonstration of fill procedure</li> </ul>	In Progress	A manual ball valve has been installed, and an integrated fill demonstration is scheduled.
6.4.3	The ethanol tank fill valve shall be located below the fuel tank.	<ul style="list-style-type: none"> <li>• Review of piping layout</li> <li>• Physical location check in run bay</li> </ul>	Complete	The fill valve is installed at a tee below the ethanol tank, enabling bottom fill.
7.1.1	The combustion chamber casing shall have a yield FOS of greater than 1.5 at the maximum expected operating pressure.	<ul style="list-style-type: none"> <li>• Stress analysis of chamber wall</li> <li>• Verification with final material data</li> </ul>	In Progress	Engineering calculations are ongoing to confirm an FOS above 1.5 at the operational chamber pressure.
7.1.2	The combustion chamber casing shall be capable of being connected to the TVC linear actuators.	<ul style="list-style-type: none"> <li>• CAD inspection of mounting brackets</li> <li>• Fit check with actuator ball joints</li> </ul>	Complete	The chamber includes integrated brackets designed to accept the TVC actuator connections.
7.2.1	The injector shall have no interpropellant seals between the nitrous and fuel volutes.	<ul style="list-style-type: none"> <li>• Inspection of injector design</li> <li>• Confirmation that passages are physically separate</li> </ul>	Complete	The design isolates the fuel and oxidizer paths, ensuring no single seal bridges the two volutes.
7.2.2	The injector orifices shall be sized such that a minimum stiffness of 10% is achieved for the entirety of the burn duration.	<ul style="list-style-type: none"> <li>• Pressure drop calculations</li> </ul>	In Progress	Fuel orifices yield ~60 psi drop (above 35 psi needed), and nitrous orifices achieve ~40%

		<ul style="list-style-type: none"> <li>• Simulation of feed conditions for nitrous and fuel</li> </ul>		stiffness. Hotfire tests will finalize the result.
7.2.3	The injector material shall be compatible with both ethanol and nitrous oxide.	<ul style="list-style-type: none"> <li>• Check of material specification (303 SS)</li> <li>• Review of established compatibility data</li> </ul>	Complete	303 stainless steel is recognized as compatible with both ethanol and nitrous oxide.
7.2.4	The injector material shall retain its structural integrity at the maximum expected operating temperature during the burn.	<ul style="list-style-type: none"> <li>• Previous hotfire experience on smaller injector</li> <li>• Planned post-hotfire inspection</li> </ul>	Pending	No issues were observed with similar injectors previously. The team will verify again after the full-duration burn test.
7.3.1	The combustion chamber liner shall not completely ablate away by the end of the burn.	<ul style="list-style-type: none"> <li>• Computed liner thickness vs. predicted ablation rate</li> <li>• Full-scale hotfire observation</li> </ul>	Pending	The liner is sized conservatively based on known ablation rates, and a hotfire test will confirm no burn-through occurs.
7.3.2	The combustion chamber liner shall possess sufficient strength to prevent cracking or failure throughout the duration of the hotfire test.	<ul style="list-style-type: none"> <li>• Material structural analysis</li> <li>• Post-hotfire inspection for cracks</li> </ul>	Pending	The chamber liner's strength under operating conditions will be verified during a live test.
7.3.3	The graphite insert shall not crack or become dislodged at any point during the hotfire test.	<ul style="list-style-type: none"> <li>• Verification of mechanical retention features</li> <li>• Inspection post-hotfire</li> </ul>	Pending	The graphite throat is secured with robust mounting features. The hotfire test will confirm no damage occurs.
7.4.1	The ignition system shall be capable of being activated remotely at mission control.	<ul style="list-style-type: none"> <li>• Review of remote relay wiring and battery circuit</li> <li>• Bench test of activation</li> </ul>	In Progress	A relay-based nichrome coil ignition is set up for remote activation. The final integrated test remains.
7.4.2	The ignitor shall remain fixed inside the combustion chamber	<ul style="list-style-type: none"> <li>• Inspection of epoxy mounting</li> </ul>	Pending	The ignitor puck is bonded with high-temperature epoxy.

	until stable self-sustained combustion is attained.	<ul style="list-style-type: none"> <li>• Observation during smaller-scale tests</li> </ul>		In prior smaller hotfires, it remained until flame was established.
7.4.3	The ignition system shall provide sufficient activation energy to vaporize and combust the mixed propellants during startup.	<ul style="list-style-type: none"> <li>• Reference to successful ignition on previous nitrous-ethanol engine</li> <li>• Planned hotfire test for Chimera</li> </ul>	Complete	An identical approach was used to ignite nitrous-ethanol in previous tests, demonstrating sufficient activation energy.
7.4.4	The ignitor burn duration shall be at least 7 s.	<ul style="list-style-type: none"> <li>• Measurement of burn time in bench trials</li> <li>• Verification in a live hotfire</li> </ul>	Pending	A smaller puck lasted ~20 s previously. The new puck's duration will be confirmed in upcoming tests.
7.4.5	The ignitor shall produce thick, visible smoke that can be seen using the camera system.	<ul style="list-style-type: none"> <li>• Observation of smoke production in earlier ignition tests</li> <li>• Confirmation with on-stand cameras</li> </ul>	Complete	Prior pucks produced significant black smoke visible on all cameras, so this requirement is satisfied.
8.1.1.1	The pressurization control valves shall be remotely actuated.	<ul style="list-style-type: none"> <li>• Inspection of solenoid wiring</li> <li>• Basic functional test with remote signals</li> </ul>	In Progress	Bench tests confirmed remote actuation capability. The final integration on GSE is pending.
8.1.1.2	The control valves for the GSE pressurant panel shall be configured to ensure that the N2 cylinder contents are NOT passively vented.	<ul style="list-style-type: none"> <li>• Review of schematic showing normally closed vent valve</li> <li>• Inspection ensuring supply isolation</li> </ul>	Complete	The arrangement ensures the cylinder remains isolated if power is lost, preventing passive venting of N2.
8.1.1.3	The GSE pressurant control valves shall have a pressure rating that exceeds the MEOP of the pressurant tank.	<ul style="list-style-type: none"> <li>• Datasheet rating check (5000 psi)</li> <li>• Comparison to 4000 psi tank MEOP</li> </ul>	Complete	All control valves are rated to 5000 psi, which is higher than the 4000 psi MEOP.

8.1.1.4	The GSE pressurant control panel shall contain a relief valve that passively vents pressurant in the event of pressure excursions above the maximum expected working pressure.	<ul style="list-style-type: none"> <li>• Set point inspection (4000 psi relief)</li> <li>• Verification of minimal overshoot in static lines</li> </ul>	In Progress	The relief valve is set at 4000 psi. A final system test will confirm that pressure does not exceed safe limits.
8.1.2.1	The pressurization regulator shall be hand-loaded.	<ul style="list-style-type: none"> <li>• Physical inspection of adjustment knob</li> <li>• Confirmation that no powered loading mechanism is present</li> </ul>	Complete	The cylinder-mounted regulator uses a manually adjusted spring mechanism.
8.1.2.2	The GSE pressurization control regulator shall have an inlet pressure rating that exceeds the expected supply pressure from a 6K nitrogen cylinder.	<ul style="list-style-type: none"> <li>• Datasheet review (7500 psi max)</li> <li>• Comparison to 6000 psi cylinder limit</li> </ul>	Complete	The regulator inlet rating of 7500 psi exceeds the typical 6000 psi supply cylinder pressure.
8.1.2.3	The GSE pressurization control regulator shall have an outlet pressure range that encompasses the Maximum Expected Working Pressure (MEWP) of the pressurant tank.	<ul style="list-style-type: none"> <li>• Manufacturer data on adjustable output (0–5000 psi)</li> <li>• Requirement of 3100 psi tank pressure</li> </ul>	Complete	The regulator can output up to 5000 psi, covering the 3100 psi needed.
8.1.3.1	The pressurization panel on the GSE subassembly shall passively vent pressurant contained within isolated portions of plumbing if control is lost.	<ul style="list-style-type: none"> <li>• Panel schematic review with normally open vent</li> <li>• Inspection of isolation conditions</li> </ul>	In Progress	Design includes a normally open vent to purge isolated lines upon control loss. The final system test is pending.
8.2.1.1	The oxidizer fill valve shall have a pressure rating that exceeds the MEOP of the nitrous supply cylinder.	<ul style="list-style-type: none"> <li>• Datasheet check of 2200 psi rating</li> <li>• Comparison to ~1030 psi MEOP</li> </ul>	Complete	The valve is rated at 2200 psi, comfortably above the 1030 psi cylinder MEOP.
8.2.1.2	The oxidizer fill valve shall be actuated remotely to allow for remote fill capabilities.	<ul style="list-style-type: none"> <li>• Inspection of pneumatic actuator</li> <li>• Plan for solenoid-driven fill</li> </ul>	In Progress	A pneumatic rotary actuator is used, controlled by a pilot solenoid for remote

				operation. The final fill test is forthcoming.
8.2.1.3	The wetted components of the oxidizer fill valve shall be compatible with nitrous oxide.	<ul style="list-style-type: none"> <li>Materials review (316 SS, PTFE)</li> <li>Reference to nitrous compatibility data</li> </ul>	Complete	Stainless steel 316 and PTFE are both accepted for nitrous oxide service.
8.2.1.4	The oxidizer fill valve shall be actuated pneumatically.	<ul style="list-style-type: none"> <li>Inspection of actuator mechanism</li> <li>Basic functionality test</li> </ul>	In Progress	The valve uses a pneumatic rotary actuator, which will be verified under actual fill operations.
8.3.1.1	The dome pressure loader valve shall have an inlet pressure rating that exceeds the expected supply pressure from a T nitrogen supply cylinder.	<ul style="list-style-type: none"> <li>Datasheet check (0–5000 psi)</li> <li>Typical T-cylinder ~2600 psi</li> </ul>	Complete	The valve rating of 5000 psi is above the ~2600 psi T-cylinder pressure.
8.3.1.2	The dome pressure loader valve shall be hand-loaded.	<ul style="list-style-type: none"> <li>Physical inspection of spring-loaded adjustment</li> <li>Verification that no powered pilot system is needed</li> </ul>	Complete	The selected dome valve is manually adjusted and does not rely on an external pilot load.
8.3.1.3	The dome pressure loader valve shall allow for precise control of the outlet pressure, ensuring that the dome pressure is achieved within +/- 20 psi of the target value.	<ul style="list-style-type: none"> <li>Bench or cold flow test of regulator accuracy</li> <li>Past operational data for reference</li> </ul>	In Progress	Preliminary data suggests acceptable accuracy. A dedicated cold flow test will verify +/- 20 psi control.
8.3.2.1	The GSE pneumatic regulator shall allow for precise control of the outlet pressure, ensuring that the pneumatic pressure is maintained at 100 psi +/- 5 psi.	<ul style="list-style-type: none"> <li>Bench test with calibrated gauge</li> <li>Observation of regulator drift over test period</li> </ul>	In Progress	A similar model showed ~2 psi drift previously. A final acceptance test will confirm +/- 5 psi performance.
8.3.2.2	The GSE pneumatic regulator shall have an inlet pressure rating that exceeds the expected supply	<ul style="list-style-type: none"> <li>Datasheet stating 0–5000 psi inlet</li> </ul>	Complete	The regulator rating is 5000 psi, above the 2600

	pressure range from a T nitrogen supply cylinder.	<ul style="list-style-type: none"> <li>• Comparison to 2600 psi supply</li> </ul>		psi maximum from a T cylinder.
8.4.1.1	The thrust assembly shall be capable of both static and thrust-vectorized operation of the engine.	<ul style="list-style-type: none"> <li>• CAD review of thrust mount design</li> <li>• Plan for gimbal integration</li> </ul>	In Progress	The design accommodates a static mount and a gimbal for vectoring. Assembly-level validation is pending.
8.4.1.2	The thrust assembly shall be capable of withstanding the maximum expected thrust (1500 lbf) with a yield safety factor of at least 3.	<ul style="list-style-type: none"> <li>• Structural analysis (FEA or equivalent)</li> <li>• Material yield criteria check</li> </ul>	Pending	A final analysis will confirm an FOS $\geq$ 3 at 1500 lbf thrust load.
8.4.1.3	The thrust assembly shall be capable of measuring engine thrust in the static engine configuration.	<ul style="list-style-type: none"> <li>• Integration of load cells</li> <li>• Static hotfire to record thrust data</li> </ul>	Pending	The mount includes load cells for static thrust measurement, which will be verified in an actual static hotfire.
8.4.1.4	The thrust mount gimbal shall not yield when subjected to the maximum expected thrust (1500 lbf) at all deflection angles permitted by the thrust vectoring system.	<ul style="list-style-type: none"> <li>• Gimbal stress analysis at <math>\pm 10^\circ</math></li> <li>• Final structural verification</li> </ul>	Pending	Analytical checks will ensure no yielding under peak thrust at full gimbal angles.
8.4.1.5	The thrust mount gimbal during thrust vectored operation shall permit the engine to rotate by +/- 10 degrees about both the x and y axis simultaneously.	<ul style="list-style-type: none"> <li>• Inspection of gimbal travel in CAD</li> <li>• Measurement of actual hardware deflection</li> </ul>	Pending	The gimbal is designed for $>10^\circ$ travel. The final build will be measured to confirm the required angles.
8.4.2.1	The GSE structure shall provide support for the GSE plumbing, support rails, and thrust mount.	<ul style="list-style-type: none"> <li>• CAD inspection of structural interfaces</li> <li>• Physical assembly check for each subcomponent</li> </ul>	Complete	The “Roger” structure contains attachments for all plumbing, rails, and the thrust mount as shown in CAD.
8.4.2.2	The GSE structure shall be anchored to the ground such that	<ul style="list-style-type: none"> <li>• Earth anchor design calculations</li> </ul>	Pending	Anchors have been sized. A pull test will confirm

	no movement is possible at any point during the hotfire test of the engine.	<ul style="list-style-type: none"> <li>Planned pull test of anchors</li> </ul>		they prevent structural movement under thrust or wind loads.
8.4.2.3	The GSE structure shall have a winch that allows for raising and lowering of the support rail.	<ul style="list-style-type: none"> <li>CAD review of winch mounting location</li> <li>Observation of integrated assembly</li> </ul>	Complete	The design includes a dedicated mount for the winch, verified in the model and partially in assembly checks.
8.4.2.4	The GSE structure shall have load cells for measuring the propellant feed system during fill.	<ul style="list-style-type: none"> <li>Inspection of load cell installation</li> <li>Verification in fill demonstration</li> </ul>	In Progress	Load cells are installed to weigh the system. A final instrumentation test will verify correct readings during fill.
8.4.3.1	The support rail shall be capable of being raised, lowered and disassembled into 10 ft segments for transportation.	<ul style="list-style-type: none"> <li>Physical check of rail segmentation</li> <li>Verification of pinned or bolted joints</li> </ul>	Complete	The rails can be taken apart into 10 ft sections, facilitating easier transport and handling.
8.4.3.2	The support rail shall be supporting the propellant system as it is raised and lowered without structural failure.	<ul style="list-style-type: none"> <li>Reference to guy tower specifications for load</li> <li>Integrated lift test planned</li> </ul>	In Progress	The rail is rated for taller towers. A system-level lift test will ensure it withstands the propellant load safely.
8.4.3.3	The support rail shall be rigidly supported in its upright position to minimize movement and oscillation of the propellant system during testing.	<ul style="list-style-type: none"> <li>Inspection of locking pins or bracing</li> <li>Final upright test to check stability</li> </ul>	In Progress	The design includes pins that lock the rail in the upright position. A final assembly test will confirm minimal movement.
8.4.3.4	The support tail shall contain scaffolding to minimize the impact of wind on the load cell measurements.	<ul style="list-style-type: none"> <li>Plan for scaffolding design</li> <li>Observation of actual structure in place</li> </ul>	Pending	A scaffolding or enclosure will be added to shield the load cells from wind-induced error.
8.4.4.1	The actuators used during thrust-vectorized operation shall provide an actuation force that is sufficient to overcome the inertial,	<ul style="list-style-type: none"> <li>Dynamic force analysis in TVC model</li> </ul>	In Progress	Preliminary modeling indicates 55 lbf is sufficient to pivot the engine under full thrust.

	static friction, and dynamic friction forces experienced during all points of the test.	<ul style="list-style-type: none"> <li>• Comparison of 55 lbf actuator rating to required forces</li> </ul>		Detailed verification is still under way.
8.4.4.2	The actuators used during thrust-vectored operation shall have a travel rate that permits at least one full circular sweep of the engine during the 9.2 s burn.	<ul style="list-style-type: none"> <li>• Measurement of actuator speed (0.9 in/s)</li> <li>• Calculation of required travel vs. burn duration</li> </ul>	Pending	Based on 0.9 in/s, a full sweep is expected to take less time than 9.2 s. The actual speed under load will be measured.
8.4.4.3	The actuators used during thrust-vectored operation shall be capable of interfacing with COTS ball joints.	<ul style="list-style-type: none"> <li>• Inspection of actuator rod ends</li> <li>• CAD confirmation of ball-joint attachment</li> </ul>	Complete	The actuators feature rod ends compatible with standard ball joints, as verified by the CAD model and supplier info.

## 5.0 SUBSYSTEM OVERVIEW

The Chimera liquid engine has been subdivided into 9 different subsystems and 68 subassemblies. The subassemblies are designed and managed by the three technical subteams; propulsion, structures and telemetry & control. The proceeding technical descriptions have been grouped based on both the subsystem and subteam organization presented in Figure 4.1.

### 5.1 PROPULSION SUBTEAM

The Chimera engine is a pressure fed liquid bipropellant engine. The fuel is ethanol and the oxidizer is nitrous oxide. As denoted in Figure 4.1, the core propulsion system is composed of six individual subsystems. Five of the systems function as the propellant feed system for the engine subsystem. The ground station feed system, contained within the GSE subsystem, is responsible for both supplying regulated pressurant and allowing for remote nitrous fill capabilities. The propulsion system was designed to meet several key performance targets. The initial design point for the propulsion system was a 10 second burn duration with 1500 lbf of thrust on startup. Based on the initial design point, the feed system and engine were sized accordingly. A summary of the parameters have been presented in Table 5.1.1.

Table 5.1.1: Propulsion System Specifications

Parameter	Value
Propellants	Ethanol (5.5 kg), N <sub>2</sub> O (23 kg)
Specific Impulse	189 s
Nominal Burn Duration	9.2 s
Initial Thrust	6.4kN (1420 lbf)
Mass Flow Rate	0.60 kg/s Ethanol 2.8 kg/s N <sub>2</sub> O
O/F Ratio	4.7
Initial Chamber Pressure	350 psig
Cooling System	Silica Phenolic Ablative
Injector	Like-like impinging

As demonstrated in Table 5.1.1, the predicted thrust and burn duration vary slightly from the initial design point. This variation was due to the collection of data from hotfire tests of the team's previous engine design. From this data, models were refined to reflect combustion inefficiencies that stem from the selected injector configuration. While it is a design goal for the combustion efficiency to be improved through refinement to the injector and chamber design, the 83% combustion efficiency from previous hotfire tests was used as a baseline for preliminary sizing of the system. As the team progresses further through the detailed design process, further refinements to the specifications will be made as required.

### 5.1.1 TRANSIENT ENGINE PERFORMANCE PREDICTION

Due to the use of self-pressurizing nitrous oxide, the performance of the engine is expected to vary throughout the 9.2 second burn. Accurate predictions of the transient engine performance help to ensure that the injector is able to remain choked, eliminating the likelihood of low-frequency coupling instabilities. A thermodynamic model of the nitrous oxide run tank was used to compute the nitrous fluid properties during the full-flow 9.5 second nitrous blowdown. The resulting pressure and mass flow rate plots have been presented in Figure 5.1.1.1 and 5.1.1.2 respectively. A description of the thermodynamic model along with Flownex validation has been provided in Appendix A.

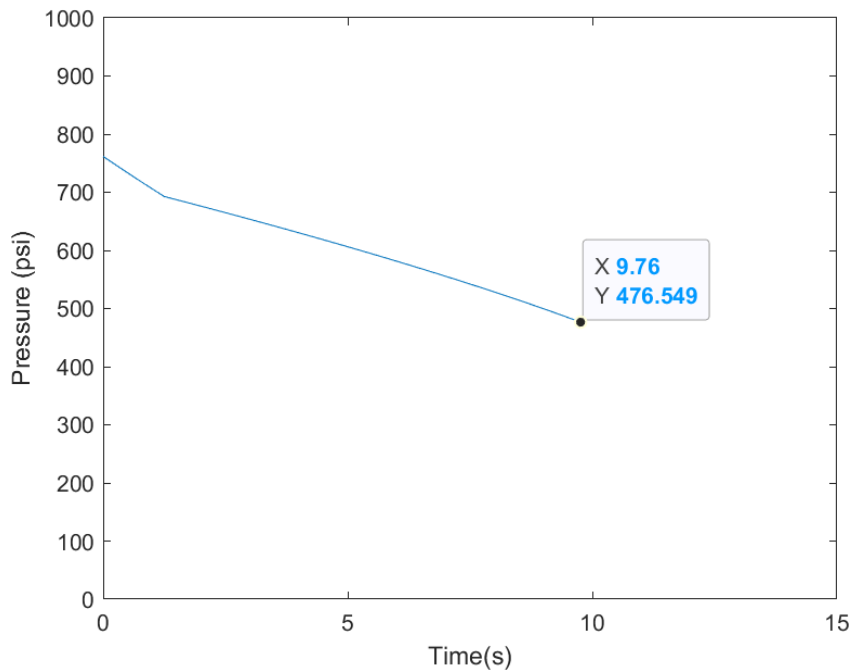


Figure 5.1.1.1: Transient nitrous oxide tank pressure

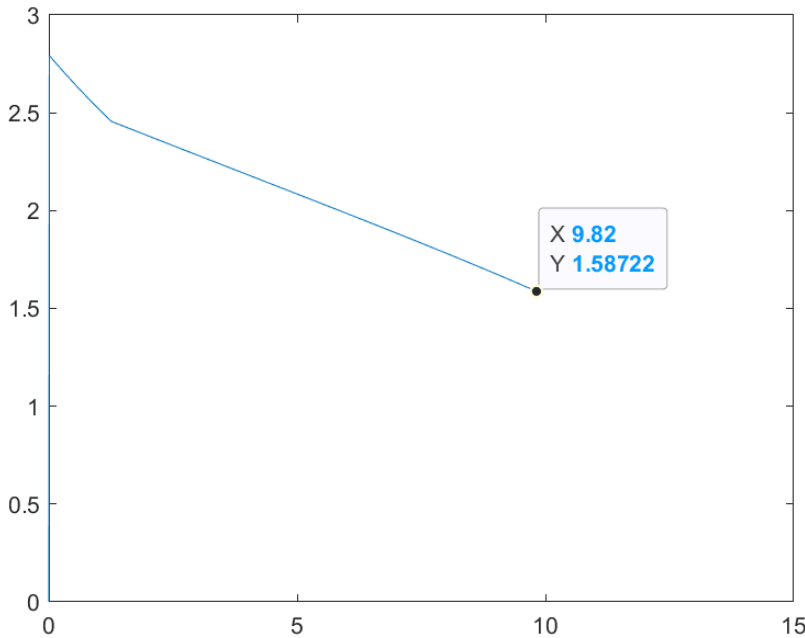


Figure 5.1.1.2: Transient nitrous oxide flow rate

Since the ethanol flow is to be controlled using a regulated supply of nitrogen and a cavitating venturi, the mass flow rate will remain constant at 0.60 kg/s for the entirety of the burn. The nozzle has been sized to result in an initial chamber pressure of 350 psi for the initial total mass flow rate of 3.4 kg/s using the hand calculations presented in Appendix A. Additional performance parameters for the start of the burn have been presented in Table 5.1.1.

The engine performance at the end of the burn was computed using an iterative process. The blowdown simulation allowed for the mass flow rates of each propellant to be determined at the end of the burn. Iterative calculations were subsequently performed using C\* results from CEA to approximate the final chamber pressure. A C\* efficiency of 83 % was assumed based on experimental combustion data collected for the team's previous ethaNOS engine. The final chamber pressure was computed to be 217.1 psi using this iterative process.

The computed chamber pressure was subsequently used to determine the equilibrium composition of the exhaust products. The pertinent theoretical CEA results have been presented in Table 5.1.1.1.

Table 5.2.7.1: CEA Results for End of Burn

Parameter	Value
$C^*$ <sub>Theoretical</sub>	1474.8 m/s
$C^*$ <sub>Predicted</sub>	1224.084 m/s
Gamma	1.22

Computations of the theoretical thrust coefficient yielded a value of 1.4478 for perfectly expanded flow. Using a vacuum thrust coefficient efficiency of 97.4%, the predicted thrust coefficient at sea level was determined to be 1.33. The preceding results were used to compute the final specific impulse and thrust. Sample calculations for the transient engine performance calculations have been provided in Appendix A. The predicted thrust curve has been presented in Figure 5.1.1.3.

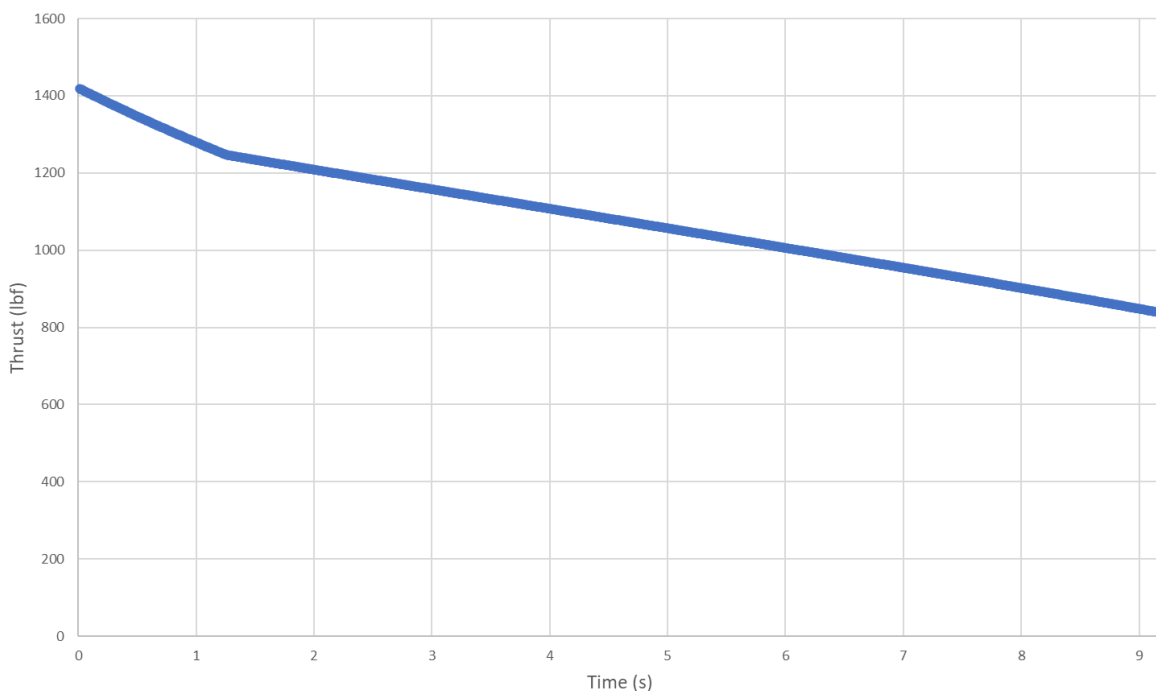


Figure 5.1.1.3: Predicted thrust curve for Chimera 9.2s burn

## 5.1.2 PROPELLANT SYSTEM

The propellant feed system consists of many subsystems. A P&ID of the entire propellant feed system has been provided in Figure 5.1.2. The proceeding subsections describe aspects of the P&ID in further detail.

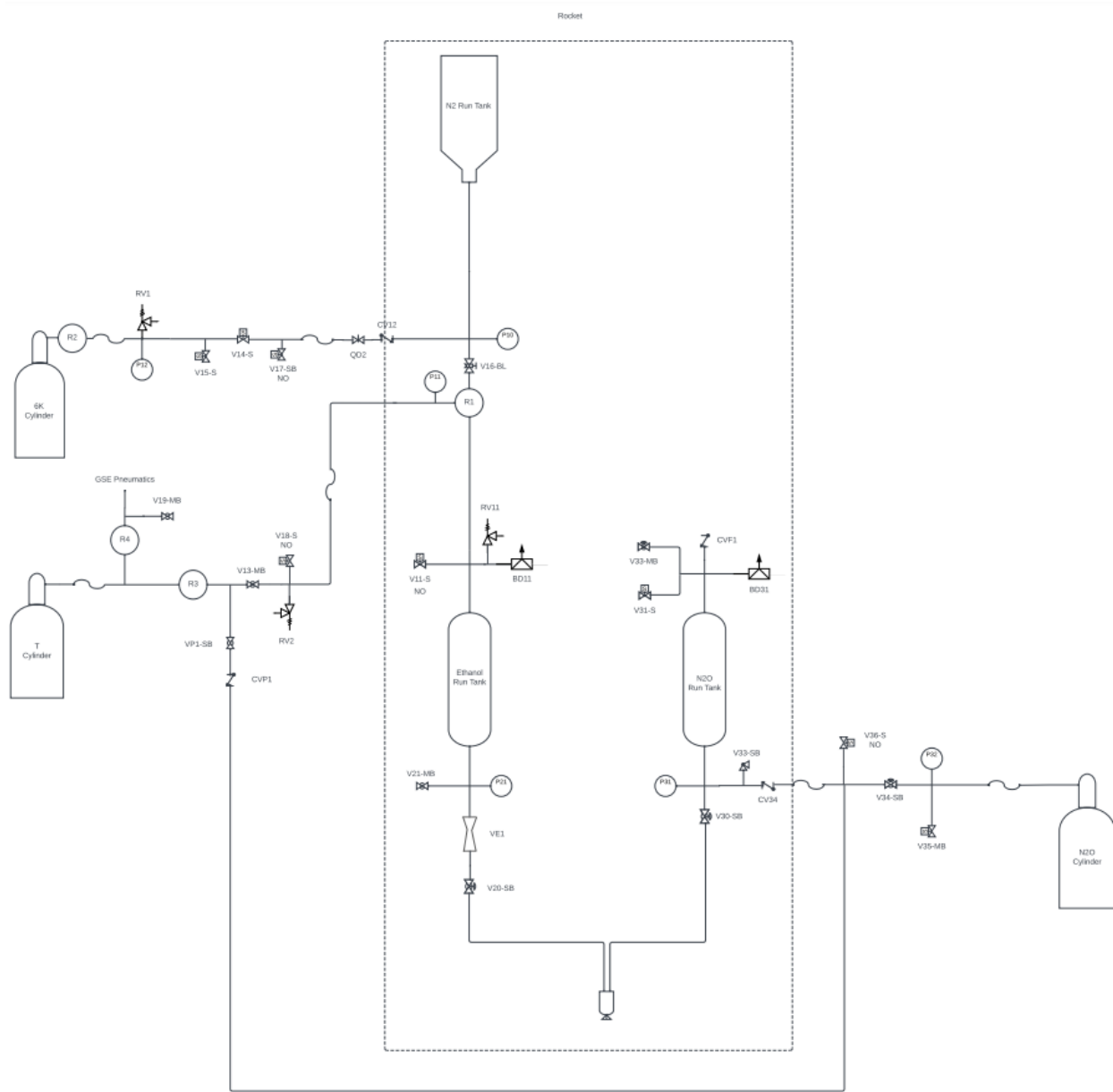


Figure 5.1.2.1: Complete P&ID of Day-Glo Propellant Feed System

The propellant system has been arranged in a vertically stacked configuration. This configuration was chosen due to the fact that the system is designed to fit within an airframe. In addition, due to the limited OD and the resultant heights of the tanks, it was determined that the resultant form factor would be best suited for a singular propulsion system unit that can be raised vertically. The relative positions of the propulsion subsystems can be observed in Figure 5.1.2.1.

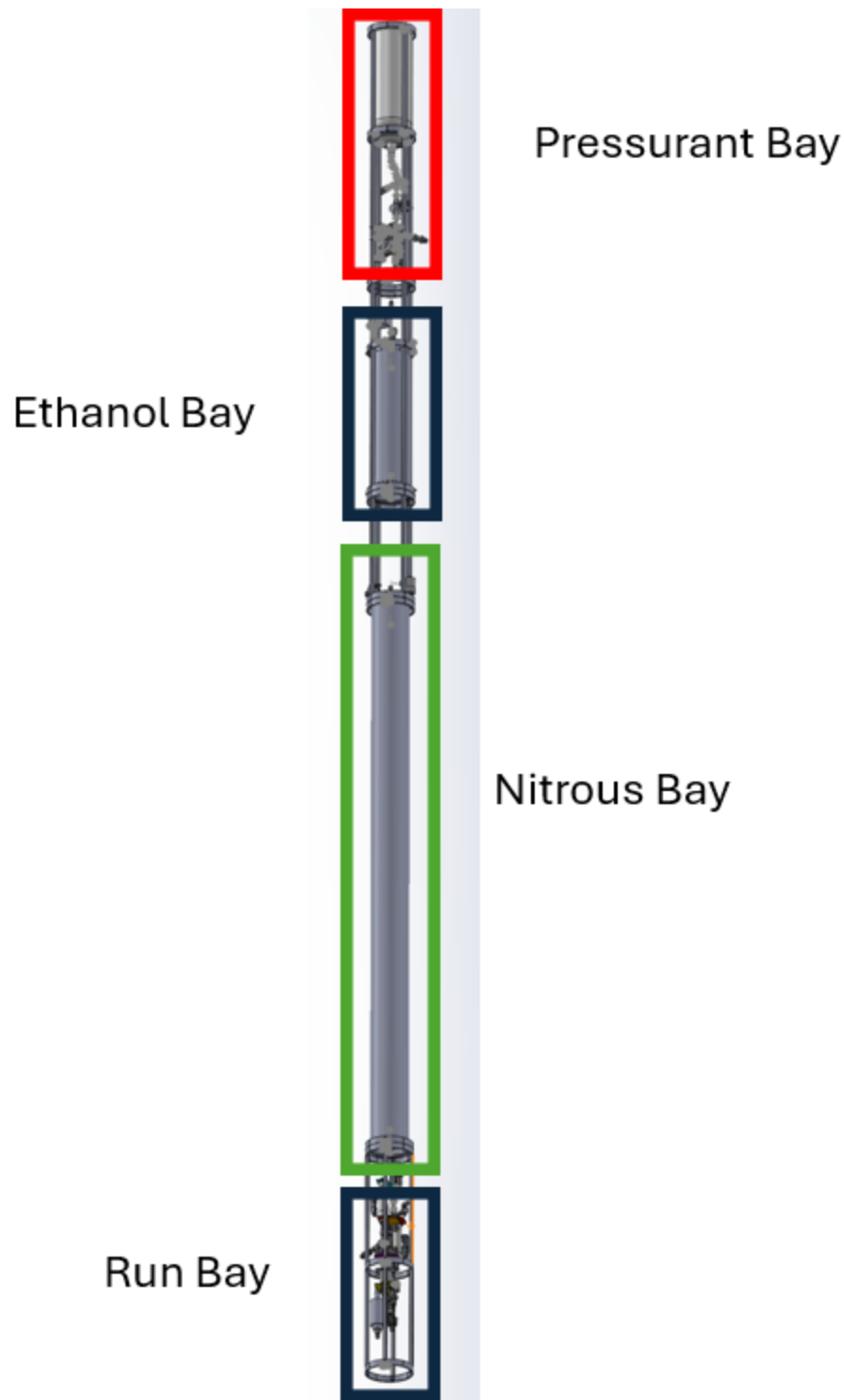


Figure 5.1.2.2: Vertically stacked propulsion system layout

### **5.1.2.1 PRESSURANT BAY SUBSYSTEM**

The pressurant bay subsystem is responsible for pressurizing the fuel tank. Two candidate designs were considered for the fuel pressurization system. A traditional regulated pressurization system was evaluated alongside a piston tank, designed to use nitrous oxide to pressurize the fuel. The piston tank design was not selected due to the additional manufacturing resources that would be required, a key constraint that dictates many of the team's design decisions.

With the regulated pressurization system, a source of inert pressurant is required. With the current design, the pressurant is to be stored in a commercial off the shelf pressure vessel, and filled from a supply cylinder connected to the ground support system. Two approaches were considered for providing the pressurant supply. The first candidate design involved the use of a run tank to supply the inert pressurant, while the second option involved a direct connection to the pressurant supply cylinder. The first design approach was selected due to the excessive pressure drop that was predicted in the flexible hose line that would have connected the pressurant bay to the supply cylinder. The excessive pressure drop was an expected outcome as the flexible hose was required to be approximately 20 ft in length, a byproduct of the team's decision to vertically stack the propulsion system. The selected architecture allows for future iterations to be flown in a flight vehicle, something that would not have been possible without redesign effort with the second candidate design architecture.

The selected pressure vessel was a TUXING 6.8L COPV, rated to 4500psi. For safety, the pressure vessel has been derated to 3100 psi per the requirements of the feed system. With this initial pressure, it is expected for the tank pressure to decay to 1018 psi over the 9.2s burn duration as per the flow simulations that were performed for the propellant system. A plot of the expected pressurant supply pressure has been provided in Figure 5.1.1.1.1.

The pressurant supply is regulated through the use of a dome-loaded pressure regulator. The dome-loaded regulator was selected due to its superior droop and drift characteristics relative to its equivalent spring-loaded configuration. The use of a dome-loaded regulator also allows for an on-ground loader valve to be used to manipulate the dome regulator set pressure, allowing for the regulator set pressure to be changed while the propulsion system has been raised vertically. The ground support system was therefore designed to interface with the dome port of the dome-loaded regulator to provide a consistent dome pressure via the loader valve. A further description of the ground support equipment subsystems that interface with the dome regulator have been provided in Section 5.1.2.3.

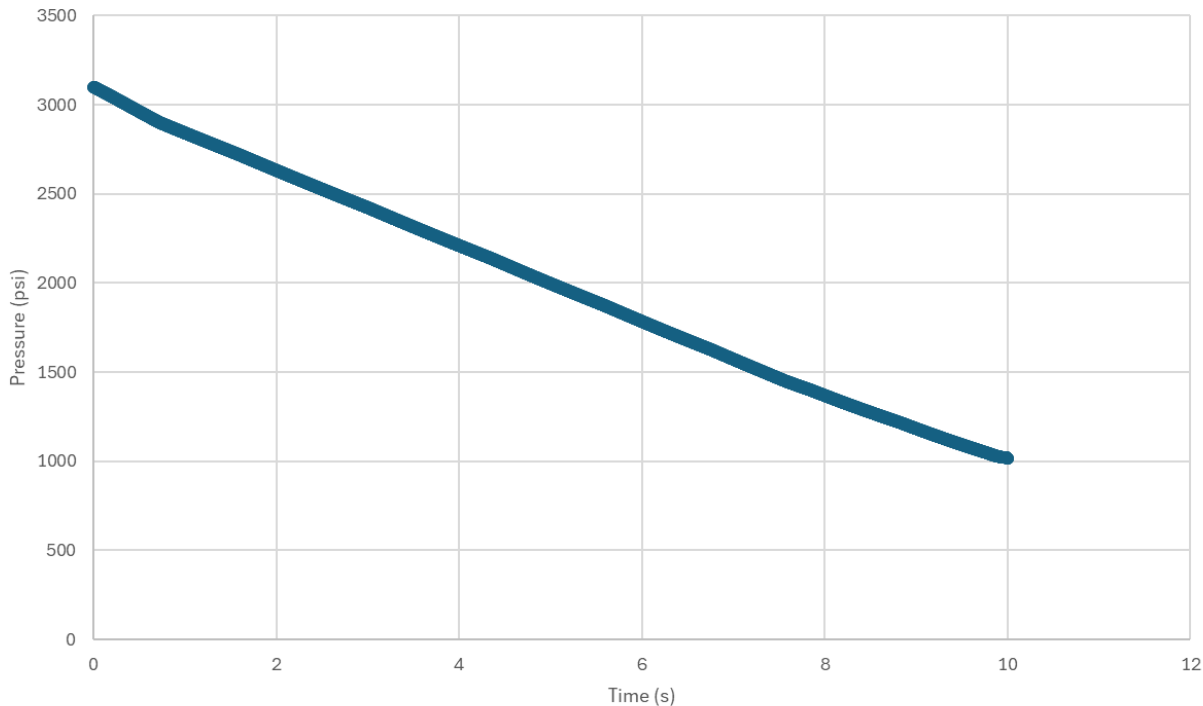


Figure 5.1.2.1.1: Pressurant tank pressure vs. time

In the highly unlikely event that complete dome pressure is lost, the regulator would revert to its fully closed position. As there is no dedicated passive vent in the pressurant section, a hand-operated bleed valve was added for emergency depressurization of the pressurant tank. This was deemed to be a highly unlikely failure mode due to the presence of both a constant pressurant supply to the dome port and a check valve to ensure that pressurant is both fed and kept in the plumbing that interfaces with the regulator's dome port. In an abort scenario, the pressurant nominally vents through the normally open solenoid valve connected to the ethanol tank. A further description of this passive relief mechanism has been provided in Section 5.1.2.2.2.

To size the pressure regulator, the volumetric flow rate was calculated. To calculate the volumetric flow rate, the previously mentioned flownex model was used. The resulting curve of volumetric flow rate versus time has been presented in Figure 5.1.2.1.2. Per the plot, a maximum volumetric flow rate of 153 SCFM is required to maintain a constant fuel tank pressure.

The design constraints for the regulator have been formally specified in Section 4. The constraints on the pressure and flow rates can be summarized as follows:

Pressure Adjustment Range: 0-1500 psi

Maximum Inlet Pressure: 4000 psi

Flow Capacity: 150 SCFM

The dome-loaded regulator has a strict flow capacity requirement. An Aqua Environment 873 series dome-loaded regulator was selected to satisfy this requirement. Per the supplier's flow curves, the regulator is capable of handling 450 SCFM at an outlet set pressure of 900 psi and an inlet pressure of 1500 psi [1]. While the specified inlet pressure on the flow curve is above the expected 1000 psi tank pressure at the end of the burn, the regulator is only required to handle 150 SCFM, leading to the decision to select this regulator for further testing. This indicates that the pressurant supply pressure would at most need to be raised by an additional 500 psi if further testing reveals that the regulator is unable to handle the required volumetric flow rate towards the end of the burn. This can easily be achieved as the pressure increase would result in an initial supply pressure that is within the specified pressure vessel rating per the manufacturer. However, due to the low magnitude of the required and maximum volume flow rates, it was determined that this was an unlikely outcome.

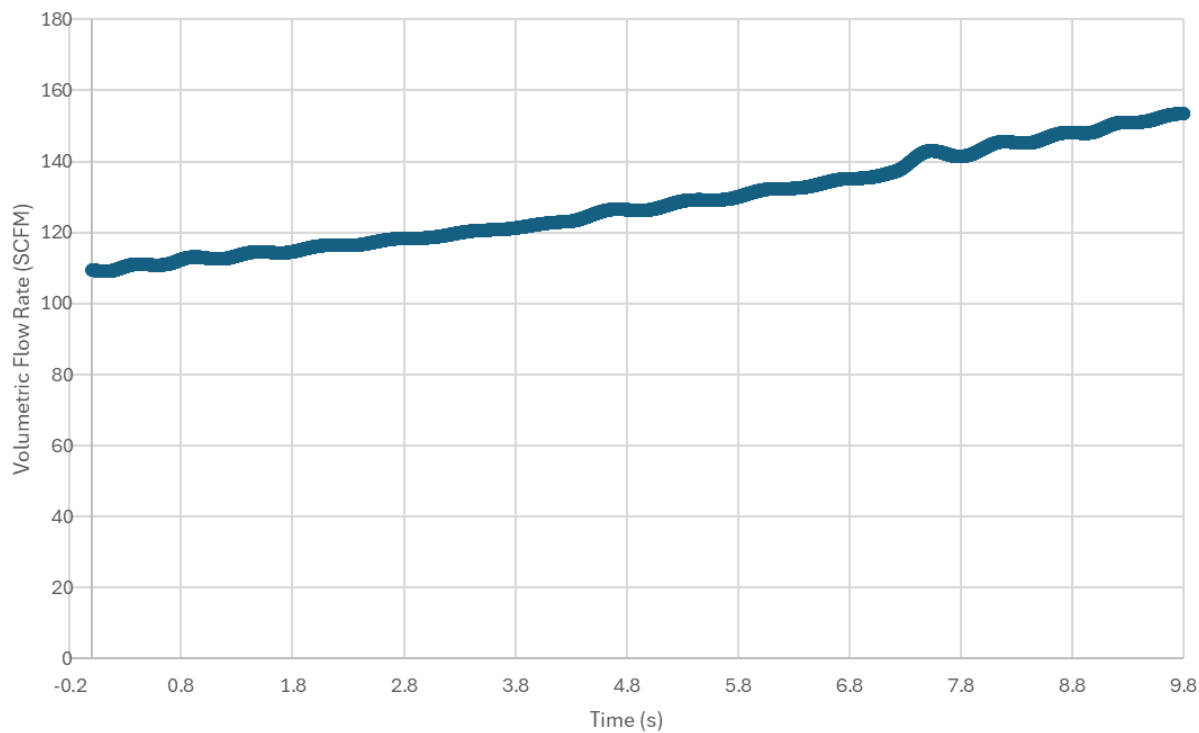


Figure 5.1.2.1.2: Dome regulator (R1) volumetric flow rate vs. time

The pressurant bay plumbing has largely been completed and is ready to be integrated with adjacent subsystems. Progress pictures have been presented in Figure 5.1.1.1.3.

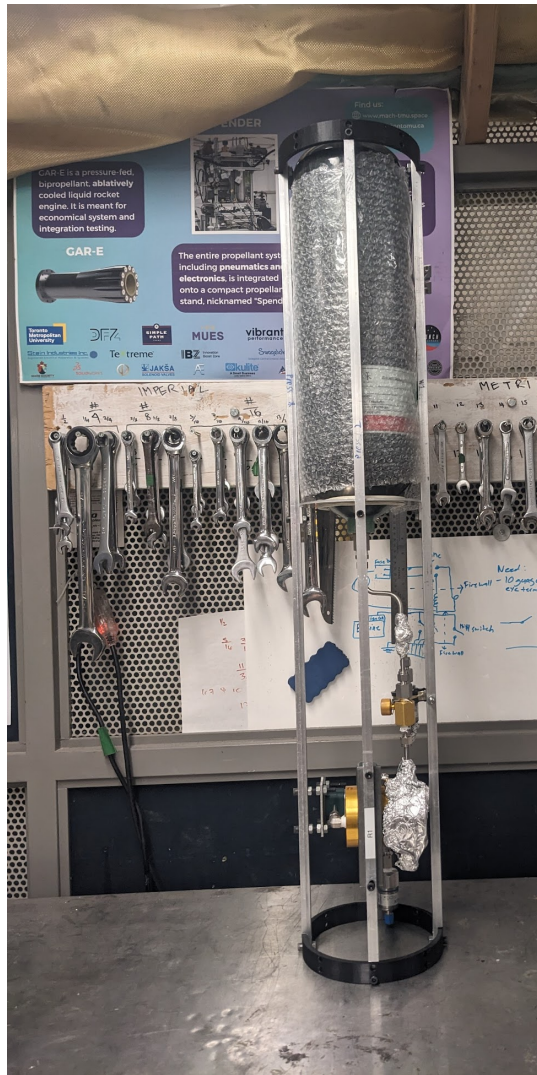


Figure 5.1.1.1.3: Completed pressurant bay plumbing

### 5.1.2.2 ETHANOL AND NITROUS BAY SUBSYSTEMS

As the names suggest, the ethanol and nitrous bays house the pressure vessels that contain the pressurized ethanol and nitrous oxide respectively. These two bays also contain the vents and relief mechanisms designed to protect the system from overpressure events and enable passive venturing in the case of control loss.

#### 5.1.2.2.1 PRESSURE VESSEL DESIGN

The design of the ethanol and nitrous run tanks are notably identical to simplify the manufacturing process. This decision was considered acceptable as the design provided

sufficient safety factors for both yield and burst for the ethanol run tank, which has the slightly higher maximum expected operating pressure (MEOP) of the two. Modifying the manufacturing process to tailor the design of the nitrous run tank, the pressure vessel with the lower pressure rating, was deemed an unnecessary complication that offered only marginal weight optimization benefits.

The ethanol run tank was initially sized based on the calculations presented in Table 5.1.1. During manufacturing, the casing length was cut to 2ft, resulting in a total internal tank volume of 7.4L. The resulting ullage volume was verified to be acceptable per the relief calculations presented in Section 5.1.1.2.2. Based on the assumed mass flow rate of 0.6 kg/s, a total ethanol mass of 5.5 kg was calculated as the required ethanol mass. Based on the flow simulations discussed in Appendix A, a nominal tank pressure of 800 psi was calculated. Per the aqua environment data sheet for the 873-D dome loaded regulator, compliance with the flow curve volumetric flow rate requirements results in at most a 10% droop. For a nominal tank pressure of 800 psi, this corresponds to an expected droop of ~90psi. It is therefore expected for the ethanol run tank to be pressurized to 900 psi immediately prior to a hotfire. Based on the revised pressure level definitions presented in R3 of the Launch Canada DTEG [2], 900 psi was defined as the maximum expected working pressure (MEWP). To define the maximum expected operating pressure (MEOP), simulations of regulator creep were performed for various assumed leakage rates. As further described in Section 5.1.1.2.2, the maximum fully open relief valve pressure of 1030 psi was used to define the MEOP of the ethanol run tank.

The nitrous oxide run tank was sized according to the 23 kg mass requirement highlighted in Table 5.1.1. AIGA guidelines for safe handling of nitrous oxide recommend a filling ratio of 0.68 kg/L [3]. As demonstrated in Appendix A, application of this standard notably yields a ullage gas volume in excess of 10%, a baseline notably recommended to the MACH team in previous years at the Launch Canada competition. Applying the filling ratio yielded a required nitrous run tank volume of at least 33L. During manufacturing, it was easiest to cut the run tank casing to a length of 90 inches, resulting in a total internal volume of 34L. In preparation for future iterations of the Chimera engine and feed system intended for flight, self-pressurization was selected to pressurize the run tanks instead of incorporating an additional pressure feed system. As demonstrated in the calculations in Appendix A, self-pressurization minimizes engine impulse loss while significantly simplifying the feed system design and reducing weight. The run tank working pressure is therefore a direct function of the ambient temperatures. As the Launch Canada 2025 competition is set to take place near the end of August, the selected run tank nitrous equilibrium temperature was reasonably set to 21C. This ambient temperature corresponds to an equilibrium pressure of 760 psi. As it is intended for means of supply cylinder cooling to be present on pad, 760 psi was defined as the WP. At the Launch Canada 2024

competition, temperature extremes resulted in nitrous equilibrium pressures on the order of 960 psi. Based on this result and the relief valve sizing process highlighted in the proceeding section, the MEOP of the tank was set to 1000 psi, notably lower than the ethanol tank's MEOP of 1030 psi. As a result 1030 psi was used as the MEOP for verifying the design's compliance with the requirements highlighted in Section 4.0.

Both run tanks are student research and developed (SRAD) aluminum pressure vessels. The design features two 6061-T6 aluminum bulkheads and a 6" OD and 3/16" thick 6061-T6 aluminum casing. The bulkheads are retained using 24 18-8 steel clevis pins. Four failure modes were considered while performing the stress analysis for the run tanks; clevis pin shear, casing tear-out, casing bearing failure, and casing tensile failure. The analysis indicated that the selected design has a factor of safety of 1.995 at the MEOP of 1030 psi. The expected failure mode is shearing of the clevis pins per the analysis results presented in Table 5.1.1.2.1.1. A summary of the calculation procedure has been provided in Appendix A. Similarly, at the nitrous tank MEOP of 1000 psi, the safety factor is exactly 2.

Table 5.1.2.2.1.1: Ethanol Tank FOS

Mode of Failure	Yielding FoS
Bearing Failure of Tank Wall	2.5
Tensile Failure of Tank at Min. Cross. Sect.	3.6
Shear Pin Failure	1.995
Pin Tear-Out Failure	2.4

Table 5.1.2.2.1.2: Nitrous Tank FOS

Mode of Failure	Yielding FoS
Bearing Failure of Tank Wall	2.5
Tensile Failure of Tank at Min. Cross. Sect.	3.7
Shear Pin Failure	2.06
Pin Tear-Out Failure	2.4

Both tanks were hydrostatically tested to 1300 psi for a duration of fifteen minutes. Elongations were measured in both the pressurized and unpressurized state. Other than a

minor leak from one of the fittings that was quickly addressed, no leakage was observed from either of the tanks. Further details on the testing results have been provided in Section 6.0.

#### **5.1.2.2.2 PRESSURE RELIEF AND VENTING**

Both the ethanol and nitrous run tanks are connected to spring-loaded relief valves that reduce the tank's pressure in the event of transient excursions above the corresponding working pressure. The relief valves have been sized to ensure that most common failure modes of the pressure feed system do not result in exceedances of the tank's MEOP. Per the risk analysis conducted in Section 7.0, the most critical failure mode for the pressure feed system involved failure of the pressure regulator in the fully open position. In the unlikely event that this were to occur, a large unregulated volumetric flow of nitrogen would be permitted to enter the nitrogen tank. The magnitude of this volumetric flow rate was so high that it would have increased the relief valve mass and cost by several orders of magnitude. To address this unique failure mode of the ethanol run tank, a  $\frac{1}{2}$ " burst disc has been connected in parallel with the run tank's relief valve. Simulations have been performed in flownex to verify that the relief valves and burst disc satisfy the subsystem requirements described in Section 4.0.

The pressure relief valves on both run tanks were selected to be Aqua Environment 1607 spring-loaded relief valves. The valves have an orifice diameter of 0.11 inches. To model the pressures in the system during relief valve operation, leakage was assumed to occur through the pressure regulator. The assumed leakage area was increased until a satisfactory volumetric flow rate was achieved. Following multiple iterations of the relief system, the team converged on a relief valve orifice diameter of 0.11 inches and a ESEOD of 0.067" for the leakage path in the regulator. In this configuration, a relief valve set pressure of 950 psi and an upstream pressure increase of 80 psi resulted in a sustained volumetric flow rate of about 130 SCFM to be exhausted from the valve. This level of leakage is notably incredibly high and is on the order of what is expected during transient operation of the pressure regulator, as demonstrated in Figure 5.1.2.1.2. It is also important to note that this level of leakage is only possible if significant damage to the regulator sealing surface were to occur. Damage to the regulator sealing surface most often occurs due to foreign object debris (FOD) that is either left from assembly or introduced through poor cleanliness during transport, or operation of the system [3]. To prevent this, The 873-D regulator comes with a built-in 10 micron filter [1]. Additionally, excessive leakage, like that which was modeled in the relief valve simulations, are likely to be caught during low pressure leak checks where the pressure source does not approach the MEOP of the tank. The results were therefore deemed to be acceptable for the provided reasons and the

upstream pressure of 1030 psi, corresponding to the fully open relief valve position, was chosen as the MEOP.

As previously mentioned, it was impractical to size a relief valve to handle the full volumetric flow rate associated with failure of the regulator in its fully open position. It is for this reason that an additional burst disc was added to the ethanol run tank. The selected burst disc is a PB series burst disc from Zook. The burst pressure is 1200 psi and the corresponding flow area is 0.17 in<sup>2</sup>. Per the supplier, the standard operating pressure of the disc is 75% of the burst pressure, or 900 psi [5]. As shown, the burst disc is compatible with the selected working pressure of the system. Transient relief simulations were performed to demonstrate that failure of the regulator in its fully open position would not result in excursions above the tank's proof pressure. The results of that simulation have been presented in Figure 5.1.1.2.2.1. Per the team's interpretation of DTEG requirement 2.2.1.1, it is acceptable for the burst pressure of the disc to be above the MEOP of the tank so long as the fully open position of the relief valve is able to handle the common and expected mechanisms of pressure excursions above the working pressure [2]. Due to the use of a COTS regulator, the fully open regulator failure mode was determined to be highly unlikely and was therefore not considered for the sizing of the relief valve and selection of the corresponding MEOP.

An identical relief package was selected for the nitrous run tank. Transient excursions above the selected working pressure are most likely to occur due to temperature changes of the fluid contained in the tank post-fill. As heat transfer to the fluid in the tank is an ambiguous process to model that depends on several external factors, engineering judgement was used to conclude that this process of heating would be unlikely to produce substantial volumetric flow rates that would be in excess of what has been predicted to occur in the ethanol pressurant system. The highest risk failure mode per the risk analysis presented in Section 8.0 corresponds to a runaway thermal decomposition reaction of saturated vapor trapped in the tank. While it is highly unlikely for this to occur due to the high temperatures that would be required to initiate this reaction, the identical PB series burst disc was plumbed in parallel with the relief valve to mitigate the potential impacts of this failure mode. It is important to note that nitrogen purging and premature closing of the main oxidizer valve (MOV) are additional mitigations that would help to prevent thermal decomposition initiation.

### **5.1.2.3 RUN BAY SUBSYSTEM**

The run bay subsystem is responsible for containing the plumbing that controls the flow of liquid fuel and oxidizer. It contains the valves and flow control mechanisms used for fill,

dumping and hotfire operations. The run bay is notably the only part of the core propulsion system that requires pneumatic pressure for valve actuation.

Upon confirmation that the ignitor has begun to burn, the main valves are to be opened at the same time, allowing propellant to flow to the injector. The oxidizer valve is positioned slightly ahead of the fuel valve, resulting in a slight oxidizer lead to the combustion chamber. This will be verified during full scale cold flow tests. The main valves were selected to be Sharpe 2-piece ball valves. Ball valves were selected due to their high flow coefficient and low cost relative to other valve types. The flow coefficients of the main oxidizer and fuel valves are 47 and 5.5 respectively. To comply with standards for safe handling of nitrous oxide, an upstream vent will be manually bored in the ball of the MOV prior to the use of nitrous oxide for testing.

Due to the high torque requirements of the main valves, pneumatic pistons were selected as the preferred actuation mechanism to allow for both fast and remote valve control. The pistons were selected over rotary pneumatic actuators due to their compliance with the spatial constraints of the run bay. The valve and actuator are connected using a waterjetted aluminum frame and steel linkage. The independent frame pieces sandwich the valve on each of its ends and are held together with two  $\frac{3}{8}$ -16 bolts. The fully assembled and integrated MOV and MFV assemblies can be seen in Figure 5.1.2.2.1.



Figure 5.1.2.2.1: Run bay with installed MOV and MFV assemblies.

The run bay subsystem also contains the plumbing required for fill operations of both fuel and ethanol. Fuel is filled by opening V21-MB, and manually pumping ethanol into the tank. For the oxidizer, a flexible hose is to be connected to the AN fitting upstream of CV34. The oxidizer is filled through this fitting and the check valve ensures that the oxidizer cannot flow backwards into the GSE plumbing once it has entered the main propulsion system. The dump valve, V33-SB, is a COTS Aqua Environment 1094 poppet valve with a flow coefficient of 0.8 [6]. This valve was selected as the dump valve due to its compact 90 degree design, relatively low cost and high flow coefficient. The valve is pneumatically actuated and therefore interfaces with the same pneumatic system that supports the main valves.

High pressure stainless steel tubing was selected to connect the plumbing components in the run bay. The oxidizer feed line consists largely of 1" OD tube and was sized according to the

AIGA guidelines for safe handling of nitrous oxide [3]. Compliance with this standard helps to minimize the presence of two-phase flow in the feed lines, making the flow rates and pressures much more steady and predictable. The fuel feed line consists mostly of 0.5" OD tube and was selected due to the present availability of hardware (Tube bender, cutters, etc) for handling this size of tube. Pressure drops were calculated and verified to be acceptable at these tube sizes.

The mass flow rate of the oxidizer is controlled using choked injector orifices, further described in Section 5.1.3.1. The mass flow rate of the fuel is controlled using student researched and developed (SRAD) cavitating venturi. The cavitating venturi was sized per the calculations presented in Appendix A. A discharge coefficient of 0.83 from the team's previous experience with similar hardware in the past. An identical internal contour as what was used for previous venturis will be used, allowing for a diffuser efficiency that is consistent to the previous designs. Coldflow testing will be used to verify that the discharge coefficient matches the assumed value. Currently, the design of the cavitating venturi is in the process of being finalized and will be sent out for manufacturing in the near future. The cavitating venturi is designed to interface with a male -8 AN fitting, in a similar fashion to the design presented in Figure 5.1.2.2.2.



Figure 5.1.2.2.2: SRAD Cavitating Venturis Used for Previous Engine.

### 5.1.2.3 GROUND SUPPORT PLUMBING

The ground support plumbing supplies oxidizer and pressurant to the main propulsion system. As shown in Figure 5.1.1.1, it includes all components outside the rectangular box labeled "Rocket." This plumbing system is divided into three sections based on its specific support functions for the core propulsion system: the pressurant fill subsection, the dome pressurant fill

subsection, and the nitrous fill subsection. Each of the subsections of the GSE plumbing has been described in further detail in the proceeding sections. The GSE plumbing has been presented in Figure 5.1.2.3.1.

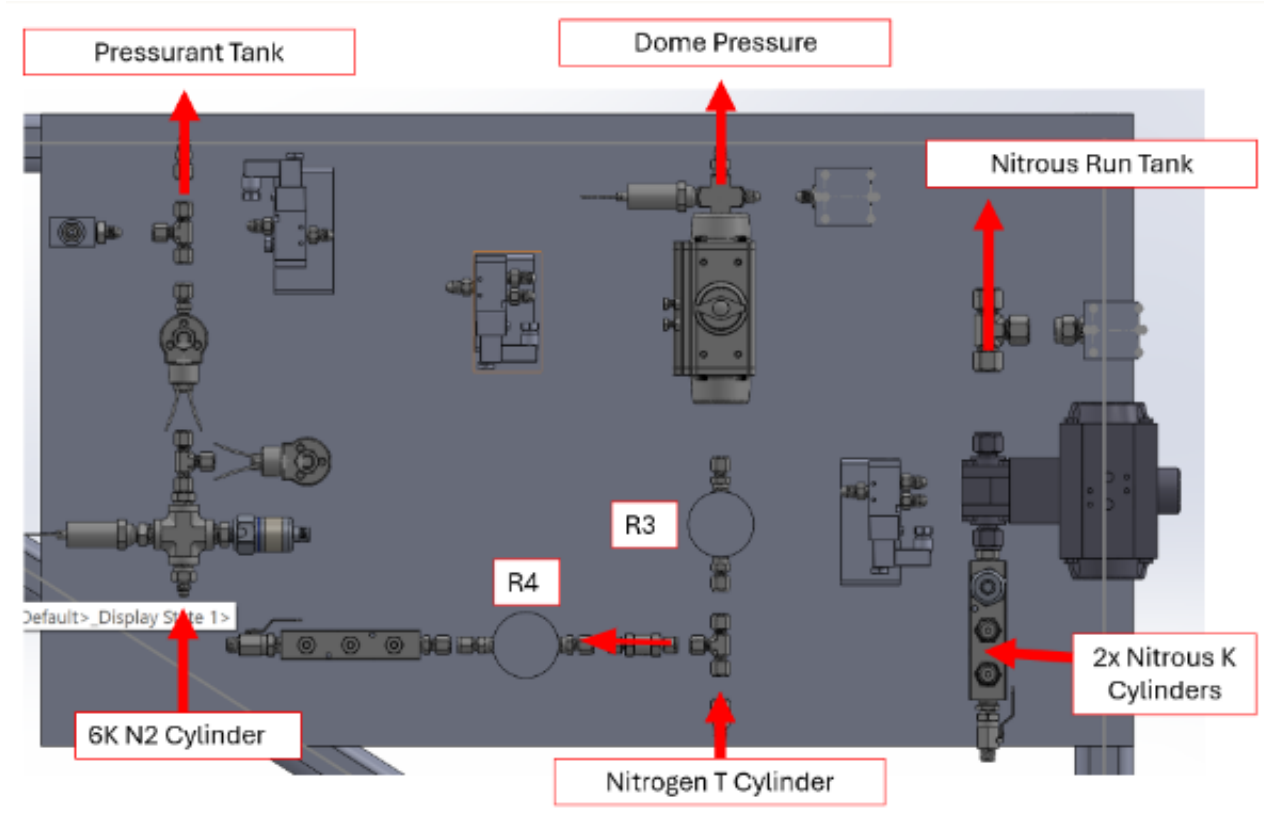


Figure 5.1.1.3.1: GSE Plumbing CAD.

As can be seen in the preceding figure, the GSE plumbing components are to be mounted on a common panel. Pneumatic pressure supply to the pneumatic valves is supplied from a tap-off from the dome pressurant supply. It is important to note that dedicated mounts for the major plumbing components are in the process of being designed and fabricated, hence their absence from Figure 5.1.1.3.1. Most of the fittings have been torqued and installed, leaving the team with some remaining work prior to upcoming testing. The current assembled state of the GSE panel of plumbing has been presented in Figure 5.1.1.3.2.

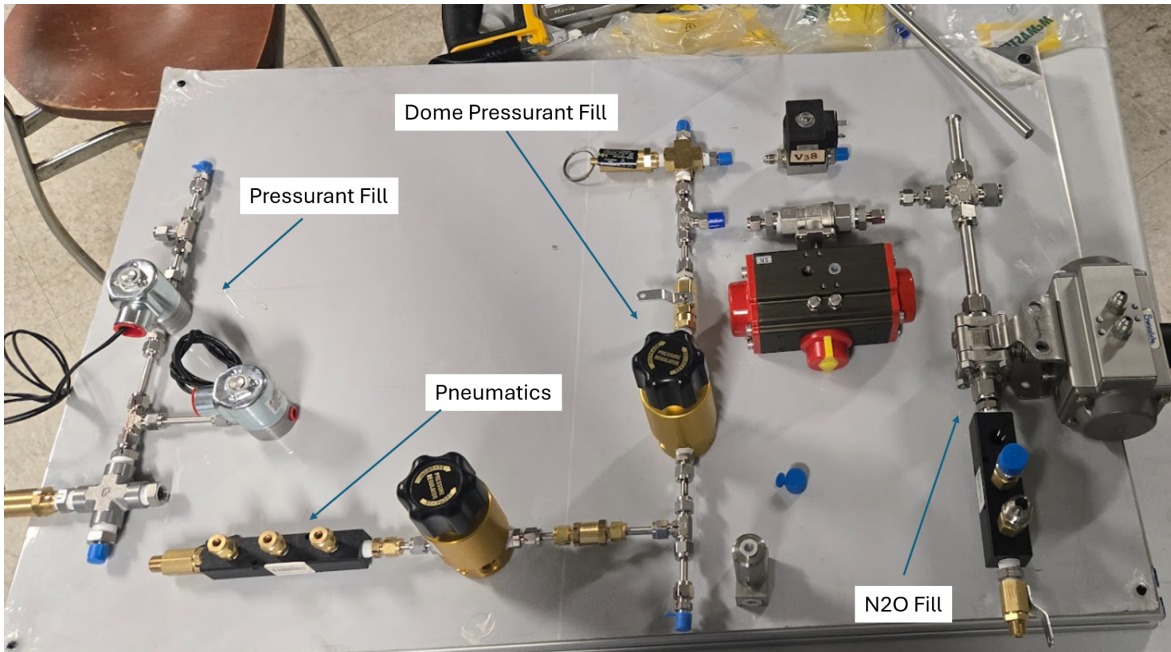


Figure 5.1.1.3.2: GSE plumbing panel in currently assembled state.

### 5.1.2.3.1: GSE PRESSURANT SUBASSEMBLY

The GSE pressurant subsystem, shown as the leftmost subassembly in Figure 5.1.1.3.1, is responsible for pressurizing the propulsion system's COPV pressurant supply. Both the control valve (V14-S) and cylinder vent valve (V15-S) were selected to be 5000 psi Normally Closed (NC) Peter Paul solenoid valves. These valves were chosen due to their high pressure rating and low cost compared to similarly-rated valves. The cylinder vent valve, V15-S, was selected to be NC to prevent uncontrolled venting of the pressurant in the event of control loss.

The vent directly downstream of V14-S was selected to be a Jaksa P2NNO pneumatic poppet valve, rated to 5801 psi. This valve was selected due to its normally open configuration, high pressure rating, and its ability to interface with the existing pneumatic pressure supply. A normally open configuration was selected for this valve as it allows the trapped volume inside the downstream flexible hose to be vented passively in the event of control loss, making it possible to approach and safe the system.

The pressurant supply regulator (R2) reduces the pressure from the 6000 psi supply cylinder to the working pressure (WP) of the pressurant tank. An Aqua Environment 1575 hand-loaded regulator was chosen for this purpose, as its inlet pressure rating of 7000 psi exceeds the supply cylinder pressure. To address challenges in sourcing valves and plumbing rated for such high

pressures, the regulator is to be tank-mounted, eliminating the need for ultra high-pressure hoses and plumbing. This design choice enhances system safety while reducing costs. A relief valve exists downstream of the regulator to prevent the system from exceeding its MEOP of 4500 psi. The relief valve set pressure is 4000 psi and has an airflow capacity of 820 SCFM per the supplier. It is important to note that this is significantly higher than the expected flow rates at any point in the operation of the panel due to the strict upper limit on the volumetric flow rate to the COPV.

#### **5.1.2.3.2: DOME PRESSURANT FILL & PNEUMATICS SUBASSEMBLY**

The dome pressurant fill and pneumatics subassembly is responsible for supplying pneumatic pressure to all required valves and delivering regulated pressure to the dome port of R1 through the loader valve. This sub assembly includes two valves: the dome pressure control valve (V13-MB) and the supply line vent valve (V18-S). The dome pressure control valve was chosen to be a manual ball valve to provide direct manual control of the pressurant flow to the dome port. Although a remotely controlled valve was an option, it was determined that all dome pressurization operations would be performed manually due to the use of a conventional hand-loaded regulator, offering minimal to no additional safety benefit from a remotely actuated valve. The supply vent line utilizes a Jaksa D22NNO normally open solenoid valve, which enables passive venting of isolated pressure within the flexible hose in the event of control loss.

The dome regulator loader valve (R3) was selected as an Aqua Environment 415 series regulator. This regulator features a 6000 psi inlet pressure rating, well above the supply bottle pressure of 2600 psi. Its outlet pressure range is 0-1500 psi, with an expected operating outlet pressure of 900 psi, positioned near the midpoint of the regulator's outlet pressure range. Coldflow testing will be required to characterize the difference between the dome pressure and the corresponding R1 outlet pressure, however, it is unexpected for this difference to be greater than 100 psi per anecdotal evidence collected from other amateur rocketry teams. The use of an on-ground loader valve allows for the dome regulator set pressure to be changed while the propulsion system is in its vertical position, making the resulting operations significantly easier relative to other configurations that were considered. A relief valve (RV2) with a set pressure of 1500 psi was connected to the plumbing downstream of the loader valve. This relief valve limits the dome supply pressure to below 1500 psi, ensuring that gross exceedances of the ethanol tank's working pressure cannot occur due to accidental movement of the loader valve handle.

A purge valve (VP1-SB) was added between the dome and nitrous fill subassemblies to supply pressurant to the oxidizer feed lines via the nitrous fill port. This valve is intended to be opened

during the engine's shutdown sequence during on-ground static testing. Since this valve connects to plumbing designed to hold liquid nitrous during pre-fire filling operations, the procedure will include steps to thoroughly vent the common volume before the hotfire test. This ensures that nitrogen is supplied through the fill port and into the oxidizer feed lines during shutdown rather than a mixture of liquid nitrous and gaseous nitrogen. Sequencing will be refined during coldflow testing to ensure that risks related to adiabatic compression of the nitrous will be sufficiently mitigated. It is important to note that this purging configuration was selected as it dramatically reduced the complexity and cost of the oxidizer feed lines. Following the selection of this configuration it was observed that a similar practice is used on similar nitrous liquid engines [7].

#### **5.1.2.3.3: NITROUS FILL SUBASSEMBLY**

The nitrous fill subassembly is responsible for providing the means to remotely fill the nitrous run tank via the GSE. The nitrous fill subassembly contains a common manifold that connects to two nitrous K cylinders. This manifold interfaces with the flex hoses that carry the fluid via two -8 AN fittings. The nitrous fill valve (V34-SB) is located downstream of the manifold and is responsible for controlling the flow of propellant to the feed system. The valve was selected to be a Swagelok 63 series ball valve with an upstream vent. This valve was chosen due to its availability in the workshop from previous tests involving nitrous oxide. The upstream vent is required to be compliant with AIGA guidelines for safe handling of nitrous oxide [3]. A pneumatic actuator is responsible for opening and closing this valve, allowing for remote actuation from mission control. A normally open vent (V36-S) is connected to the plumbing downstream of the fill valve, allowing the isolated section of plumbing between the feed system and fill valve to be passively vented in the event of control loss.

#### **5.1.3 THRUST CHAMBER**

The objective of the thrust chamber for the bi-propellant liquid rocket engine (nitrous oxide and ethanol) is to sustain combustion of the fuel and oxidizer. The design of this system includes an ablative cooled combustion chamber, and a graphite insert around the nozzle throat section. This design is effective because the liner provides sufficient ablative cooling to the hot gasses caused by combustion. The graphite insert can withstand any deformation to ensure consistent performance through burn duration.

The engine system needs to be able to have a specific envelope to be used inside of a flight ready rocket, and the engine needs to be able to create the desired performance. The expectations of the desired performance can be seen in Table 1. This table outlines the internal

dimensions of the engine system required to create the desired performance characteristics. Not shown in the table is the dimensions of the envelope, which has a diameter of 7.5". This packing constraint outlined the dimension characteristics while Table 5.1.1 outlined the desired performance characteristics.

The particular parts of the project include the graphite insert, combustion chamber liner, chamber wall and retaining ring. Starting with the chamber liner, the inner diameter was determined from the Interface Control Document. This was 5.26" while the length of the chamber from the injector to the throat was to be 12.4". The contour of the nozzle section was determined from Basic Simulation and Optimization of Liquid Rocket Engines as shown in Figure 3 [8]. Along with this diagram and information a formula for nozzle length was established. The length of the nozzle was determined to be 2.77 and such calculations are found in the Appendix E [8]. The graphite insert geometry was determined from Solid Rocket Motor Nozzles [9]. A graphite insert is machined to have the desired performance characteristics inside of the engine assembly.

This philosophy was applied to the Chimera Bi-prpellant engine where a graphite insert cylinder can be inserted before a combustion chamber liner is set. Due to the load created by the exhaust gasses on the chamber liner and throat, a retaining ring was placed at the end of the liner. The purpose of this is to hold the contents in place due to compression at the retainer. This design approach was determined after a hot fire test in Pefferlaw, ON. During this test a test article graphite insert was fired on a rocket engine, and due to shear forces the nozzle broke at the throat. This determined that the approach for Chimera should have the load supported by compression. The chamber wall geometry was generated by encapsulating the system in 2/5" T6 6061 aluminum. Aluminum is the desired choice for Chimera as T6 6061 aluminum is a lightweight alloy which is optimal for flight applications. Although the material lacks in strength properties at high temperatures, the use of a chamber liner aids to alleviates concerns of any deformation in the chamber wall. Throughout development, different solutions were conceptualized to solve the problems of shear in the graphite insert, and the graphite insert geometry itself was a point of contention. Most notably, this design lacks the feature of a retaining ring and graphite at the throat. A pin was originally placed at the bottom to create a compression force from the liner. The team moved away from this approach as the pin is small in size and is not as effective as the retaining ring in supporting against the forces. In addition, the geometry of the liner was changed to the new approach because it was determined that hot gasses would persist after the throat. Since the purpose of the insert is to avoid thermal degradation the insert must be extended. The length of the extended portion was determined from Testing and CFD Simulation of Diaphragm Hybrid Rocket Motors, where a simulation of heat inside a rocket nozzle gave the team a visualization to build the geometry around. Overall

these were some challenges faced in development of the Chimera graphite insert and liner geometry.

### 5.1.3.1 INJECTOR

A like-like doublet injector was selected for Chimera, based on the success of the design in MACH's previous engine, GAR-E. A functional decomposition diagram of the injector is presented in Figure 5.1.3.1.1 with the major design considerations included.

Manifolding is accomplished similarly to the LR101 vernier engine, with an oxidizer dome and a fuel ring manifold. This was selected to allow for the adoption of a regeneratively-cooled chamber later down the line; fuel passages can easily feed directly into the ring manifold. For this ablative engine, the fuel inlet is a brazed fitting tangent to the ring manifold.

A central 1-5/16" ORB fitting was selected for the oxidizer inlet, mirroring the oxidizer tank outlet. A tangential fuel inlet was selected to induce a swirl in the ring manifold. Brazing the fuel inlet was selected in order to keep the inlet dimensions small and avoid a large inlet flange. Threading the engine case itself was not feasible without increasing manifold wall thickness, and as a result, the required stock size for milling beyond 7.5". Figure 5.1.3.1.2 presents a cross-section of the injector assembly.

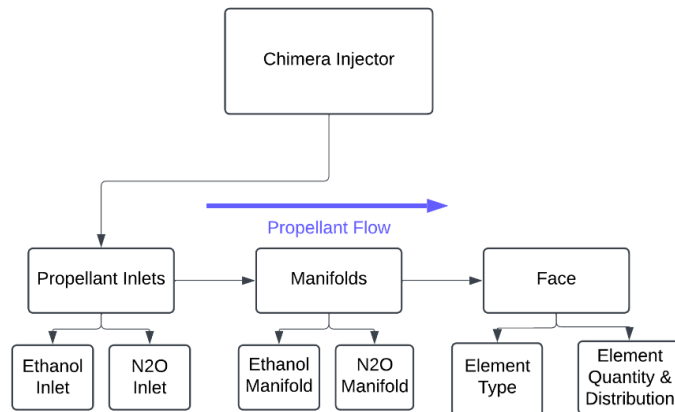


Figure 5.1.3.1.1: Broad functional decomposition of the injector with major considerations.

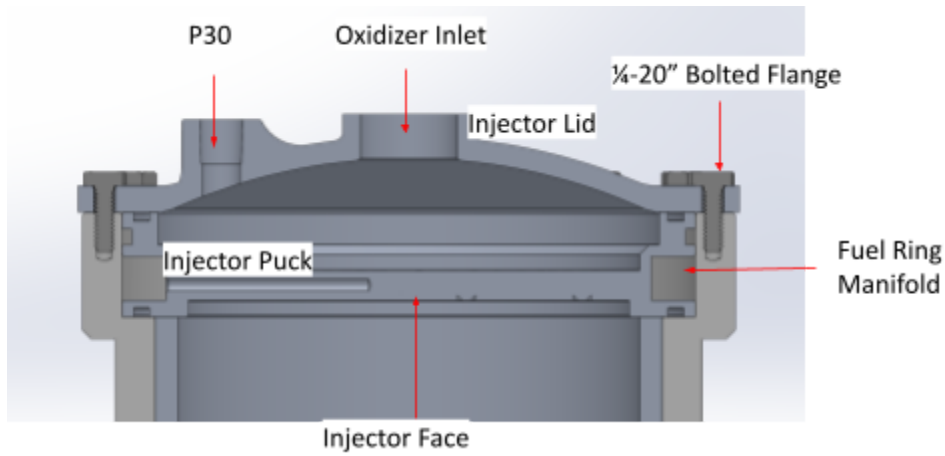


Figure 5.1.3.1.2: Cross-section of injector geometry.

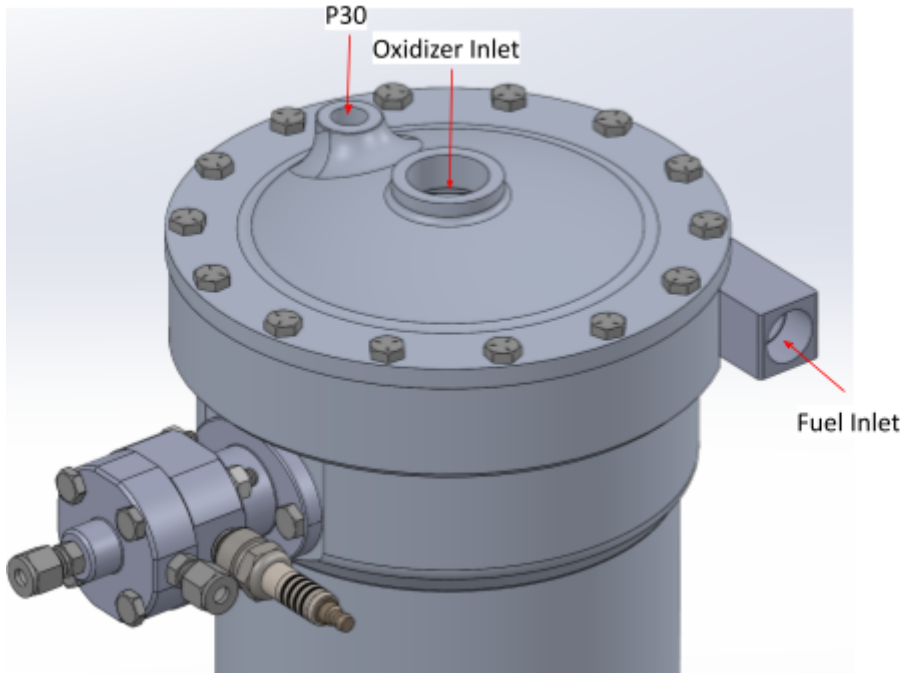


Figure 5.1.3.1.3: External view of the injector assembly.

Sealing is accomplished by three silicone o-rings on the injector puck. Additionally, RTV (room temperature vulcanizing) silicone sealant is used as the primary seal between the ablative chamber liner and the injector puck.

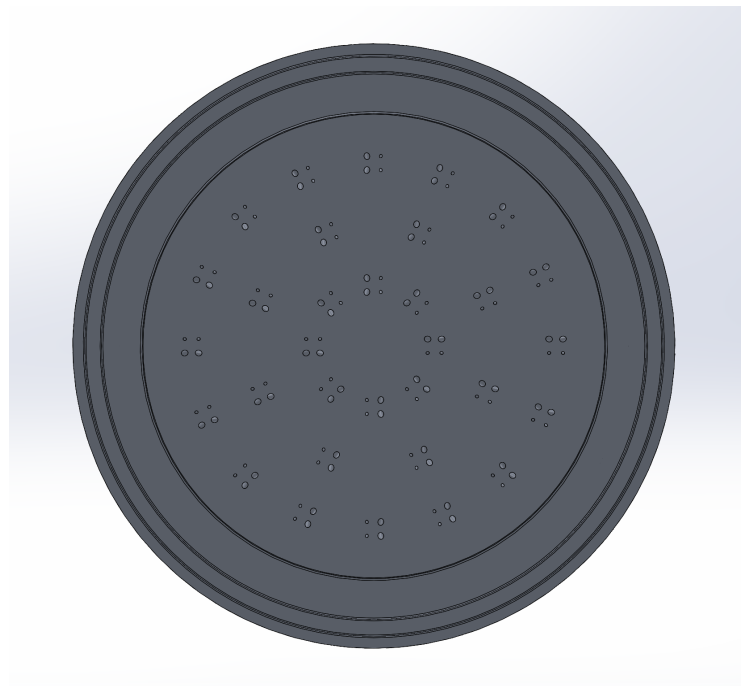


Figure 5.1.3.1.4: View of the injector face.

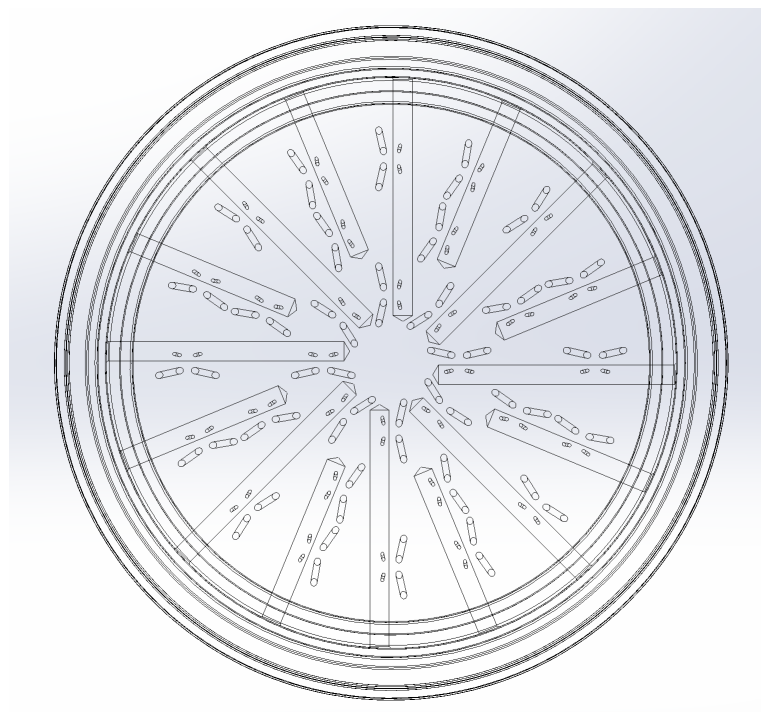


Figure 5.1.3.1.5: Wireframe view of the injector face, showing fuel feed passages.

The fundamental unit of the injector face is a like-like doublet element. The dimensions of this element were directly borrowed from GAR-E, and originally taken from Falk [10]. A close-up of the element is shown in Figure 5.1.3.1.6. Each oxidizer orifice is  $1/16''$  diameter; each fuel orifice is  $1/32''$  diameter. Total element count was then found using the total orifice area in conjunction with the nitrous model.

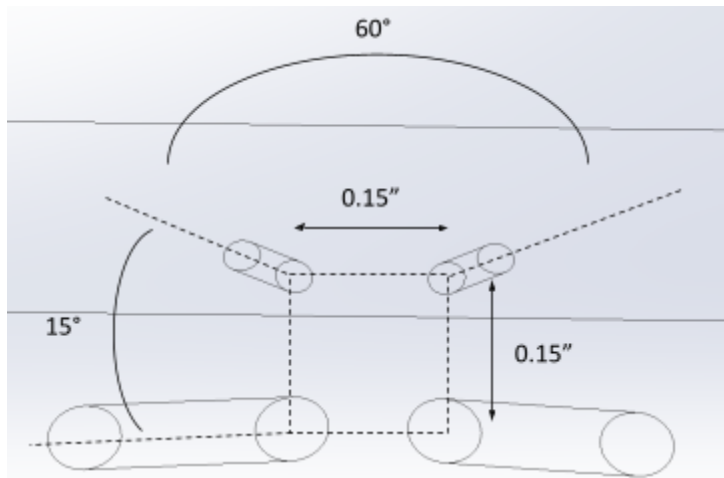


Figure 5.1.3.1.6: Close-up of element geometry.

A series of 16 radial fuel lines feed each fuel orifice. Manifolding the face geometry took careful planning of the fuel feed lines to avoid the oxidizer orifices.

### 5.1.3.2.1 INJECTOR STRESS ANALYSIS

The oxidizer dome was initially sized using hand calculations in accordance with the ASME 2023 Boiler and Pressure Vessel Code [11]. This gave preliminary dimensions for the head and flange thickness. These calculations are provided in Appendix A. In summary, a head thickness of  $0.25''$  and a flange thickness of  $0.67''$  were found to provide a FOS of 2 over the MEOP of 1030 psi, to comply with the Launch Canada Rules & Requirements Guide.

The failure mode of the bolted flange was deemed to be bolt failure rather than thread tearout, as the thread engagement length was made purposefully long - 2 x the nominal bolt

diameter, or 0.5 in - in accordance with machining rules of thumb for aluminum. Initial bolt count was selected by performing normal stress calculations on the dome. Taking the total force on the bolts as the product of pressure and inside dome area normal to the flange, and using a 2 x FOS over MEOP, it was found that 14 bolts are required to retain the flange. Rule of thumb calculations for the bolt load  $W_{m1}$  differed from the basic normal force calculation by 6%. These calculations are also provided in Appendix D.

Stress analysis will soon be performed in ANSYS at MEOP and 2 x MEOP with varying flange thicknesses, as a 0.67" flange thickness appeared overly large and presented integration issues with the rest of the engine assembly. The team recognizes the limitations of handbook calculations and plans to run several FEA simulations to confirm that the assembly will behave as expected.

#### **5.1.3.2 SRAD ABLATIVE LINER**

An SRAD ablative mixture is being developed for deep pours of the chamber lining. The goal of this project is to develop a pourable ablative liner with an ablation rate below 0.020"/s (comparable to Half Cat's CHAMBERSAFE). A two-part mandril, joined at the throat and enclosing the graphite insert, will be used to produce the engine geometry.

Testing is being carried out in several phases. Each phase involves pouring dog-bone samples of each mixture, conducting tensile tests of the material, and finally conducting comparative ablation testing with an oxy-acetylene torch of the broken tensile testing samples. Tensile testing allows for some stress calculations to be carried out on the engine liner later on in the design process. Ablation rate will be calculated by piercing the resulting char layer and measuring the final thickness of the virgin material using a micrometer with a cone attachment.

The first phase of testing compares additions of single additives to a base epoxy/hardener mixture, to characterize the effect of each additive. West Systems 105 & 205 were selected as they were on hand, though consideration will be given to more affordable products. Later phases will include mixtures of several additives, and cease when a mixture shows an ablative rate equal to or slower than CHAMBERSAFE, while still being pourable.

To date, 19 mixtures of West Systems 105 Epoxy & 205 Hardener and varying levels of single additives have been tested for tensile strength, with the first round of ablative testing planned for one week from the date of writing.

The total list of additives and mixture ratios to-date is presented in Table (5.1.3.2.1)

Table 5.1.3.2.1: Ablative Mixtures To Date

Additive	% By Weight
3M Glass Microballoons	5 10 15 20
Alumina Powder	5 10 15 20 30 40 50
1/32" Milled Glass Fiber	5 10 15 20
Sodium Bicarbonate	5 10 15 20

3M glass microballoons were initially selected as they were on hand and provide a source of silica, which has been shown to improve the performance of ablative mixtures through the production of a film of liquid silica on the surface of the char layer [12]. However, glass microballoons severely thickened the matrix and proved extremely difficult to pour. 1/32"

milled glass fiber also provided a source of silica, while being easy to pour and contributing somewhat to the tensile strength in low quantities.

Alumina powder was selected for its high heat resistance and its potential to strengthen the epoxy matrix. Baking soda was selected as a source of transpiration cooling; water vapour and carbon dioxide have been shown to produce a film of vapour at the char layer [13]. Figure 5.1.3.2.1 shows the results of tensile testing to date. Many more tests are required to ensure that the liner performs as expected.

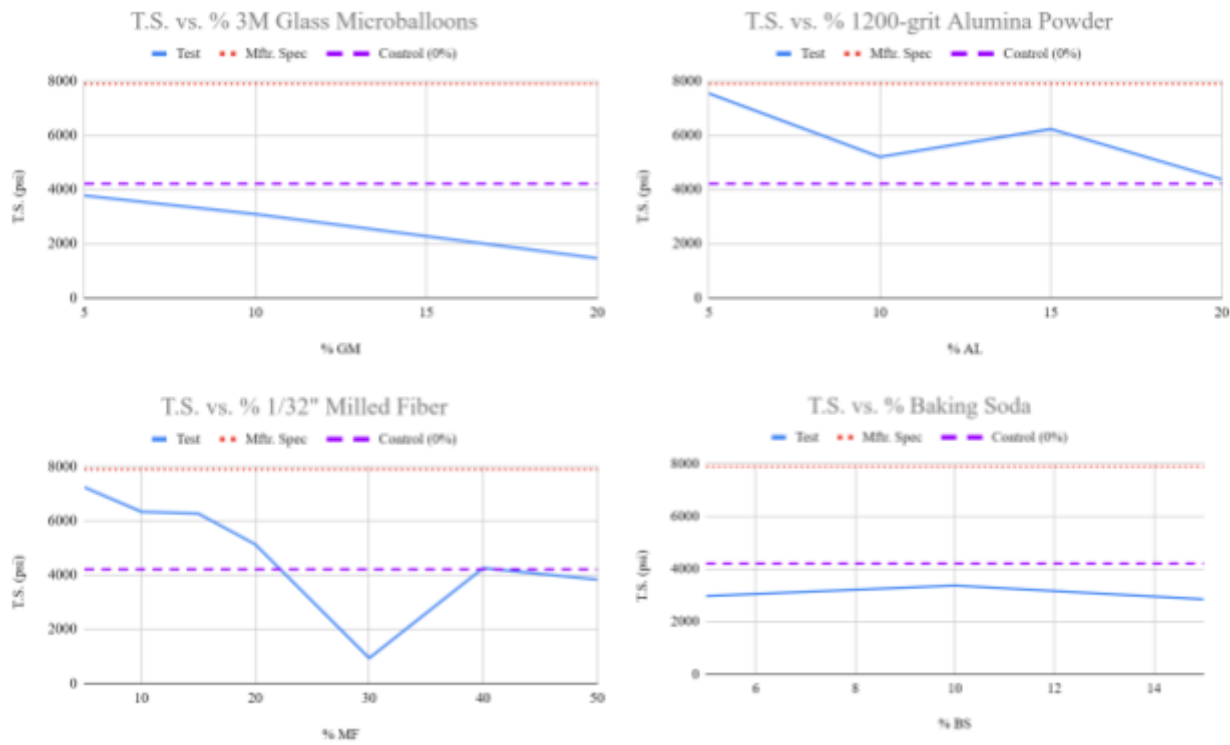


Figure 5.1.3.2.1: Ablative Mixtures To Date



Figure 5.1.3.2.2: Sample undergoing tensile testing ahead of ablative testing.

### 5.1.3.3 IGNITION

MACH has successfully achieved ignition in past designs with a casted puck ignitor, a combination of potassium nitrate and epoxy. The current plan is to use this casted pack for ignition at the Launch Canada 2025 competition. However, it is important to note that a torch igniter is currently in development. If the technology readiness level has increased to a sufficient degree, the team may attempt to use the torch igniter for the hotfire test at the competition. **However, the team does not intend to use the torch ignitor at the competition and presently wishes to be graded as such.**



Figure 5.1.3.3.1: Puck igniter used in MACH's first successful hot fire

After the fuel and oxidizer have travelled into the injector they at a certain point downstream of the injector plate in order to adequately mix for combustion (impingement). The impingement process is a significant step in order to achieve combustion, as inadequate impingement may lead to incomplete combustion, and in some cases no combustion at all. This impingement design has successfully achieved combustion in a September 2024 test in Pefferlaw, ON and also at Launch Canada 2024 in Timmins, ON.

The orifice geometry also aids in atomization of the flow of propellant. Atomization is when the liquid breaks apart into droplets due to the shear forces and expansion of the high velocity stream of flow. With the propellant broken up into droplets, the contact area inside of this spritz increases. With more surface area, the fuel and oxidizer spritz can achieve a more efficient mix which aids in achieving combustion. This atomized flow reaches the impingement point (fuel and oxidizer make contact) at 1.15" downstream of the injector plate. Giving adequate time for the propellant to mix, the fuel interacts with the flame of the torch igniter at 1.5" downstream.

The torch igniter burns hotter than 3000°K, therefore it is capable of decomposition of the oxidizer (nitrous oxide) and capable of achieving combustion of the fuels. The decomposition of the nitrous oxide is crucial to achieving combustion in the chimera chamber, as the oxygen is bonded to the nitrogen atoms in the nitrous oxide molecule. In order for the oxygen to interact with the ethanol, it must be separated from the nitrogen in the nitrous oxide. The torch igniter

achieves this and additionally inputs the required energy needed for combustion to occur in the thrust chamber.

#### 5.1.4 TORCH IGNITER

The propellant system of the torch igniter will re-use as many of the existing components from spender as possible (previous team propellant system). It will be integrated into the existing Day-Glo propellant feed system to route ethanol and nitrous oxide to the torch igniter. The ethanol line will be connected to the main fill valve on the Day-Glo system, utilizing its tank and pressurant system. The nitrous system will connect upstream of the fill valve, directly to the bottle. This will allow vapour-phase nitrous to be utilized. A schematic for the propellant system of the torch igniter is shown below. The torch orifice diameter is 0.01" for the fuel, as the fuel flow rate is significantly small. Despite the low Cv of the torch system, the propellant flow rates are substantially low given the orifice geometry that a low Cv should not cause implications with the design, and furthermore  $\frac{1}{4}$ " check valves are placed right before the injector to prevent backflow.

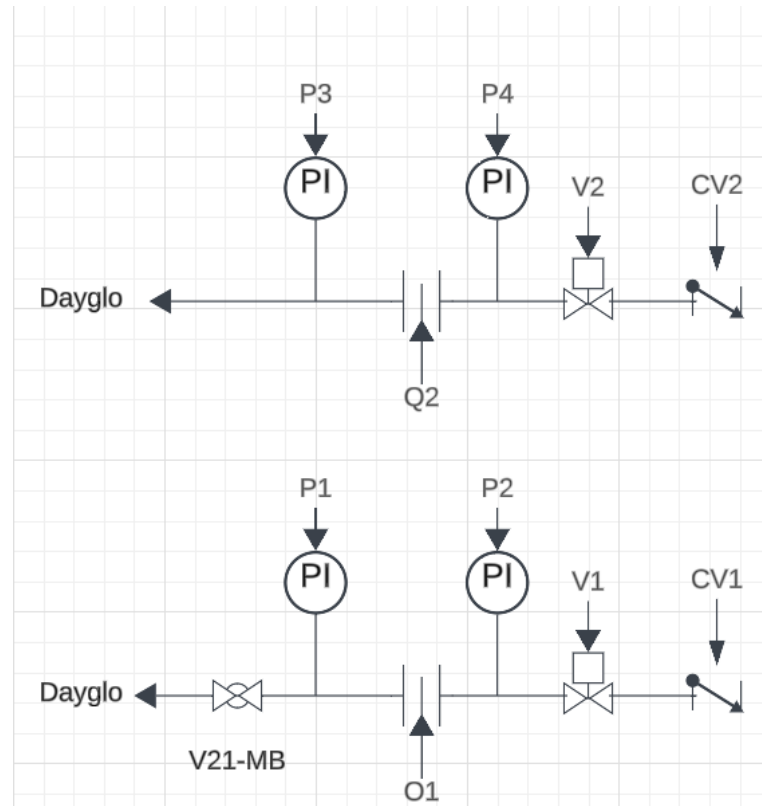


Figure 5.1.4.1 Preliminary P&ID.

Table 5.1.4.1: Propellant System BOM

P&ID Label	Description	Component
P1	Pressure transducer	
O1	1/4" orifice	<a href="#">2275N39</a>
P2	Pressure transducer	
V1	1/4" NC solenoid	<a href="#">1190N24</a>
CV1	1/4" check valve	<a href="#">45385K54</a>
P3	Pressure transducer	
O2	1/4" orifice	<a href="#">2275N39</a>
V2	1/4" NC solenoid	<a href="#">1190N24</a>
CV2	1/4" check valve	<a href="#">45385K54</a>
T	1/4" Tee	<a href="#">5182K434</a>
Nozzle	Oil furnace nozzle	<a href="#">3178K61</a>

A general layout of the system is shown below. It will be assembled on a piece of acrylic, roughly 50 cm by 20cm. This makes the system easily transportable which is crucial for ground testing in preparation of an isolated test. For testing, it can be attached to the current thrust stand, making it easy to incorporate to current test procedures.

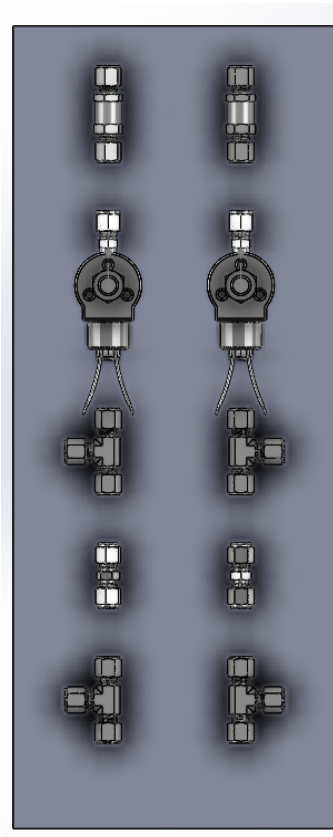


Figure 5.1.4.2: Propellant System Layout.

#### 5.1.4.1 TORCH INJECTOR

The torch injector is a single piece design, reducing both manufacturing complexity as well as the number of seals. The design of the torch injector is shown below. Figure 5.1.4.5 presents a cross section of the tapped orifice holes for the fuel. Oxidizer inlets are placed on either side of the central fuel inlet. NPT threads are used throughout for ease of assembly.

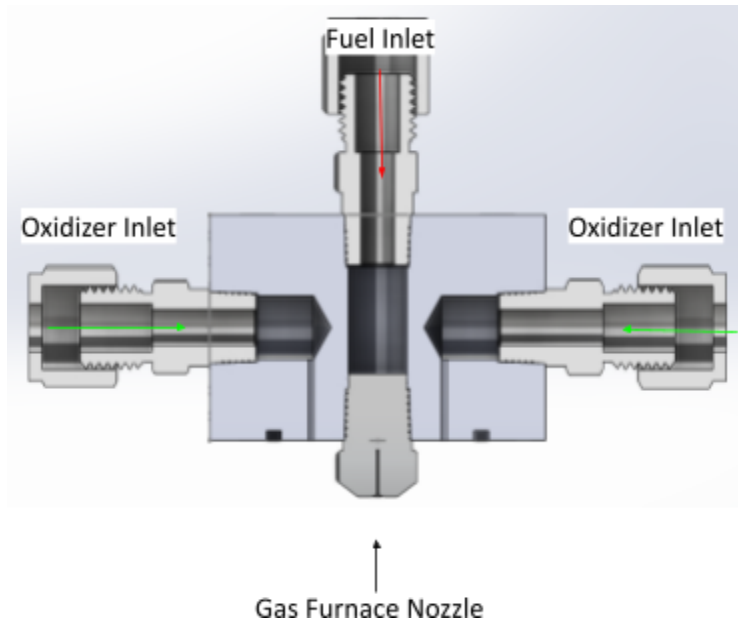


Figure 5.1.4.1.1: Torch injector section view.



Figure 5.1.4.1.2: Torch injector side view.

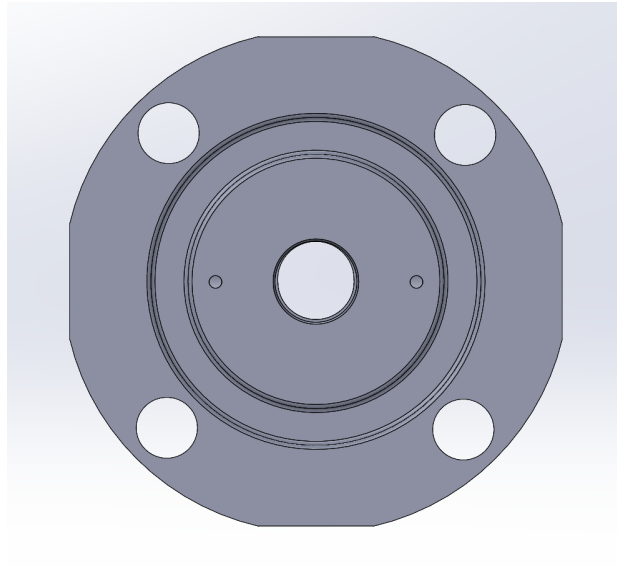


Figure 5.1.4.5: Torch injector face view.

The nozzle is a commercially available oil furnace nozzle. A solid-cone, 1.35 GPH, 70 deg nozzle was selected. A -216 silicone o-ring seals the torch igniter flange.

#### 5.1.4.2 TORCH COMBUSTION CHAMBER

In order to size the combustion chamber the team had to create a few assumptions such as the main chamber pressure. The torch chamber is set as  $1.2 * \text{Main chamber pressure}$ , to ensure no backflow upon main chamber ignition. This is because if the torch chamber was lower than the main chamber pressure, there would be a flow of pressure leading into the torch. The injector chamber pressure with this correction is 504 psi. The next is the mass flow rate and mixture ratio. The mixture ratio is kept the same as the main chamber. The mass flow rate was selected to be in line with those of other torch igniters used in similar systems, which is around 5 g/s.

The injector and the torch chamber are going to be machined separately. The torch igniter can be utilized as a heat sink if manufactured out of stainless steel. This is because stainless steel has a high melting point of 1800 and a high specific heat capacity. This means that a stainless steel torch can absorb a large quantity of energy before being damaged.

The torch injector will attach via bolts and make a seal via a  $\frac{1}{8}$  in thick o-ring. This design

incorporates a flat face machined to easily tap a space for the spark plug and it also has an open bolt section under the injector and torch tip plate which allows for attaching a nut and a washer. The torch chamber is also mated to the main chamber in a similar manner to the torch injector. In order to mate the torch igniter to the main chamber a bolt and flange was devised. A circular flange allows an attachment to the main chamber with large surface area on a flat face, and ensures that an RTV silicone seal can be achieved easier.

Moving on to the spark plug, the plug itself avoids the melting and damage of the system as it is only penetrating its spark gap electrode. Furthermore, the spark plug is also situated downstream from the injector face by  $\frac{1}{2}$ ". This allows the system to keep more heat away from the top of the chamber. Avoiding heat in the torch injector is important as it can cause the O-ring to become heated which can create deformation in the seal. The O-ring chosen is from The Parker Handbook [14] it's a  $\frac{1}{8}$  inch cross sectional thickness ring and its size is Parker Size No. 217.

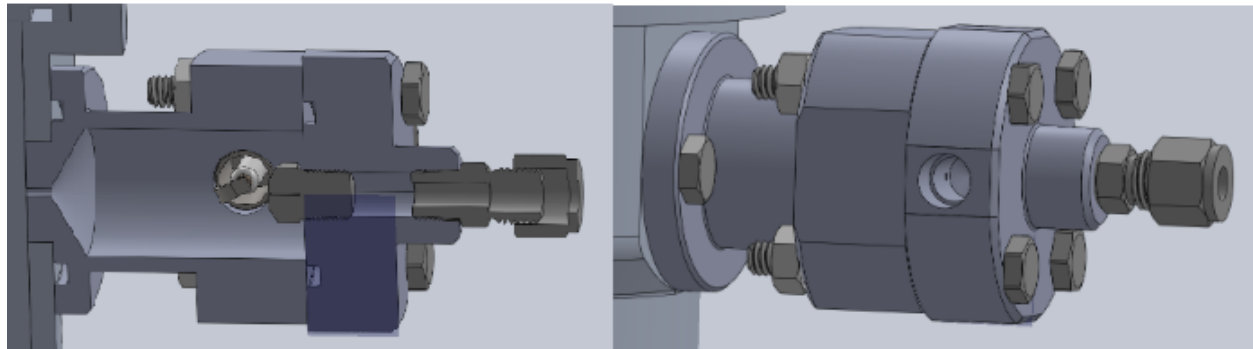


Figure 5.1.4.6: Full assembly of torch ignitor.

### 5.1.5 THRUST VECTOR CONTROL

Thrust vector control (TVC) is the action of controlling a rocket's thrust direction to orient its yaw and pitch axis. The purpose of TVC for MACH's case is to have a gimballed static test fire for the technology development category at Launch Canada 2025. The engine will be mounted to a gimbal, allowing it to rotate independently on the rocket. The final design MACH chose was using linear actuators connected to the gimbal and engine, allowing for accurate, controlled movement of the engine. Sections below will go more in depth on the gimbal and actuators

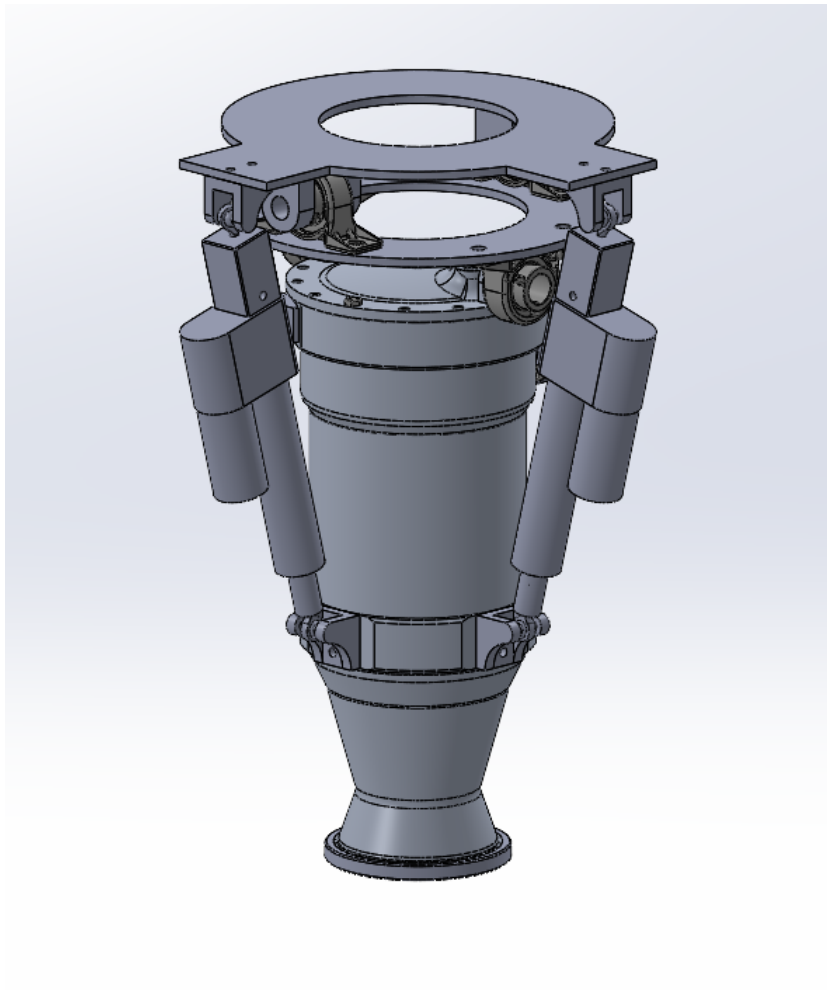


Figure 5.1.5.1 CAD of the TVC system on the engine

The TVC system, shown in Figure 5.1.4.1, will use linear actuators to control the rocket's thrust direction to orient its yaw and pitch axis. A gimbal mount will be attached to the top of the engine, allowing the engine to move independently from the rocket. This gimbal will allow the large 1-inch nitrous lines to remain in the rocket's center, which must be done due to their small bending radius. The linear actuators are connected to the gimbal and engine through ball and pin joints, respectively, allowing the engine to have proper degrees of freedom.

The TVC system is engineered to accommodate a peak thrust of 1650 lbf with a gimbaling range of 10 degrees. It utilizes two linear actuators positioned 90 degrees apart, integrated with a custom SRAD gimbaling mechanism that is unprecedented at this scale in amateur rocketry. Key design considerations included actuator performance, gimbal architecture, attachment point optimization, and dynamic movement capabilities.

### **5.1.5.1 LINEAR ACTUATORS**

The strengths of the linear actuators were determined through simplification, with the 3D dynamic model reduced to a 2D static model for ease of analysis. Following the guidelines in “Considerations for Thrust Vector Control in Load Predictions” [15], the gimbal force was estimated to be approximately 50 lbf. This value accounts for the engine's inertial and gravitational forces. While these estimates provide a baseline, they will require refinement once the full CAD assembly is completed. The relevant calculations have been added in the appendix. Additionally, the stroke length needed to achieve a gimbal range of  $\pm 10$  degrees is relatively short—minimum 3-4 inches— actuator selection will be finalized after completing the CAD model. The current recommendation for the actuator is the Pololu glide force 25 kgf, 6” stroke length for the fastest actuation speed. The actuator base is located as far as feasibly possible from the pivot point and the actuator head is located at the converging section of the rocket engine to maximize leverage and reduce needed actuation force. The Actuators will also be tested pre-hotfire to verify theoretical values.

Custom parts for the actuator will be manufactured, for easy and proper connection to the entire assembly. The actuator is manufactured with a pin connection in mind, on both sides of the actuator; However, a ball joint is to be used, which uses a  $\frac{1}{4}$ ” - 28 male thread. To allow threads to be used instead of pin connection, two custom parts are to be made. The first part is the custom coupler, labeled in Figure 5.1.5.2. This coupler slips over the square joint at the end of the actuator, and has a pin to secure it in place. The other side of the coupler has a female thread, for the ball joint to screw into. The second custom part, labeled in Figure 5.1.5.2, is the actuator arm. The new actuator arm will be slightly longer, allowing for threads to be tapped into the end of it. The original actuator arm uses a pin joint, as well as having internal threads for movement taking up most of the internal section of the arm. Due to such reasons, the new arm will be longer, giving space for threads to be tapped into the end, allowing the ball joint to be connected.

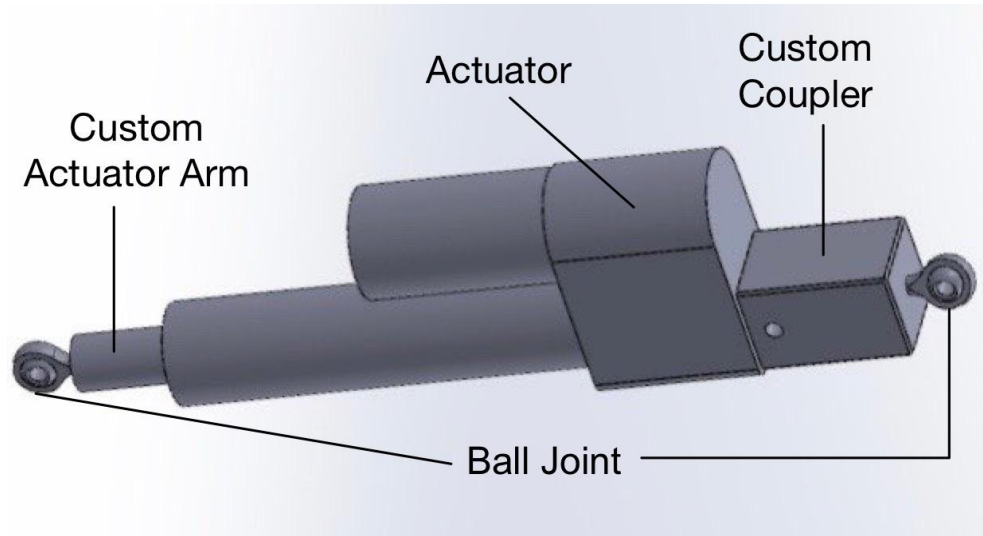


Figure 5.1.5.2 Linear Actuator used in TVC

### 5.1.5.2 GIMBAL

The current gimbal ring design, shown in Figure 5.2.4.2, accommodates a nitrous oxide feedline routed through the center of the combustion chamber. This approach deviates from the traditional axial propellant feed system, which typically allows for a ball joint pivot as the bearing mechanism. However, this design offers distinct advantages, including reduced actuator loads due to fewer inertial forces acting on the system.

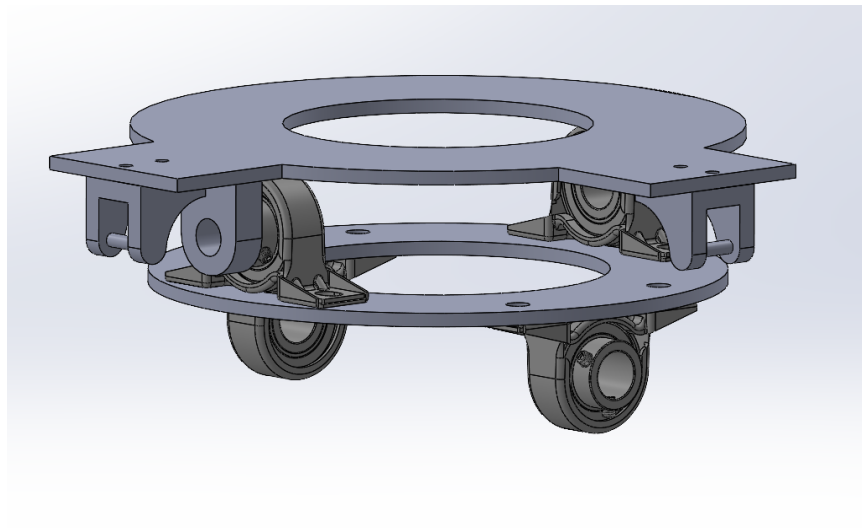


Figure 5.1.5.3 CAD of the engine gimbal

The gimbal ring consists of 4 bearings, 2 of each begin set 90 degrees apart. This gives 2 degrees of rotation to the engine, allowing it to rotate independently to the rocket. The middle plate of the gimbal is a simple disk with 8 holes used to bolt in the bearings. The top

plate is similar however it includes blocks to connect the bearings to it using pins, as well as extenders allowing the actuators to be connected to the rocket at a distance of 4 inches.

The structural integrity of the system is still being evaluated via FEM. Some preliminary concerns have been raised from the high deformation and stress on the first gimbaling platform. The first platform may have to be made from steel depending on future evaluations of the deformation and stress.

## **5.2 TELEMETRY & CONTROL SUBTEAM**

### **5.2.1 HARDWARE**

The telemetry & control hardware is based around the Labjack T7. This is a data acquisition device (DAQ), that will be used to collect sensor data and control valve actuation. It will be connected and powered via USB to an ASUS NUC 13 Rugged, which is a small form factor computer that will be mounted in the ground support equipment (GSE) electronics enclosure.

Pressure transducers and thermocouples are directly connected to the analog inputs on the Labjack, while the output from load cells are first sent to a load cell amplifier to be conditioned before they are sent to the labjack.

The solenoid valves are actuated using custom control boards with surface-mount technology (SMT) solid state relays (SSR). The SSRs are controlled by the digital pins on the Labjack and switch the 24V power that actuates the solenoids on and off. To prevent inductive voltage spikes when the solenoids are turned off, the control boards have flyback diodes on each of the SSR outputs. Easily replaceable glass fuses are also used in series with the outputs of the control boards to prevent damage in the case of a short.

To house and connect the GSE electronics, a 610x610x150mm IP66 rated steel enclosure will be used with a DIN rail system inside. The DIN rail is a standardized mounting system for electronics and terminal blocks, which we will use to make cable management and any future changes to the hardware setup easier, while also providing more secure connections.

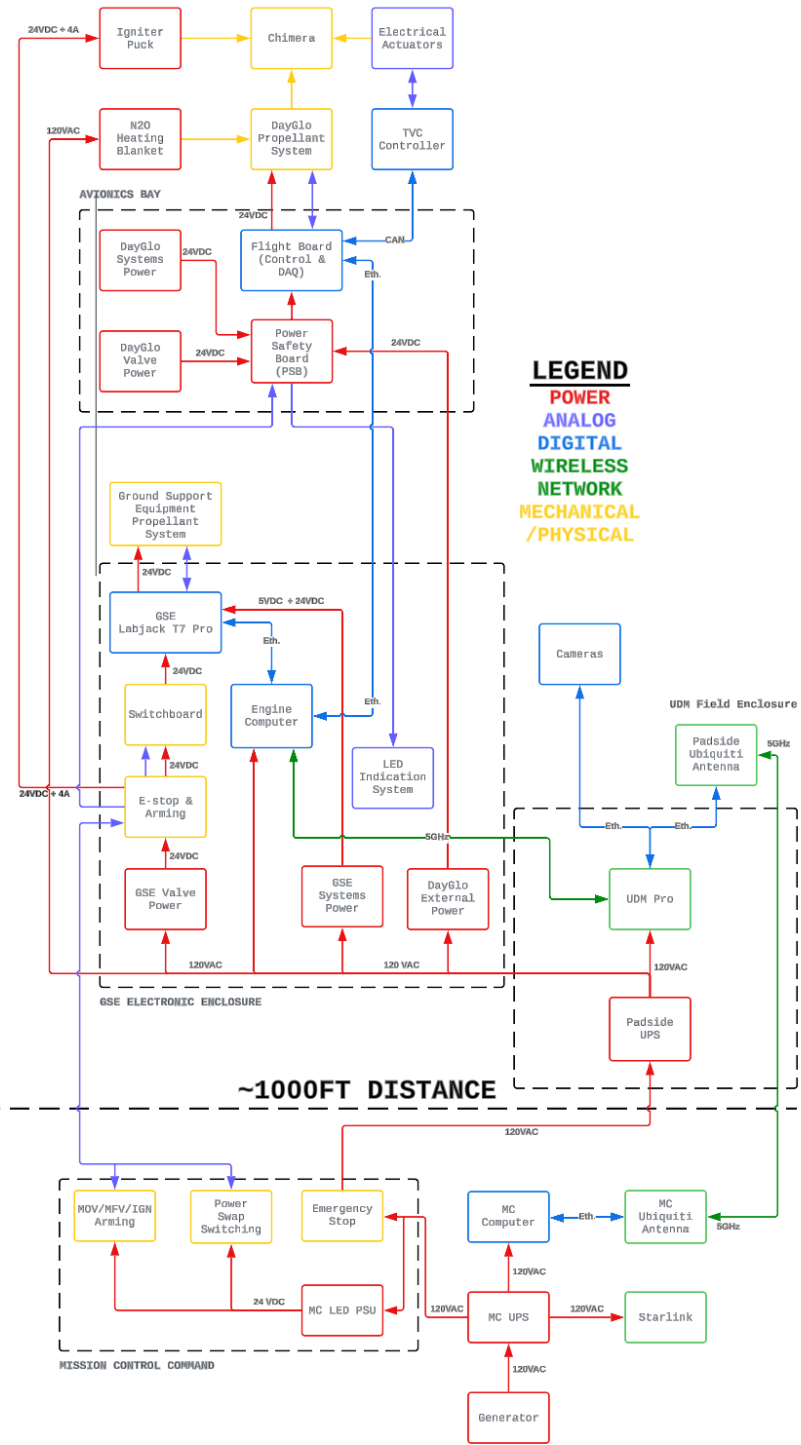


Figure 5.2.1.1 Overall System Architecture

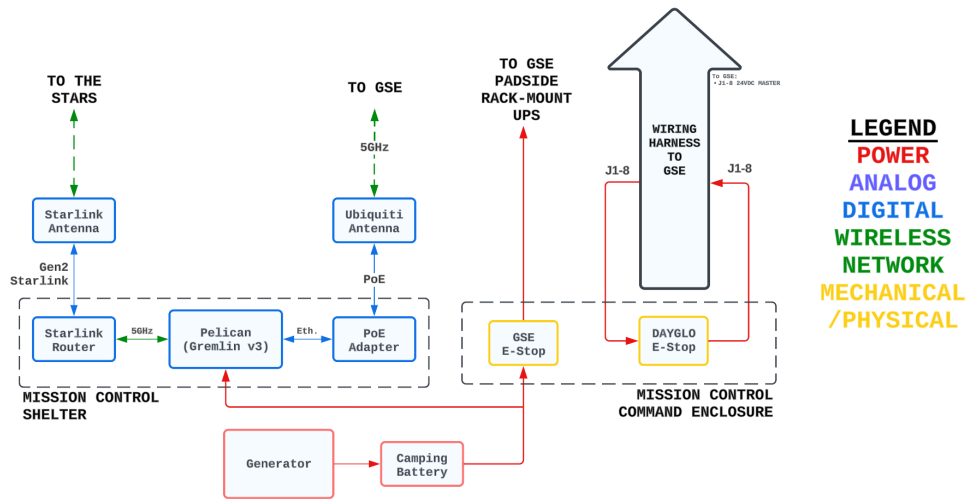


Figure 5.2.1.2 Mission Control Architecture

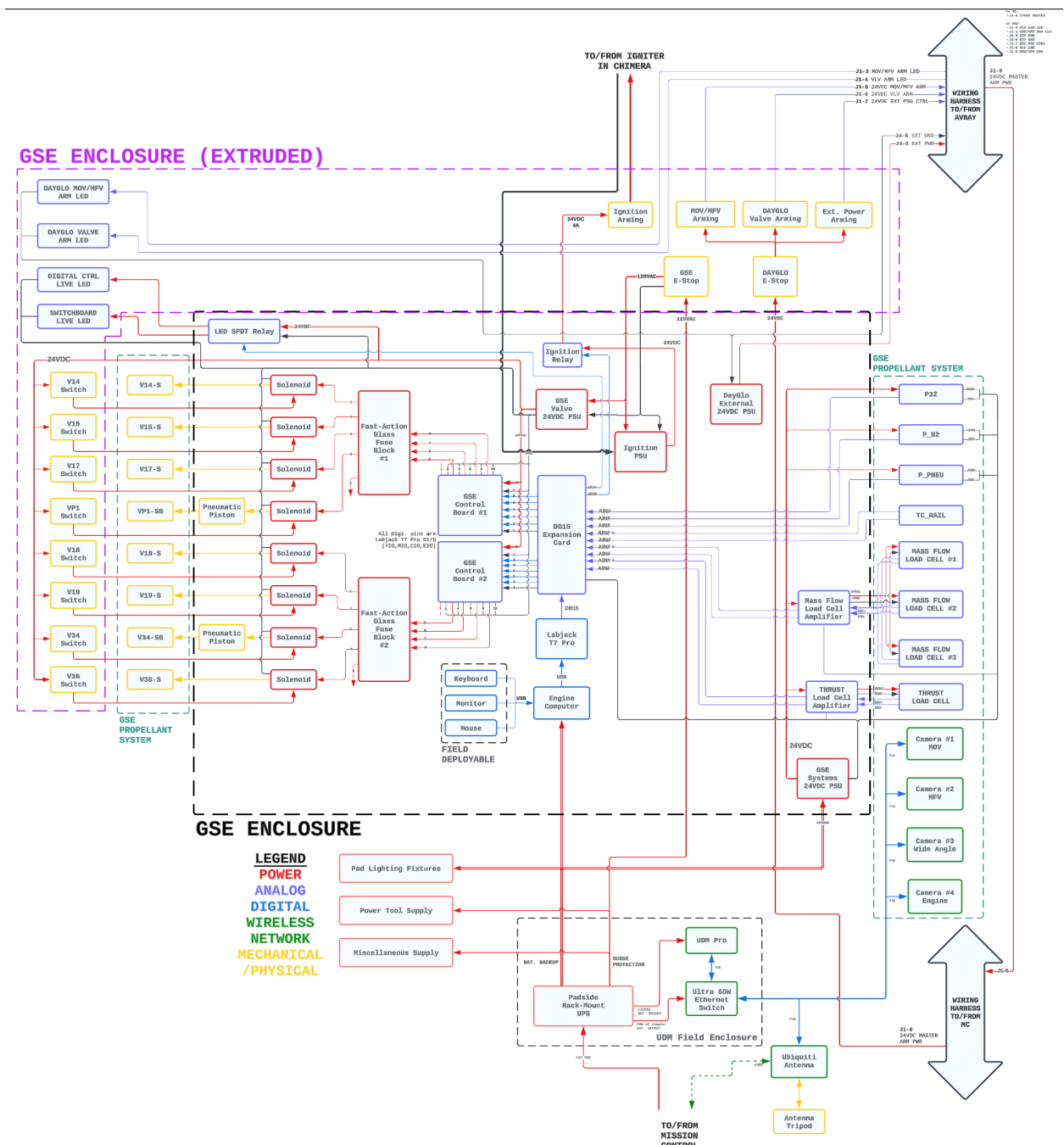


Figure 5.2.1.3 GSE Architecture

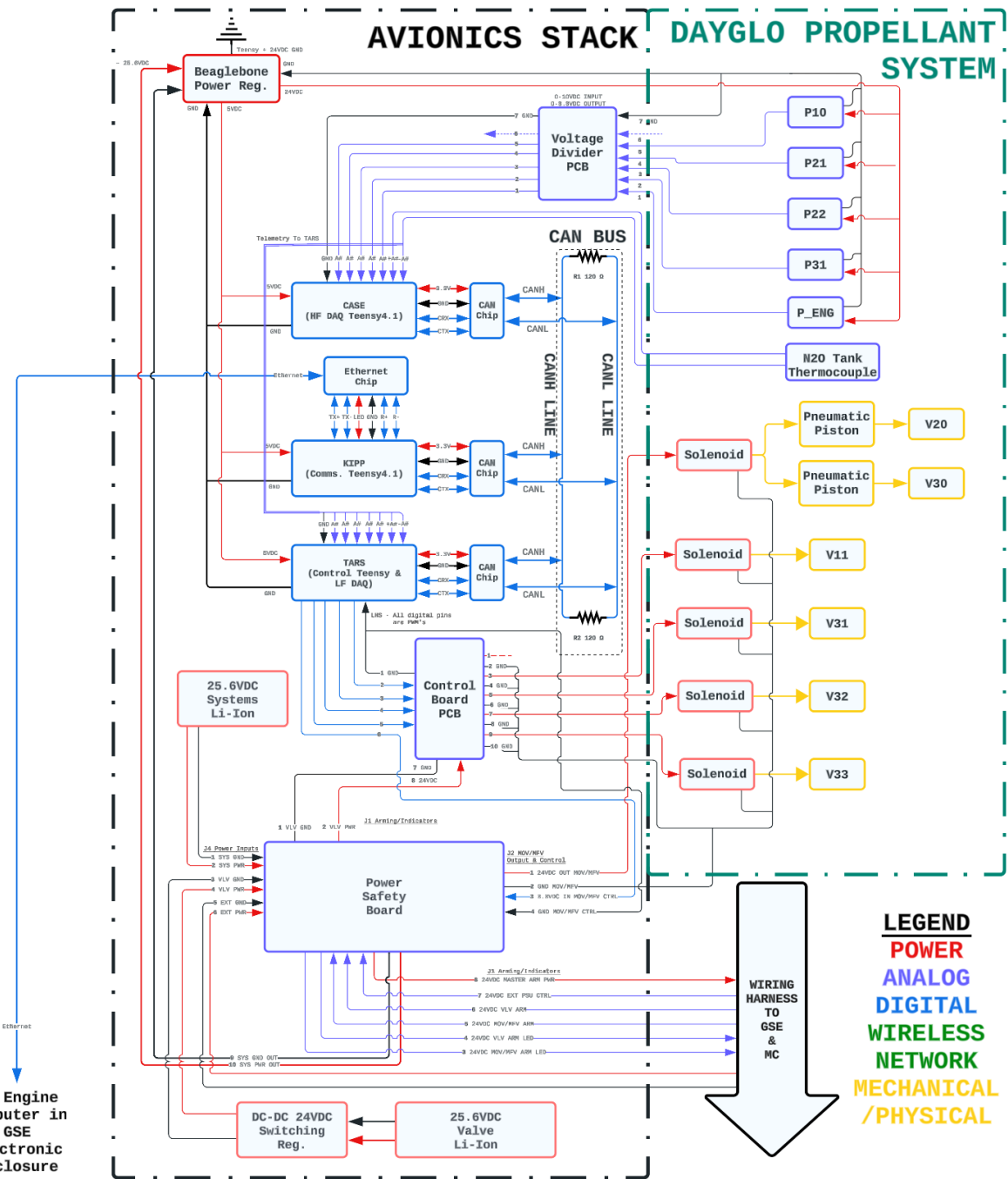


Figure 5.2.1.4 Avionics Stack Architecture

## **5.2.2 SOFTWARE**

### **5.2.2.1. INTRODUCTION**

MACH's Chimera software architecture is being improved and simplified, borrowing heavily from previous experience with Labjack. A broad overview of the software architecture is presented in Figure 5.2.2.1.

The Chimera Control Program (CCP) manages engine operations through a structured software architecture. It includes configuration parsing, device management, execution control, and gRPC-based communication. The system coordinates subsystems to handle telemetry data, execute commands, and manage real-time interactions with hardware.

### **5.2.2.2. SYSTEM ARCHITECTURE**

The system consists of several modules. Configuration management loads runtime parameters from YAML files. Device management controls actuators and sensors. Execution control runs command sequences, while the gRPC communication layer handles external control. Python functions process telemetry data and update the UI. The software uses C++ for core logic, Go for networking, and Python for data handling.

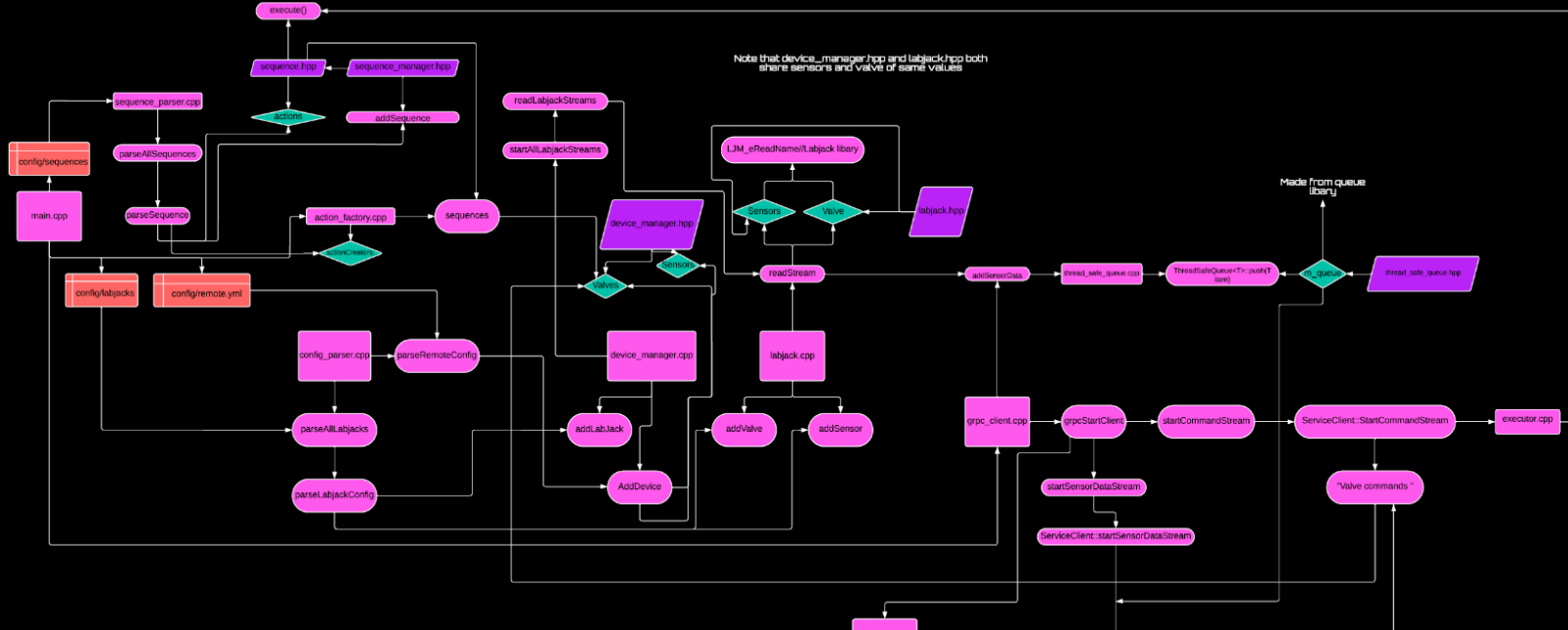
### **5.2.2.3. DATA FLOW & EXECUTION PROCESS**

The system follows a structured flow. Initialization loads parameters from config.yaml, and device\_manager sets up actuators and sensors. The execution module processes commands, while gRPC handles remote inputs. Telemetry data is logged and streamed for real-time monitoring. Modules interact via function calls, network protocols, and shared memory.

### **5.2.2.4. COMMUNICATION & CONTROL MECHANISMS**

The system uses gRPC for remote communication. SERVER\_GRPC receives and forwards commands. Device\_manager.cpp manages hardware communication, while telemetry data updates the UI in real-time.

# Legend



## Day-Glo Software Breakdown

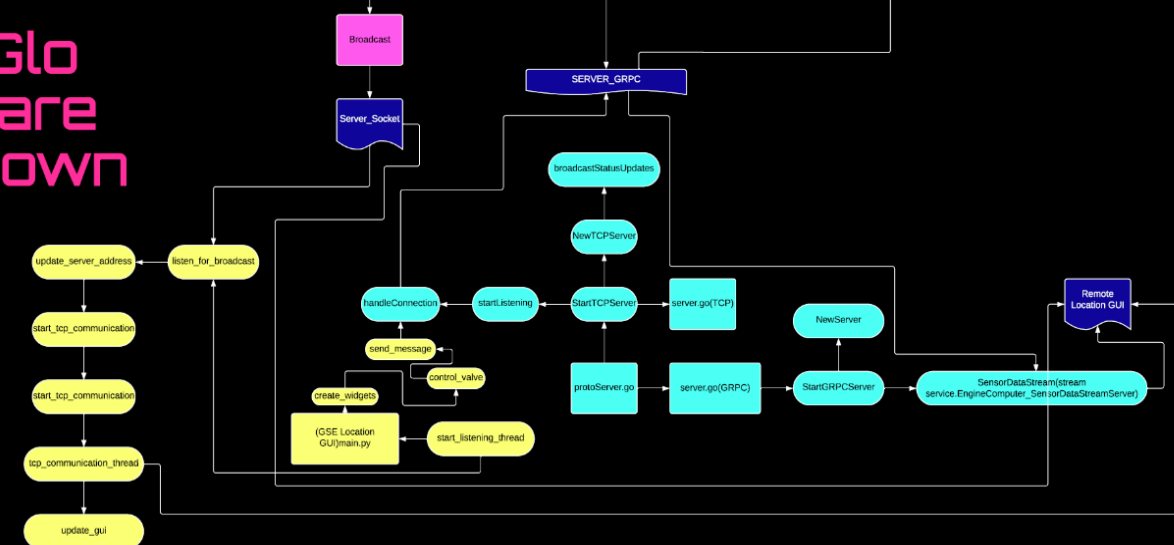


Figure 5.2.2.1 Chimera Control Program flow chart diagram

## **5.3 STRUCTURES SUBTEAM**

### **5.3.1 PLUMBING AND PROPULSION SYSTEM INTEGRATION**

The plumbing and propulsion system has been meticulously designed to integrate seamlessly with the ground support equipment (GSE), optimizing setup, maintenance, and operational efficiency. This system is engineered to remain in a horizontal configuration during initial assembly, repairs, and leak testing, ensuring accessibility and ease of modification. Once all pre-operational procedures are completed, the system is elevated to a vertical position for propellant filling and ignition.

The core design philosophy of the GSE is centered on modularity, allowing for the efficient combination of multiple critical components, including the raising tower, ground plumbing infrastructure, engine thrust stand, and electrical mounting systems. This modular design enables rapid assembly and disassembly, facilitating transportation and deployment in various environments, including remote test sites, competition venues, and university research facilities. The adaptability of this system not only enhances operational flexibility but also streamlines troubleshooting and maintenance processes, reducing downtime between tests.

### **5.3.2 LEVER ARM**

The lever arm plays a crucial role in supporting the structural framework of the raising tower, which houses the propulsion system during the elevation and lowering process. To ensure its structural integrity, a preliminary buckling analysis was conducted to assess its load-bearing capabilities under expected operational stresses. Based on these findings, the lever arm was fabricated using  $2 \times 2$  in.,  $1/8$  in. thick mild steel square tubing, which was selected for its strength-to-weight ratio and durability. The individual steel sections were welded together to form a rigid structure capable of withstanding repeated loading cycles without deformation or failure.

In addition to supporting the raising tower, the lever arm contributes to the overall stability of the GSE, ensuring smooth and controlled movement during system adjustments. The same material used in the lever arm was also incorporated into the base structure of the thrust stand, reinforcing the modular nature of the design. This allows for efficient component interchangeability and future modifications without requiring a complete redesign of the GSE framework.

### **5.3.3 WINCH EXTENSION**

To enhance the efficiency of the propulsion system's lifting mechanism, a winch extension was developed to increase mechanical advantage and reduce strain on the raising system. The extension was iteratively refined through the application of various numerical analysis methods, including buckling analysis and weld stress concentration analysis, to ensure structural reliability. By systematically evaluating stress distribution and failure points, the design was optimized for both safety and performance.

Once the final design was validated, the winch extension was fabricated and integrated into the GSE. It was specifically designed for bolted attachment to the thrust stand, providing a secure and stable lifting mechanism. To further enhance stability, the extension is weighed down using strategically placed sandbags, preventing unwanted movement or shifting during operation. This design not only improves the safety and reliability of the propulsion system but also enhances ease of use, reducing the effort required to transition between horizontal and vertical system orientations.

### **5.3.4 SUPPORT TOWER**

The launch tower was designed around the functionality of allowing the propulsion system to move freely up and down, allowing it to sit on a set of load cells for a mass change analysis. The tower is being assembled with a set of COTS radio towers from an independent manufacturer in Peterborough. The launch tower and base plate are bolted onto the lever arm, allowing the stress experienced by the tower to be relieved by both the lever arm, and support cables attaching the top of the lever arm and support tower.

## 6.0 PLANNED TESTING

The testing plan has been developed such that each step allows for incremental improvements to the technology readiness level (TRL) of key subsystems. The steps of the testing plan have been summarized in Table 6.1. Subsequent descriptions, and explanations of applicable test results have been presented in the proceeding subsection.

Table 6.1: Testing Plan Summary

Test Name	Description	Measurements & Instrumentation	Objectives
Tank Hydrostatic Testing	Hydrostatically pressurize tanks to 1300 psi (~1.3× MEOP) to ensure the design withstands pressures above the operating limit without permanent damage.	- Bulkhead Separation: Measured with calipers at a 1/16" gap (before, during, and after pressurization). - Tank Pressure: Monitored via a gauge connected to the pump to detect leaks.	- Hold pressure for 15 minutes without rapid loss. - Avoid permanent plastic deformation when subjected to pressures >1.1× MEOP.
Control & Actuation Tests	Unpressurized evaluation of the control system's ability to manually and automatically operate valves via the GUI.	No specialized instrumentation; the test primarily involves operational commands via the GUI.	- Demonstrate manual valve operation through the GUI. - Validate automatic valve sequencing upon activation.
Integrated Structure Lift Test	Integrate all structural components and lift the propulsion system support rail vertically using an electric winch to test structural integration and dynamic load capacity.	No specific measurements or instrumentation are planned.	- Demonstrate seamless integration of structural subsystems. - Validate winch sizing and ensure the support tower and pivoting mechanisms withstand dynamic loads during lifting.
Sub-Scale Coldflow	Flow test of the nitrous run line using CO <sub>2</sub> as an inert stand-in, with a flow article that replicates the full-scale orifice geometry (with fewer orifices).	- Mass Measurements: Load cells record system mass during fill and discharge. - Tank Pressure: Gauged to monitor pressure changes during autogenous pressurization. - Video: High-speed footage to	- Verify setup/teardown procedures and refine workflows. - Validate valve sequencing. - Measure transient mass reduction (flow) and increase (fill). - Collect video data for

		qualitatively assess injector mixing.	injector mixing characterization.
Full Scale Injector Coldflow	Flow test for both fuel and oxidizer run lines using distilled water and CO <sub>2</sub> , conducted in three phases (individual and simultaneous) to assess full-scale injector behavior.	<ul style="list-style-type: none"> <li>- Pressure Measurements: At the venturi inlet (via a slave transducer), nitrous tank, and within the fuel and oxidizer domes (as per the P&amp;ID).</li> <li>- Mass Measurements: Load cells measure propellant system mass during fill and flow for direct flow rate calculation.</li> </ul>	<ul style="list-style-type: none"> <li>- Verify installation procedures including engine mounting.</li> <li>- Refine workflow and pad operations.</li> <li>- Accurately measure mass flow rates and pressure drops.</li> <li>- Ensure robust valve control and software/GUI performance.</li> <li>- Collect comprehensive data for subsequent analysis.</li> </ul>
Ignitor Test (Puck)	Test the Chimera-sized puck ignitor to verify burn characteristics critical for engine ignition.	<ul style="list-style-type: none"> <li>- Burn Duration: Determined via video analysis.</li> <li>- Peak Temperature: Measured using high-temperature laboratory thermocouples.</li> </ul>	<ul style="list-style-type: none"> <li>- Ensure a minimum burn duration of 7 seconds.</li> <li>- Confirm energetic burn characteristics similar to previous tests.</li> <li>- Achieve a peak temperature above 1000 K.</li> </ul>
Full Duration Static Hotfire Test	Fire the engine in its static configuration to characterize performance and validate combustion models.	<ul style="list-style-type: none"> <li>- Pressure Measurements: Across tanks, runlines, injector bulkheads, and chamber (as defined in the P&amp;ID).</li> <li>- Mass Measurements: Load cells record propellant mass during fill and flow.</li> <li>- Force Measurements: Engine load cell measures thrust for performance characterization (C* and Ct efficiencies).</li> </ul>	<ul style="list-style-type: none"> <li>- Validate setup/teardown (injector, mounting hardware, load cells, chamber).</li> <li>- Accurately measure mass flow and pressure throughout operations.</li> <li>- Confirm reliable valve control and sequencing via the GUI.</li> <li>- Demonstrate successful ignition and thrust measurement.</li> <li>- Verify structural subsystem performance under full</li> </ul>

			engine load.
Full Duration TVC Hotfire Test	Fire the engine in its TVC configuration to demonstrate full-thrust gimbaling ( $\pm 10^\circ$ ) while monitoring key performance parameters.	<ul style="list-style-type: none"> <li>- Pressure Measurements: At tanks, runlines, injector bulkheads, and chamber (per the P&amp;ID).</li> <li>- Mass Measurements: Load cells measure propellant mass during fill and flow.</li> <li>- Force Measurements: Engine load cell records thrust (with some inaccuracies due to gimbaling).</li> <li>- Linear Actuator Position: Feedback from actuators tracks TVC movement for real-time corrections.</li> </ul>	<ul style="list-style-type: none"> <li>- Validate setup/teardown (including additional instrumentation for TVC).</li> <li>- Accurately measure mass flow and pressure during operations.</li> <li>- Demonstrate reliable valve control and sequencing (including torch ignitor ignition).</li> <li>- Achieve full TVC motion (<math>\pm 10^\circ</math> sweep) during the burn.</li> <li>- Ensure overall engine thrust and structural integrity under TVC conditions.</li> </ul>

## 6.1 TANK HYDROSTATIC TESTING

This test involves hydrostatically pressurizing the tanks to 1300 psi (approximately 1.3× MEOP) to confirm that the tank design can tolerate pressures above the Maximum Expected Operating Pressure without incurring permanent structural damage. During the test, calipers are used to measure the bulkhead separation (before, during, and after pressurization) at a designed 1/16" gap between the casing and the bulkheads. Additionally, a pressure gauge connected to the pump monitors any pressure drops over time, which would indicate leaks. The objectives are twofold: first, to ensure that each tank maintains the applied pressure for a duration of 15 minutes without rapid loss, and second, to verify through measurements that no permanent plastic deformation occurs when the tank is subjected to pressures greater than 1.1× MEOP.

The hydrostatic test of both tanks was successfully completed on October 26th, 2024. Per the testing plan, each tank was pressurized to 1300 psi and sustained pressure for 15 minutes. No measurable pressure lost was measured for the hydrostatic test of the ethanol tank. From the initial gap of 1/16", an elongation of approximately 17 thou was measured between the bulkheads and casing. This elongation can be explained by the fact that there the casing,

bulkhead and clevis pins were manufactured with a small clearance fit. Once pressurized, the clearance between the pins and hole are eliminated, allowing the bulkhead to settle in a new equilibrium position. The ethanol tank hydrostatic test setup can be observed in Figure 6.1.1.



Figure 6.1.1: Ethanol tank hydrostatic test

The nitrous tank was tested under similar conditions. Upon initial pressurization, a noticeable drop in pressure was initially observed. This was traced to an observable leak from the  $\frac{1}{4}$ " NPT fitting intended for the relief valve (Capped for purpose of the test). This leak was quickly remedied by slight tightening of the fitting. Upon re-pressurization the pressure drop was not observed and the tank held 1300 psi for 15 minutes. The gap between the bulkheads and casing was measured to increase by approximately 24 thou. This increase in the gap relative to the ethanol tank can be attributed to the difference in manufacturing technique used for each of the tanks. The process used for the nitrous tank resulted in a greater clearance between the pins, bulkhead and casing, causing the bulkheads to travel a greater distance before settling in its equilibrium position. The nitrous tank hydrostatic setup can be observed in Figure 6.1.2.



Figure 6.1.2: Nitrous tank hydrostatic test

## 6.2 CONTROL & ACTUATION TESTS

In an unpressurized setting, the control system's ability to operate the valves is put to the test. This phase evaluates both manual operations via a graphical user interface (GUI) and automatic valve sequencing. The primary goal is to demonstrate that all valves can be reliably opened and closed manually through the GUI, and that the system correctly executes the pre-programmed automatic sequencing when commanded. This test is critical for confirming the responsiveness and functionality of the control and actuation subsystems before progressing to more integrated tests.

### **6.3 INTEGRATED STRUCTURE LIFT TEST**

The focus of the integrated structure lift test is to verify the successful assembly and mechanical integrity of all structural components of the propulsion system. In this test, the propulsion system support rail is lifted vertically using an electric winch. Although no specific measurements or instrumentation are deployed, the test is designed to confirm the seamless integration of structural subsystems, validate that the winch is appropriately sized, and ensure that the support tower and pivoting mechanisms are capable of withstanding the dynamic loads encountered during lifting.

### **6.4 SUB-SCALE COLDFLOW TEST**

This test evaluates the flow characteristics of the nitrous run line by substituting CO<sub>2</sub> as an inert stand-in for nitrous. The setup uses a flow article featuring a reduced number of orifices that maintain the same sizes and impinging geometry as the full-scale design. Instrumentation for this test includes load cells that measure the mass of the propellant system during both the fill and discharge phases, as well as pressure gauges that record tank pressure changes during autogenous pressurization. High-speed video footage is also captured to provide qualitative insights into the impinging injector mixing characteristics. The objectives here are to verify the setup and teardown procedures, refine workflows and pad operations, validate valve sequencing, and accurately record transient mass changes during both fluid discharge and tank filling.

### **6.5 FULL SCALE INJECTOR COLDFLOW TEST**

In this test, both the fuel and oxidizer run lines are exercised using inert stand-ins—distilled water for fuel and CO<sub>2</sub> for the oxidizer. The main valves are connected to the full-scale injector to assess pressure drops at full flow rates. Conducted in three phases (testing each run line individually followed by a simultaneous coldflow of both), this test employs comprehensive instrumentation. Critical pressure measurements include the venturi inlet pressure (monitored with a slave pressure transducer), nitrous tank pressure, and pressures within the fuel and oxidizer domes. Load cells record propellant system mass data to enable precise calculations of mass flow rates. Objectives include verifying the proper setup and teardown procedures (which now involve mounting the engine), refining workflow and pad operations, ensuring accurate measurements during both fill and flow operations, maintaining reliable valve control and

communication, validating the software and GUI performance, and collecting data for subsequent analysis.

## **6.6 IGNITOR TEST (PUCK)**

The ignitor test focuses on the Chimera-sized puck ignitor, which is critical for engine ignition. The test uses high-temperature laboratory thermocouples to capture the peak ignitor temperature and high-speed video analysis to determine the burn duration. The objectives are to confirm that the ignitor burns for at least 7 seconds, to demonstrate that it burns with energetic characteristics comparable to previous puck tests, and to verify that the peak temperature exceeds 1000 K.

## **6.7 FULL DURATION STATIC HOTFIRE TEST**

This test fires the Chimera engine in a static configuration to characterize engine performance and validate key assumptions in the combustion modeling process. Extensive instrumentation is employed, including pressure transducers located at strategic points (tanks, runlines, injector bulkheads, and chamber) to ensure that pressure drops remain within acceptable limits. Load cells provide mass measurements of the propellant system during both fill and flow operations, while an engine load cell records force data for thrust measurement—critical for evaluating engine efficiencies such as  $C^*$  and  $C_t$ . The objectives are to verify installation and teardown procedures (with the injector, mounting hardware, load cells, and chamber in place), to ensure accurate mass and pressure measurements during operations, to validate the control system's valve sequencing and GUI functionality, to demonstrate successful ignition and thrust measurement, and finally, to confirm that the structural subsystem performs as expected under full engine thrust loads.

## **6.8 FULL DURATION TVC HOTFIRE TEST**

In the final test, the engine is fired in its Thrust Vector Control (TVC) configuration to demonstrate the ability to gimbal  $\pm 10^\circ$  at full thrust. Like the static hotfire test, this phase uses pressure measurements at critical system points, mass measurements from load cells, and force measurements from the engine load cell. In addition, linear actuator position feedback is used to track the TVC motion and enable real-time corrections. The objectives extend those of the static hotfire test by also requiring the demonstration of successful ignition of a torch ignitor,

valve sequencing, and a full sweep of TVC motion during the burn, all while ensuring that the engine thrust and structural responses remain within acceptable limits.

## 7.0 PROJECT TIMELINE

	ALL											
	H1						H2					
	Q1			Q2			Q3			Q4		
	SEP	OCT	NOV	DEC	JAN	FEB	MAR	APR	MAY	JUNE	JUL	AUGUST
THRUST VECTOR CONTROL	Initial Design Proposal	Sourcing parts	Manufacturing	Testing								
TORCH IGNITOR	Initial Design Proposal	Manufacturing			Testing							
INJECTOR	Initial Design Proposal	Preliminary design review	Manufacturing									
COMBUSTION CHAMBER	Preliminary design review		Manufacturing									
SYSTEM INTEGRATION										Integration of propulsion systems with T-C		
ABLATIVE TESTING	Initial Design Proposal	Manufacturing and testing										
COMPETITION									Preparing system integration		Competition	
COLD FLOW									Cold Flow			
HOT FIRE										Hotfire		
<b>Add Row</b>												

Figure 7.1: Project timeline for Chimera liquid engine project

## 8.0 PROJECT RISKS

### 8.1 SAFETY AND OPERATIONAL RISKS

Safety and operational risks are important considerations in the design and execution of the Chimera engine project. These risks encompass hazards associated with propulsion system failures, structural integrity issues, and personnel safety. Ensuring proper mitigation strategies is essential to prevent catastrophic failures and maintain operational efficiency. This section outlines the primary risks, categorized into propulsion system risks, structural risks, and personnel safety risks.

Table 8.1: Summary of Key Safety and Operational Risks

Risk Category	Key Risks
<b>Propulsion System Risks</b>	Nitrous Oxide Thermal Decomposition, Pressure Vessel Failure, Premature Ignition, Valve Sequencing Errors, Flow Control Issues
Structural Risks	Support Tower Failure, Lift System Malfunction, Engine Mount Failure, TVC System Structural Issues
Personnel Safety Risks	Chemical Exposure, High Pressure Systems, Fire/Explosion Hazards, Mechanical Hazards

#### 8.1.1 PROPULSION SYSTEM RISKS

The propulsion system represents the core operational element of the Chimera engine and incorporates multiple subsystems working in concert, each with associated failure modes. Analysis of these failure modes reveals several critical risk categories requiring systematic evaluation and mitigation.

##### 8.1.1.1 NITROUS OXIDE THERMAL DECOMPOSITION

Nitrous oxide decomposition presents a primary risk due to the oxidizer's inherent chemical instability. The decomposition reaction follows an autocatalytic pathway, where the heat released accelerates the reaction rate. This behavior can manifest under two conditions: elevated temperatures exceeding 570K or exposure to catalytic contaminants [3]. The resulting rapid pressure rise can exceed the pressure vessel's structural limits within milliseconds.

#### **8.1.1.1.1 CURRENT MITIGATION STRATEGIES**

To mitigate risks of nitrous oxide thermal decomposition, the team has implemented several strategies. Temperature control is critical during operations. The team will carefully monitor temperatures to prevent conditions that could trigger thermal decomposition. All components in the propellant feed system have been selected for chemical compatibility with nitrous oxide. This reduces the potential for chemical interactions that could destabilize the oxidizer. Relief devices, detailed in Section 5.1.2, are installed to manage pressure changes. These mechanisms allow controlled pressure release if unexpected conditions arise. An emergency dump system has been designed to quickly evacuate the oxidizer if critical risks are detected. This provides an additional safety mechanism during the operational sequence. These mitigation strategies aim to manage the inherent risks of nitrous oxide handling through careful design and operational protocols.

#### **8.1.1.1.2 ADDITIONAL RECOMMENDATIONS**

To further enhance safety and reduce the risk of nitrous oxide thermal decomposition, the team recommends two additional strategies. First, implement a comprehensive monitoring system that continuously tracks temperature and pressure thresholds for the nitrous oxide system. This real-time monitoring will allow for early detection of potentially hazardous conditions that could lead to thermal decomposition. Second, apply thermal insulation around the oxidizer tanks to minimize external temperature variations and reduce the risk of uncontrolled temperature-driven pressure changes. Proper insulation can help maintain a more stable thermal environment for the nitrous oxide, further mitigating decomposition risks.

#### **8.1.1.2 PRESSURE VESSEL FAILURE**

The potential failure of oxidizer and fuel tanks due to excessive pressure or material degradation poses significant risks, including structural rupture, uncontrolled fluid release, and potential ignition. To mitigate these risks, the team has implemented several critical strategies. Hydrostatic testing serves as a primary validation method for tank structural integrity. The tanks are pressurized to 1300 psi, which represents 1.3 times the Maximum Expected Operating Pressure (MEOP). This testing helps identify potential weaknesses in the tank structure before operational deployment. Pressure relief devices are strategically integrated into the tank design to ensure controlled venting during unexpected pressure increases. These devices provide a critical safety mechanism that prevents catastrophic over-pressurization. Burst discs have been carefully designed and installed to safely release excess pressure in extreme scenarios. These passive safety components act as a final line of defense, preventing tank rupture by allowing controlled pressure dissipation when other relief mechanisms are insufficient.

#### **8.1.1.3 PREMATURE IGNITION**

Unintended ignition presents a significant risk to the rocket engine system, with potential consequences including engine damage and serious safety hazards for personnel. To mitigate these risks, the team has developed comprehensive strategies. The ignition system incorporates a remote activation mechanism with multiple safety interlocks. These interlocks prevent accidental or unauthorized ignition by requiring specific, sequential activation steps. Valve sequencing protocols have been strictly defined to control the precise timing and order of fuel and oxidizer valve operations. This approach minimizes the risk of improper valve interactions that could create dangerous mixing conditions. Non-sparking materials have been deliberately selected for use in the ignition circuitry. This material choice reduces the potential for electrical sparks that could trigger unintended combustion.

#### **8.1.1.4 VALVE SEQUENCING ERRORS**

Valve sequencing errors pose a risk to the rocket engine's performance and safety. Incorrect timing or activation of fuel and oxidizer valves can lead to significant operational problems, including combustion instability, incomplete ignition, or dangerous over-pressurization of the combustion chamber. To address these potential risks, the team has implemented several mitigation strategies. An automated sequencing logic has been developed with real-time validation capabilities. This system accounts for the precise timing and order of valve operations, ensuring that fuel and oxidizer are introduced to the combustion chamber according to carefully designed parameters.

#### **8.1.1.5 FLOW CONTROL ISSUES**

Inconsistent fuel or oxidizer flow can lead to multiple issues, including combustion instability, chamber over-pressurization, and inefficient propellant utilization. To mitigate these risks, the team has implemented several design and monitoring approaches. A choked injector design has been developed to maintain stable oxidizer flow. By restricting the flow at a critical point, the system ensures a more consistent and predictable oxidizer mass flow rate, reducing potential variations that could disrupt combustion. A cavitating venturi has been incorporated for precise fuel flow regulation. This specialized flow control device helps standardize the fuel flow rate, minimizing variations that could impact engine performance. Comprehensive monitoring systems have been installed to track pressure and mass flow rates at critical points in the propellant feed system. These real-time measurement capabilities allow for immediate detection of any flow rate anomalies, enabling rapid response to potential performance issues.

## **8.1.2 STRUCTURAL RISKS**

The structural integrity of the Chimera engine and its support systems is crucial to ensuring successful operation. Failures in structural components can lead to uncontrolled collapse, loss of system stability, and severe damage to the propulsion unit. Key structural risks are as follows:

### **8.1.2.1 SUPPORT TOWER FAILURE**

A potential structural failure could lead to a catastrophic collapse, posing significant risks to equipment, personnel, and the overall testing process. To mitigate these risks, the team has implemented several strategic approaches: High-strength steel components have been selected for the support tower construction. These materials provide enhanced structural reliability and load-bearing capacity compared to standard structural materials. Comprehensive load analysis has been conducted using two complementary methods: finite element modeling (FEM) and detailed analytical calculations. These analytical approaches allow for a thorough assessment of potential stress points, load distributions, and structural performance under various operational conditions. A robust anchoring system has been designed to ensure the support tower's stability. These anchoring mechanisms are engineered to minimize movement and provide additional structural reinforcement, reducing the risk of unexpected tower displacement or failure.

### **8.1.2.2 LIFT SYSTEM MALFUNCTION**

The lift system is responsible for precisely raising and lowering the propulsion unit. Mechanical failures in this system represent a significant safety and operational risk, with the potential to cause uncontrolled drops that could result in substantial equipment damage and serious personnel safety hazards. A high-capacity electric winch has been selected as the primary lifting mechanism. This choice provides several advantages over manual or lower-capacity systems, including more precise control, consistent lifting performance, and reduced human error during the raising and lowering process. Redundant safety latches have been engineered into the lift system to prevent catastrophic free-fall scenarios. These multiple, independent locking mechanisms ensure that even if one safety component fails, additional barriers remain to prevent uncontrolled descent of the propulsion unit. Rigorous load testing has been conducted on all lift mechanisms. These tests systematically evaluate the structural integrity, load-bearing capacity, and operational reliability of each critical component in the lifting system.

### **8.1.2.3 ENGINE MOUNT FAILURE**

The engine mount interfaces the propulsion system and its support structure, serving as the main connection point that maintains the entire system's stability during testing and operation. High-strength fasteners have been strategically selected and reinforced at all mounting points. These specialized components are engineered to withstand extreme loads and provide superior structural integrity compared to standard mounting hardware. By using advanced materials and precise manufacturing techniques, the team ensures that each connection point can resist the substantial forces generated during engine operation. Finite Element Method (FEM) analysis has been conducted to validate the load-bearing capacity of the mounting system. This computational approach allows engineers to simulate and analyze complex stress distributions, identifying potential weak points before they can become critical failure modes.

### **8.1.2.4 TVC SYSTEM STRUCTURAL ISSUES**

Structural weaknesses or mechanical failures in this system could lead to a catastrophic loss of engine control, potentially compromising the entire testing process and posing significant safety risks. To mitigate these potential risks, the team has implemented a comprehensive set of engineering strategies. Finite Element Method (FEM) analysis has been conducted on all TVC structural components. This computational approach allows for detailed stress and strain analysis, enabling engineers to identify and address potential structural vulnerabilities before they can become critical failure points. The analysis provides insights into load distributions, potential deflection points, and overall system integrity. Actuators have been carefully selected based on their high load tolerance. The chosen components are specifically engineered to withstand the complex mechanical stresses encountered during thrust vector control operations. This selection process prioritizes both performance and reliability, ensuring that the actuators can maintain precise control under challenging operational conditions. Aerospace-grade fasteners have been used to secure all mounting points in the TVC system. These specialized fasteners provide superior strength, corrosion resistance, and reliability compared to standard mounting hardware. The careful selection and precise installation of these components help ensure a robust and stable connection between the TVC system and the engine structure.

### **8.1.3 PERSONNEL SAFETY RISKS**

Personnel safety risks arise from exposure to hazardous chemicals, high-pressure systems, and potential fire/explosion hazards. Ensuring safe handling procedures is critical to minimizing risks.

#### **8.1.3.1 CHEMICAL EXPOSURE**

Chemical exposure presents a potential risk to personnel working with propellants, solvents, and other hazardous materials. To mitigate these risks, the team has implemented a comprehensive safety approach focused on personal protection and environmental controls. Personal protective equipment (PPE) is mandatory during all handling operations. This includes NIOSH-approved respirators, chemical-resistant gloves, and full-face shields designed to provide complete protection against potential chemical splashes or vapors. Ventilation systems have been carefully designed in all fueling and handling areas to minimize the concentration of potentially harmful chemical vapors and ensure a safe working environment.

#### **8.1.3.2 HIGH PRESSURE SYSTEMS**

High-pressure systems in the propulsion setup present potential safety risks due to the possibility of pressure vessel ruptures or unexpected leaks, which could result in significant personnel injury. To mitigate these risks, the team has implemented multiple engineering controls. Specifically, all high-pressure tanks are equipped with pressure relief devices designed to prevent pressure excursions beyond safe operating limits. Additionally, each pressure vessel undergoes comprehensive hydrostatic testing, which involves pressurizing the tanks to 1.3 times their maximum expected operating pressure to verify structural integrity and identify potential weaknesses before operational use.

The hydrostatic testing protocol involves carefully measuring tank deformation using calipers and monitoring pressure stability over a 15-minute period. This approach allows engineers to confirm that the tanks can withstand pressures significantly above their normal operating range without experiencing permanent structural damage or developing critical leaks.

### **8.2 TECHNICAL PERFORMANCE RISKS**

Technical performance risks impact the reliability and efficiency of the Chimera engine during operation. These risks include challenges related to combustion efficiency, control system reliability, and thrust vector control (TVC) functionality. Addressing these risks is critical for ensuring consistent engine performance and successful mission execution.

Table 8.2: Summary of Key Technical Performance Risks

Risk Category	Key Risks
<b>Combustion System Risks</b>	Injector Performance, Chamber Liner Degradation, Combustion Instability, Ignition Reliability
<b>Control System Risks</b>	Sensor Failures, Data Acquisition Issues, Communication Loss, Software Malfunctions
<b>TVC System Risks</b>	Actuator Performance, Gimbal Mechanism Issues, Control Algorithm Failures, Position Feedback Errors

## 8.2.1 COMBUSTION SYSTEM RISKS

The combustion system is a critical aspect of propulsion performance. Risks in this category primarily relate to fuel injection efficiency, thermal durability, and stability of the combustion process.

### 8.2.1.1 INJECTOR PERFORMANCE

Suboptimal injector characteristics such as inadequate propellant atomization or uneven fuel and oxidizer distribution can significantly compromise engine performance, potentially resulting in reduced thrust output and combustion instabilities. To mitigate these potential risks, the team has implemented a multi-faceted approach to injector design and validation. Analytical models are employed to optimize the injector geometry, as well as standardized assumptions are made to model and predict propellant mixing and spray characteristics before physical fabrication. These computational models help refine the injector design to ensure optimal propellant atomization and distribution. Complementing the initial analysis, the team conducts experimental cold flow testing to empirically verify the predicted spray patterns. These tests use inert fluids to simulate actual propellant behavior, providing direct experimental validation of the injector's performance characteristics. Additionally, the team emphasizes precision manufacturing techniques for the injector orifices, ensuring consistent and accurate geometries that meet the stringent requirements for propellant mixing and combustion efficiency.

### **8.2.1.2 CHAMBER LINER DEGRADATION**

The combustion chamber liner experiences extreme thermal and mechanical stresses during engine operation, with potential risks of material degradation, erosion, and subsequent loss of structural integrity. These conditions can critically compromise the engine's performance and safety.

To address these challenges, the team has developed a comprehensive approach to liner design and validation. The primary mitigation strategy involves using a silica phenolic ablative liner, which is engineered to withstand high-temperature environments by progressively and predictably eroding while protecting the underlying chamber structure. This material was selected based on its ability to provide thermal protection through controlled ablation.

Thermal modeling plays a crucial role in understanding and predicting the liner's behavior, allowing the calculation of anticipated ablation rates and assessing the material's performance under simulated conditions. To validate these computational predictions, the team conducted initial hotfire testing, which provided empirical data on the liner's actual performance and durability under real operational conditions.

### **8.2.1.3 COMBUSTION INSTABILITY**

The potential for combustion instability is an important consideration in rocket engine design, characterized by potentially destructive pressure oscillations within the combustion chamber. These oscillations can arise from complex interactions between the combustion process, chamber geometry, and propellant injection dynamics.

For the Chimera engine, the team preliminarily assesses that combustion instability risks are mitigated by the engine's relatively small size. The compact dimensions and carefully designed injector geometry - which features a like-like impinging design with specific orifice characteristics - reduce the likelihood of significant pressure oscillations.

### **8.2.1.4 IGNITION RELIABILITY**

Unreliable ignition can result in failed engine start sequences or incomplete combustion, affecting performance. To enhance reliability, the team has developed a custom pyrotechnic initiator system as a baseline ignition method. This backup system provides an additional layer of confidence for test day operations, ensuring that even if the primary torch igniter encounters issues, an alternative ignition mechanism is available. Laboratory testing rigorously validates the ignition system's performance, examining critical parameters such as burn duration, peak temperature, and consistent ignition characteristics. The remote activation capability further enhances operational safety, allowing precise control of the ignition sequence.

## **8.2.2 CONTROL SYSTEM RISKS**

The control system is responsible for engine telemetry, actuation of valves, and real-time adjustments to maintain stability. Failures in this system can compromise mission objectives.

### **8.2.2.1 SENSOR FAILURES**

Failures in pressure, temperature, or position sensors can result in inaccurate data readings, leading to compromised decision-making. To mitigate these risks, current strategies include deploying redundant sensors for critical measurements, conducting regular calibration and validation of sensor outputs, and utilizing industrial-grade sensors designed to withstand extreme environments.

### **8.2.2.2 DATA ACQUISITION ISSUES**

Data loss or corruption can impede performance assessments and real-time decision-making. To mitigate these risks, strategies include high-speed data acquisition with redundant storage to ensure data reliability, the use of shielded cabling to minimize electromagnetic interference, and regular system integrity checks to maintain system performance and accuracy.

### **8.2.2.3 COMMUNICATION LOSS**

Loss of telemetry signals can prevent monitoring and control of the engine during tests, posing significant risks. To mitigate this, current strategies include implementing multiple communication channels for redundancy, real-time telemetry monitoring to detect signal degradation, and hardwired fail-safe triggers for emergency shutdowns to ensure safety and reliability.

### **8.2.2.4 SOFTWARE MALFUNCTIONS**

Bugs or failures in control algorithms can cause incorrect valve actuation or unstable flight control, leading to potential system failures. To mitigate these risks, current strategies include software-in-the-loop testing for all control algorithms, implementing manual override capabilities for unexpected behavior, and conducting regular updates and bug fixes through iterative testing.

### **8.2.3 TVC SYSTEM RISKS**

The Thrust Vector Control (TVC) system is responsible for adjusting engine orientation during operation. Failures in this system can lead to loss of directional control and mission failure.

#### **8.2.3.1 ACTUATOR PERFORMANCE**

Linear actuators control engine movement during thrust vector control (TVC) operations, and malfunctions can lead to a loss of thrust vectoring capability. To mitigate this risk, strategies include selecting actuators rated for the full expected load range, conducting FEM analysis to ensure actuator mounts can withstand operational loads, and implementing a soft-start feature to minimize mechanical stress and extend actuator lifespan.

#### **8.2.3.2 GIMBAL MECHANISM ISSUES**

The gimbal must support engine loads while allowing controlled movement, and mechanical failures could result in a loss of stability. To mitigate this risk, strategies include FEM validation to ensure structural integrity, the use of high-strength fasteners to secure all components, routine inspections and load testing, and upgrades to bearing and joint materials for enhanced durability.

#### **8.2.3.3 CONTROL ALGORITHM FAILURES**

Errors in thrust vector control (TVC) algorithms can lead to unstable flight trajectories, compromising mission success. To mitigate this risk, current strategies include extensive hardware-in-the-loop (HIL) testing before deployment, validation of control software through multiple simulated scenarios, and the implementation of a backup manual override for emergency control.

#### **8.2.3.4 POSITION FEEDBACK ERRORS**

Incorrect position feedback can lead to improper thrust vectoring, compromising stability and control. To mitigate this risk, current strategies include using precision encoders for accurate actuator positioning, implementing calibration routines to verify positional accuracy, and incorporating multiple feedback sources to cross-check and validate readings.

### **8.3 SCHEDULE AND RESOURCE RISKS**

Schedule and resource risks encompass factors that could impact the timely execution of the Chimera engine project. These risks include challenges in manufacturing, testing, and competition deadlines, as well as logistical and regulatory constraints. Managing these risks effectively is crucial to ensure the project stays on track and within budget.

Table 8.3: Summary of Key Schedule and Resource Risks.

Risk Category	Key Risks
<b>Manufacturing Risks</b>	Component Procurement Delays, Machine Shop Availability, Quality Control Issues, Assembly Integration Challenges.
<b>Testing Program Risks</b>	Test Site Availability, Weather Constraints, Equipment Availability, Test Schedule Delays.
<b>Competition Timeline Risks</b>	Regulatory Approval Delays, Documentation Requirements, Transportation Logistics, Resource Allocation Issues.

### 8.3.1 MANUFACTURING RISKS

The manufacturing process is crucial for ensuring that all components meet performance and safety standards. Delays or failures in this phase can disrupt the entire project timeline.

#### 8.3.1.1 COMPONENT PROCUREMENT DELAYS

Delays in procuring critical components can disrupt assembly and testing schedules, impacting project timelines. To mitigate this risk, strategies include early identification and ordering of long lead-time items, establishing multiple supplier agreements to reduce dependency on a single vendor, and maintaining a buffer stock of critical components to ensure availability when needed.

#### 8.3.1.2 MACHINE SHOP AVAILABILITY

Limited access to machine shop facilities can delay the fabrication of key components, impacting overall project timelines. To mitigate this risk, strategies include pre-scheduling machining time well in advance, identifying backup machining facilities for overflow work, and prioritizing in-house machining for critical components to ensure timely production.

#### 8.3.1.3 QUALITY CONTROL ISSUES

Inconsistent quality in manufactured components can result in failures during testing and delays in project progress. To mitigate this risk, strategies include strict adherence to quality assurance protocols, conducting pre- and post-manufacturing inspections of critical components, and implementing standardized testing procedures to ensure reliability and performance.

#### 8.3.1.4 ASSEMBLY INTEGRATION CHALLENGES

Complex assemblies require precise coordination to ensure smooth integration and avoid delays. To mitigate this risk, strategies include developing detailed assembly procedures and checklists, conducting mock assembly testing before final integration, and assigning a dedicated integration team to oversee the process and address any issues in real-time.

### **8.3.2 TESTING PROGRAM RISKS**

Delays in testing can impact overall project timelines and prevent timely identification of technical issues.

#### **8.3.2.1 TEST SITE AVAILABILITY**

Limited test site availability can cause delays in scheduled firings and system evaluations, impacting project timelines. To mitigate this risk, strategies include advanced booking of test sites with built-in schedule flexibility, establishing backup test locations, and coordinating with regulatory agencies to streamline site approvals.

#### **8.3.2.2 WEATHER CONSTRAINTS**

Adverse weather conditions can disrupt outdoor testing and transportation schedules, leading to potential delays. To mitigate this risk, strategies include scheduling tests during seasons with historically stable weather, developing indoor testing setups for critical subsystems, and implementing weather monitoring systems to anticipate and plan for potential delays.

#### **8.3.2.3 EQUIPMENT AVAILABILITY**

Limited access to necessary testing equipment can hinder validation efforts and delay project progress. To mitigate this risk, strategies include maintaining an updated list of required test equipment, partnering with universities and research institutions for shared access, and renting equipment when purchasing is not a viable option.

#### **8.3.2.4 TEST SCHEDULE DELAYS**

Unexpected issues during testing can lead to setbacks in the overall project timeline, affecting development milestones. To mitigate this risk, strategies include developing contingency schedules with built-in buffer time, conducting thorough pre-test checklists to minimize unexpected failures, and parallelizing test activities where possible to maximize efficiency. Additional recommendations include implementing automated testing procedures to streamline validation efforts and conducting regular risk assessments to proactively identify and address potential delays.

### **8.3.3 COMPETITION TIMELINE RISKS**

The project must meet specific deadlines to ensure successful participation in the Launch Canada competition. Regulatory and logistical constraints must be considered.

#### **8.3.3.1 REGULATORY APPROVAL DELAYS**

Failure to obtain required permits and approvals can significantly halt project progress. To mitigate this risk, current strategies include early engagement with regulatory authorities to fully understand compliance requirements, assigning a dedicated compliance officer to track approvals, and maintaining detailed documentation to streamline the approval process.

#### **8.3.3.2 DOCUMENTATION REQUIREMENTS**

Failure to submit required documentation on time or with complete accuracy can result in disqualification or project hold-ups. To mitigate this risk, current strategies include establishing a centralized documentation repository for organized record-keeping, assigning team members to track and compile necessary reports, and conducting periodic audits to ensure compliance with submission requirements.

#### **8.3.3.3 TRANSPORTATION LOGISTICS**

Transporting the propulsion system, test equipment, and support structures to the competition site presents significant logistical challenges. To mitigate these risks, current strategies include detailed transport planning with pre-shipment inspections to ensure all components are secure, partnering with logistics companies for reliable and timely delivery, and designing modular components to simplify transportation and assembly at the site.

#### **8.3.3.4 Resource Allocation Issues**

Competing demands for funding, personnel, and material resources can create bottlenecks that hinder project progress. To mitigate these challenges, current strategies include regular financial tracking and forecasting to ensure efficient budget management, prioritizing resource allocation based on critical project milestones, and actively seeking external sponsorships and funding opportunities to supplement available resources.

### **8.4 RISK ASSESSMENT MATRIX**

The risk assessment matrix provides a structured methodology for evaluating and prioritizing project risks based on their probability and impact. By systematically categorizing risks, the team can focus resources on mitigating high-priority risks while monitoring lower-priority ones. This section details the evaluation criteria and prioritization approach used to assess safety, technical, and resource-related risks.

## **8.4.1 RISK EVALUATION CRITERIA**

To quantify the risks associated with the Chimera engine project, each identified risk is evaluated based on probability, severity, and mitigation effectiveness. These factors are assigned numerical values to determine an overall risk score.

### **8.4.1.1 PROBABILITY RATINGS**

Probability represents the likelihood of a given risk occurring during project execution. Risks are categorized into five levels:

Table 8.4.1: Risk matrix probability standardization.

<b><i>Risk Level</i></b>	<b><i>Likelihood</i></b>	<b><i>Rating</i></b>
Almost Certain	>90%	5
Likely	70-90%	4
Possible	40-70%	3
Unlikely	10-40%	2
Rare	<10%	1

### **8.4.1.2 SEVERITY RATINGS**

Severity refers to the impact a risk would have on the project if it were to materialize. The ratings range from minimal disruption to catastrophic failure.

Table 8.4.2: Risk rating severity system description.

<b><i>Rating</i></b>	<b><i>Severity Description</i></b>	<b><i>Impact</i></b>
5	Catastrophic	Total mission failure, loss of system.
4	Major	Severe delays, significant damage, loss of critical function.
3	Moderate	Minor damage, repairable failure, moderate delays.
2	Minor	Minimal impact, easily recoverable.
1	Negligible	No significant impact, minor inconvenience.

#### **8.4.1.3 RISK CATEGORIES**

Risks are grouped into broad categories to facilitate effective mitigation planning.

- **Safety Risks:** Risks that may endanger personnel, equipment, or the environment.
- **Technical Risks:** Risks that could impact system performance or mission success.
- **Schedule Risks:** Risks related to testing and project timeline delays.
- **Resource Risks:** Risks involving funding, component procurement, or facility availability.

#### **8.5.1.4 MITIGATION EFFECTIVENESS**

Mitigation effectiveness evaluates how well existing strategies reduce the likelihood or impact of a given risk. Ratings range from low (minimal mitigation in place) to high (multiple layers of risk reduction strategies).

Table 8.5.3: Mitigation Effectiveness Matrix

<b>Rating</b>	<b><i>Mitigation Effectiveness Description</i></b>
High	Redundant safety measures, continuous monitoring, extensive testing.
Medium	Some preventive controls are in place, but gaps exist.
Low	Limited or no existing mitigation measures.

#### **8.4.2 RISK PRIORITIZATION**

Using the probability and severity ratings, risks are prioritized to determine where mitigation efforts should be concentrated.

#### **8.4.2.1 HIGH-PRIORITY RISKS**

Risks with high probability and severity scores require immediate attention. These risks could lead to catastrophic failure, severe delays, or major safety hazards. Example high-priority risks include:

- **Nitrous Oxide Thermal Decomposition:** Potential for rapid exothermic reaction if improperly handled.
- **Valve Sequencing Errors:** Could result in combustion instability or loss of control.

- **Test Site Availability:** Lack of secured facilities could delay testing phases.

#### **8.4.2.2 MEDIUM-PRIORITY RISKS**

Medium-priority risks have either a moderate probability or severity rating but do not pose immediate threats to project success. These risks are actively monitored and mitigated as necessary. Such risks include:

- **Injector Performance Variability:** Could affect engine efficiency but is mitigated through testing.
- **Equipment Availability:** Delays in test hardware could slow progress but are manageable.
- **Documentation Compliance:** While critical, it is generally within team control to resolve.

#### **8.4.2.3 LOW-PRIORITY RISKS**

Risks that have a low probability and severity are considered manageable without significant intervention. These risks are periodically reviewed to ensure they do not escalate. Examples include:

- **Minor Component Quality Issues:** Typically resolvable through standard quality control procedures.
- **Weather Constraints:** Could delay outdoor testing but mitigated by scheduling flexibility.
- **Software Bugs in Telemetry:** Usually correctable without major system impact.

#### **8.4.2.4 MONITORING REQUIREMENTS**

For risks that fall into the medium- and high-priority categories, ongoing monitoring is essential. Regular risk review meetings, data tracking, and contingency planning ensure that risks remain controlled. The following strategies are implemented for effective monitoring:

- Regular risk assessments at key project milestones
- Automated alerts for critical telemetry or system failures
- Scheduled safety and quality assurance audits
- Real-time project tracking for schedule and resource constraints

The risk matrix in the next section visually maps identified risks based on their probability and severity scores, facilitating strategic decision-making in risk mitigation planning.

## 8.5 RISK MATRICES

Table 8.5.1: Safety Risk Matrix

<b>Risk</b>	<b>Category</b>	<b>Probability</b>	<b>Severity</b>	<b>Risk Score</b>
Nitrous Oxide Thermal Decomposition	Propulsion	2	5	10
Pressure Vessel Failure	Propulsion	4	5	20
Premature Ignition	Propulsion	4	4	16
Valve Sequencing Errors	Propulsion	3	5	15
Flow Control Issues	Propulsion	2	3	6
Support Tower Failure	Structural	4	4	16
Lift System Malfunction	Structural	3	4	12
Engine Mount Failure	Structural	4	3	12
TVC System Structural Issues	Structural	3	3	9
Chemical Exposure	Personnel Safety	2	5	10
High Pressure Systems	Personnel Safety	3	5	15
Fire/Explosion Hazards	Personnel Safety	4	5	20
Mechanical Hazards	Personnel Safety	2	4	8

Table 8.5.2: Technical Risk Matrix

<b>Risk</b>	<b>Category</b>	<b>Probability</b>	<b>Severity</b>	<b>Risk Score</b>
Injector Performance	Combustion	3	4	12
Chamber Liner Degradation	Combustion	3	4	12
Combustion Instability	Combustion	4	5	20
Ignition Reliability	Combustion	4	3	12

Sensor Failures	Control	3	4	12
Data Acquisition Issues	Control	3	3	9
Communication Loss	Control	3	5	15
Software Malfunctions	Control	3	4	12
Actuator Performance	TVC	3	4	12
Gimbal Mechanism Issues	TVC	3	3	9
Control Algorithm Failures	TVC	3	4	12
Position Feedback Errors	TVC	2	4	8

Table 8.5.3: Schedule Risk Matrix

<b>Risk</b>	<b>Category</b>	<b>Probability</b>	<b>Severity</b>	<b>Risk Score</b>
Component Procurement Delays	Manufacturing	4	4	16
Machine Shop Availability	Manufacturing	3	3	9
Quality Control Issues	Manufacturing	3	4	12
Assembly Integration Challenges	Manufacturing	3	3	9
Test Site Availability	Testing	4	4	16
Weather Constraints	Testing	3	3	9
Equipment Availability	Testing	3	3	9
Test Schedule Delays	Testing	3	4	12
Regulatory Approval Delays	Competition	4	4	16
Documentation Requirements	Competition	3	3	9
Transportation Logistics	Competition	3	3	9
Resource Allocation Issues	Competition	3	3	9



## REFERENCES

- [1] Aqua Environment, "873-D High Flow Dome Loaded Reducing Regulators," Aqua Environment, [Online]. Available: <https://valvesandregulators.aquaenvironment.com/viewitems/high-flow-reducing-regulators-2/873-d-high-flow-dome-loaded-reducing-regulators>. [Accessed: 31-Jan-2025].
- [2] Launch Canada, *Design, Test & Evaluation Guide*, Revision 3, Launch Canada, Nov. 1, 2024.
- [3] Asia Industrial Gases Association (AIGA), *Safe Practices for Storage and Handling of Nitrous Oxide*, AIGA 081/20, Rev. of AIGA 081/16, Nov. 2020. [Online]. Available: <http://www.asiaiga.org>. [Accessed: 01-Feb-2025].
- [4] Swagelok Pittsburgh, "What is Fluid System Creep?" Swagelok Pittsburgh, [Online]. Available: <https://pittsburgh.swagelok.com/en/about-us/blog/news-item-35-what-is-fluid-system-creep>. [Accessed: 31-Jan-2025]
- [5] Zook Enterprises, LLC, "PB Rupture Disk," Zook, [Online]. Available: <https://zookdisk.com/products/pb-rupture-disk/>. [Accessed: 31-Jan-2025].
- [6] Aqua Environment, "1094 Open/Close Valves," Aqua Environment, [Online]. Available: <https://valvesandregulators.aquaenvironment.com/viewitems/high-flow-open-close-valves-2/1094-open-close-valves>. [Accessed: 31-Jan-2025].
- [7] Half Cat Rocketry, "Mojave Sphinx," Half Cat Rocketry, [Online]. Available: <https://www.halfcatrocketry.com/mojave-sphinx>. [Accessed: 31-Jan-2025].
- [8] M. A. K. A. Kul, Y. Seymen, M. E. Yıldız, and S. M. Köroğlu, (PDF) preliminary design, basic simulation and optimization of Liquid Rocket Engines, [https://www.researchgate.net/publication/317841320\\_Preliminary\\_Design\\_Basic\\_Simulation\\_and\\_Optimization\\_of\\_Liquid\\_Rocket\\_Engines](https://www.researchgate.net/publication/317841320_Preliminary_Design_Basic_Simulation_and_Optimization_of_Liquid_Rocket_Engines) (accessed Nov. 10, 2024).
- [9] M. Lazzarin, N. Bellomo, F. Barato, and A. Bettella, (PDF) testing and CFD simulation of diaphragm hybrid rocket motors, [https://www.researchgate.net/publication/262033007\\_Testing\\_and\\_CFD\\_Simulation\\_of\\_Diaphragm\\_Hybrid\\_Rocket\\_Motors](https://www.researchgate.net/publication/262033007_Testing_and_CFD_Simulation_of_Diaphragm_Hybrid_Rocket_Motors) (accessed Nov. 10, 2024).
- [10] Falk, A. Y. Space Storable Propellant Performance--Gas/Liquid Like-Doublet Injector Characterization, Final Report, R-8973 (NASA CR-120935), Rocketdyne, a division of Rockwell International, Canoga Park, California, October 1972

- [11] W. J. Carter and B. E. Ball, ASME Section VIII Div. 1, Pressure Vessels. McGraw-Hill Professional Publishing, 2023.
- [12] D. R. Batha, M. D. Carey, J. G. Campbell, C. D. Coulbert, and M. E. Goodhart, *Thrust Chamber Cooling Techniques For Spacecraft Engines*. 1963, p. 17.
- [13] "CHAMBERSAFE," *Half Cat Rocketry*. <https://www.halfcatrocketry.com/chambersafe>
- [14] Parker Hannifin Corporation, *Parker O-Ring Handbook*, ORD 5700, Parker Hannifin Corporation. [Online]. Available: <https://www.parker.com/content/dam/Parker-com/Literature/O-Ring-Division-Literature/ORD-5700.pdf>. [Accessed: 31-Jan-2025].
- [15] E. R. Stepp, *Thrust Vector Control Load Predictions*, NASA Technical Report, ER63, Rev. 05, 2024. [Online]. Available: [https://ntrs.nasa.gov/api/citations/20240010637/downloads/Stepp\\_ER63\\_TVC\\_Load\\_Predictions\\_rev05.pdf](https://ntrs.nasa.gov/api/citations/20240010637/downloads/Stepp_ER63_TVC_Load_Predictions_rev05.pdf). [Accessed: 01-Feb-2025].
- [16] G. P. Sutton and O. Biblarz , "Rocket Propulsion Elements, 9th edition," Wiley.com, <https://www.wiley.com/en-au/Rocket+Propulsion+Elements%2C+9th+Edition-p-9781118753651> (accessed Nov. 10, 2024).
- [17] Half Cat Rocketry, "PV Design," Half Cat Rocketry, [Online]. Available: <https://www.halfcatrocketry.com/pv-design>. [Accessed: 31-Jan-2025].
- [17] MatWeb, "ASM Material Data Sheet: 6061-T6 Aluminum," MatWeb, [Online]. Available: <https://asm.matweb.com/search/specifymaterial.asp?bassnum=ma6061t6>. [Accessed: 31-Jan-2025].
- [18] H. Ghassemi and H. F. Fasih, "Application of small size cavitating venturi as flow controller and flow meter," *Flow Measurement and Instrumentation*, vol. 22, no. 5, pp. 406–412, Oct. 2011. [Online]. Available: <https://doi.org/10.1016/j.flowmeasinst.2011.05.001>. [Accessed: 01-Feb-2025].
- [19] M. C. Louwerse, M. N. W. Groenendijk, H. V. Jansen, and M. C. Elwenspoek, (PDF) nozzle fabrication for Micropulsion of a microsatellite, [https://www.researchgate.net/publication/231136007\\_Nozzle\\_fabrication\\_for\\_micropulsion\\_of\\_a\\_microsatellite](https://www.researchgate.net/publication/231136007_Nozzle_fabrication_for_micropulsion_of_a_microsatellite) (accessed Nov. 10, 2024).
- [20] E. A. R. and K. B., Jr. R., "Solid rocket motor nozzles - NASA technical reports server (NTRS)," NASA, <https://ntrs.nasa.gov/citations/19760013126> (accessed Nov. 10, 2024).
- [21] G. V. R. Rao, Exhaust Nozzle Contour for Optimum Thrust,

<https://arc.aiaa.org/doi/abs/10.2514/8.7324?journalCode=jjp> (accessed Nov. 10, 2024).

- [22] A. Khan, S. Kumar, H. Chowdary, and S. Sharath, (PDF) design of a supersonic nozzle using method of characteristics,  
[https://www.researchgate.net/publication/281029694\\_Design\\_of\\_a\\_Supersonic\\_Nozzle\\_using\\_Method\\_of\\_Characteristics](https://www.researchgate.net/publication/281029694_Design_of_a_Supersonic_Nozzle_using_Method_of_Characteristics) (accessed Nov. 10, 2024).
- [23] P. K. Bahumanyam, Y. D. Dwivedi, and N. K. Mishra, (PDF) design of Supersonic Wind Tunnel using method of characteristics,  
[https://www.researchgate.net/publication/273460548\\_Design\\_of\\_supersonic\\_wind\\_tunnel\\_using\\_method\\_of\\_characteristics](https://www.researchgate.net/publication/273460548_Design_of_supersonic_wind_tunnel_using_method_of_characteristics) (accessed Nov. 10, 2024).
- [24] J. Singh, L. E. Zerpa, B. Partington, and J. Gamboa, “Effect of nozzle geometry on critical-subcritical flow transitions,” *Heliyon*,  
<https://www.sciencedirect.com/science/article/pii/S2405844018374164> (accessed Nov. 10, 2024).

## APPENDIX A - FLUID SYSTEM CALCULATIONS AND SIZING

### APPENDIX A.1: TRANSIENT ENGINE PERFORMANCE CALCULATIONS

The main factor influencing the transient thrust reduction of the engine is the drop in nitrous supply pressure. To model the reduction in supply pressure during the 9.2 second burn, a thermodynamic model of the tank was created. Due to the relatively short burn duration, heat transfer from the surrounding environment was neglected from the model. The following system of differential equations was implemented into a time-based iterative solver to compute the tank temperature, liquid nitrous mass and gaseous nitrous mass in the tank. Derivations of the proceeding equations have not been included in this paper and have been left as an exercise for the reader.

$$(n_{2l}C_{Vl} + n_{2v}C_{vv})\frac{dT}{dt} = \frac{dn_{2l}}{dt}(P\hat{V}_l) + \frac{dn_{2v}}{dt}(RT - \Delta H_{vap}) \quad (A.5)$$

$$\frac{dn_{2l}}{dt} + \frac{dn_{2v}}{dt} = \frac{A(10^3)}{MM}\sqrt{P_i\rho_i}\frac{\eta_{crit}}{\sqrt{\omega}} \quad (A.6)$$

$$\frac{dT}{dt} \left[ \frac{dP_0^{sat}}{dT} V_T - n_{2l} \hat{V}_{2l} \frac{dP_0^{sat}}{dT} - n_{2v} R \right] - \hat{V}_{2l} P_0^{sat} \frac{dn_{2l}}{dt} - RT \frac{dn_{2v}}{dt} \quad (A.7)$$

where

$n_{2l}$ : Moles of nitrous liquid

$n_{2v}$ : Moles of nitrous vapor

$C_{Vl}$ : Specific heat of nitrous liquid

$C_{vv}$ : Specific heat of nitrous vapor

T: Temperature

$\Delta H_{vap}$ : Heat of vaporization

$\hat{V}_l$ : Molar volume of liquid nitrous

$V_T$ : Total nitrous tank volume

$P_0^{sat}$ : Nitrous saturation pressure

$\eta_{crit}$ : Injector critical pressure ratio

$P_i$ : Injector inlet pressure

$\rho_i$ : Injector inlet density

The critical flow parameters through the injector were computed using the omega model. The critical pressure ratio and  $\omega$  can be computed using (A.8) and (A.9) respectively.

$$\eta_{crit}^2 + (\omega^2 - 2\omega)(1 - \eta_{crit})^2 + 2\omega^2 \ln(\eta_{crit}) + 2\omega^2(1 - \eta_{crit}) = 0 \quad (A.8)$$

$$\omega = \frac{x_i v_{lgi}}{v_i} + \frac{c_{li} T_i P_i}{v_i} \left( \frac{v_{lgi}}{h_{lg,i}} \right)^2 \quad (A.9)$$

where

$x_i$ : Vapor quality at injector inlet

$v_{lgi}$ : Difference between specific volumes of liquid and gas

$v_i$ : Inlet specific volume

$h_{lg,i}$ : Difference in enthalpy of liquid and gas

$c_{li}$ : Liquid specific heat capacity at inlet

The preceding equations were used to produce Figures 5.1.1.1 and 5.1.1.2. To validate the model, simulations of the two-phase nitrous discharge were performed using Flownex. The resulting plot of pressure with respect to time has been presented in Figure A.1.1.

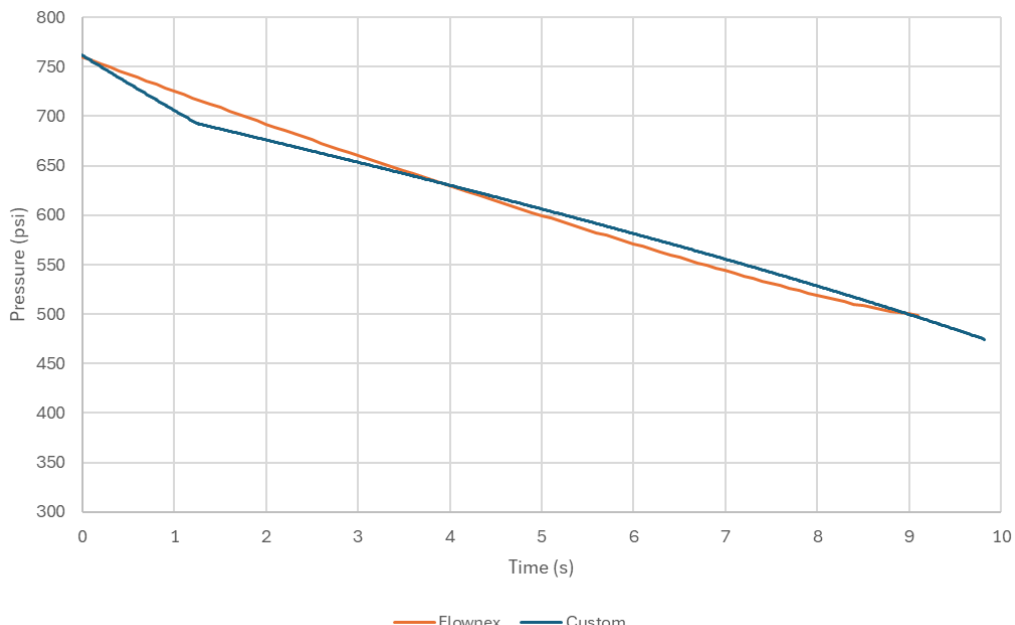


Figure A.1.1: Pressure (psi) vs. Time (s) for Custom and Flownex Models

It is important to note that the identical injector orifice area and discharge coefficient were used for both models. As demonstrated in Figure A.1.1, the custom model agrees reasonably well with the results predicted by Flownex. A summary of the flow parameters has been provided in Table A.1.1.

Table A.1.1: Custom Model & Flownex Model Results

Parameter	Flownex	Custom	% Difference
Initial Mass Flow Rate	2.54 kg/s	2.79 kg/s	9.8%
Final Mass Flow Rate	1.99 kg/s	1.59 kg/s	25%
Final Pressure	474 psi	498 psi	5.1%
Liquid Discharge Time	9.1s	9.8s	7.7%

As demonstrated in Table A.1.1 a maximum deviation of 25% is observed between the Flownex and custom models for the final mass flow rate. What is interesting is that flownex predicts a lower initial mass flow rate and a higher final mass flow rate relative to the custom model. However, since the objective of the model is to accurately predict the transient pressure and mass discharge profiles, the deviation in the final mass flow rates was deemed to be acceptable as the remaining errors were under 10%.

The computed final nitrous mass flow rate was used to calculate the chamber pressure at the end of the burn. Chamber pressure can be expressed as a function of  $C^*$  and throat area using (A.10).

$$P_o = \frac{\eta_v * C^* \dot{m}}{A_t} \quad (A.10)$$

Through consultation of experimental hotfire data, the  $C^*$  efficiency was approximated to be 83 %. Since  $C^*$  is a function of chamber pressure, a trial and error approach was utilized using CEA to calculate the chamber pressure. The iterative solution process converged on a final chamber pressure of 217 psi with a predicted  $C^*$  of 1224.1 m/s. To estimate the  $I_{sp}$ , the thrust coefficient was first calculated. The vacuum thrust coefficient was calculated since the experimental hotfire data only provided a vacuum thrust coefficient correction factor. Previous GAR-E hotfire test data was not used as the thrust data collected was not of

sufficient fidelity to determine a thrust coefficient efficiency. Equation (A.11) was used to compute the theoretical vacuum thrust coefficient.

$$(C_t)_{vacuum} = \sqrt{\frac{2\gamma^2}{\gamma-1} \left( \frac{2}{\gamma+1} \right)^{\frac{\gamma+1}{\gamma-1}} \left[ 1 - \left( \frac{P_e}{P_0} \right)^{\frac{\gamma-1}{\gamma}} \right]} + \varepsilon \left( \frac{P_e}{P_0} \right) \quad (A.11)$$

The theoretical vacuum thrust coefficient was multiplied by the thrust coefficient efficiency factor of 97.4% to estimate the actual vacuum thrust coefficient. Equation (A.12) was used to convert the vacuum thrust coefficient to the sea-level thrust coefficient.

$$(C_t) = (C_t)_{vacuum} - \varepsilon \left( \frac{P_{ambient}}{P_0} \right) \quad (A.12)$$

Application of A.12 yielded a final thrust coefficient of 1.31. The product of the thrust coefficient and C\* yielded an effective exhaust velocity of 1225.4 m/s and a corresponding I<sub>sp</sub> of 125 s. Use of a final total mass flow rate of 1.59 kg/s yielded a thrust of 817 lbf. Thus, a 41% reduction in thrust is expected for the 9.2 second burn duration.

## APPENDIX A.2 PRESSURANT TANK DISCHARGE MODELLING

Two models were created to simulate the transient pressure profile of the pressurant discharge. The first model was a custom model created in MATLAB that accounted for basic isenthalpic expansion effects. The second model was created using built-in fluid system components in flownex. The model simulates both the liquid ethanol discharge and gaseous pressurant expansion.

The initial conditions of the model include the tank volume, temperature, pressure, and regulator outlet pressure. During the design process, the required tank volume and pressure combination was not known, and was therefore iteratively determined using the model results with an initial set of assumed values.

For the custom model the initial conditions were used to determine the initial mass of nitrogen in the pressurant tank by application of the ideal gas law. This model works by subtracting the computed mass flow from the tank from the initial tank mass for each time increment of 0.01s.

From the computed mass, the subsequent density is calculated by dividing the new mass by the constant 6.8L tank volume. The ideal gas adiabatic expansion equations are then used to relate the density to the pressure and temperature. The density, temperature, and pressure are related according to (A.4.1) and (A.4.2).

$$P_0 = P_{0(initial)} \left( \frac{\rho_o}{\rho_{o(initial)}} \right)^{\gamma} \quad (\text{A.4.1})$$

$$T = T_{0(initial)} \left( \frac{\rho_o}{\rho_{o(initial)}} \right)^{\gamma-1} \quad (\text{A.4.2})$$

In the custom model, the mass flow rate is calculated by modeling the flow through the regulator as isenthalpic. This assumption is generally regarded as acceptable for modeling flow through valves and pressure regulators. For each time increment, the process of computing the nitrogen mass flow is iterative and has therefore been simplified in Figure A.4.1.

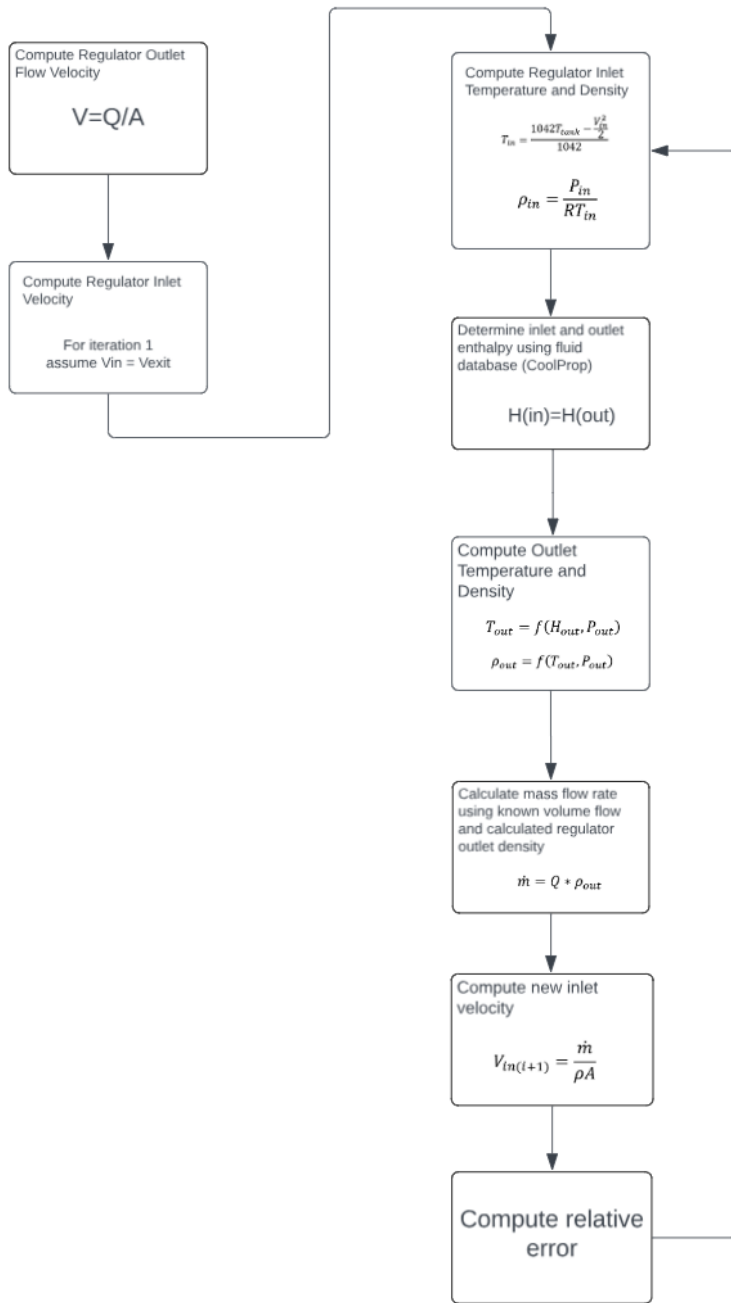


Figure A.2.1: Nitrogen Mass Flow Rate Computation Flow Chart

The flownex model starts with the same initial conditions as the custom model. The pressurant tank is modeled using the constant volume reservoir element, which is characterized by an inputted volume. A pressure and temperature boundary condition of 3100 psi and 21C was placed on this tank for the initial steady-state solution. The dome-loaded pressure regulator is

modeled using the built-in pressure regulating valve element. The flownex regulating valve element is unable to account for real-world transient effects like droop, and was therefore configured to output the expected steady-state outlet pressure of 800 psi per the analysis presented in Section 5.1.2.1. The ethanol tank and the corresponding ullage volume was modeled using the top and bottom container interface elements. These elements are configured such that the total volume is kept constant and therefore equal to the total ethanol tank volume. The initial liquid-gas interface height is inputted into the simulation, allowing for control over the initial mass of liquid ethanol in the tank.

The ethanol run line was modeled using standard pipe, valve, venturi and orifice elements. The tubes were modeled using the standard flownex pipe element with an internal diameter of 0.43 inches and a smoothness of 30 micrometers (Standard smoothness for stainless steel tubing per the built-in flownex database). As it is intended for a section of flexible hose to exist between the main valve and injector, this was modeled as a tube with an inner diameter of 0.43 inches and a roughness of 3250 micrometers. The lengths and geometries of these sections were highly approximated and largely based on ballpark values taken from the system's CAD model. The main valve was modeled using the basic valve element with a defined flow coefficient of 5.5 in the fully open position. The ethanol cavitating venturi was modeled using the 3 degree half angle venturi tube, which is able to account for choked flow due to cavitation. The calculated CdA of the throat was notably inputted as  $8.04 \text{ mm}^2$ . The injector was modeled using an orifice with an area equal to the combined area of all the injector elements. A discharge coefficient of 0.72 was assumed [16]. The model in Flownex can be observed in Figure A.4.1.

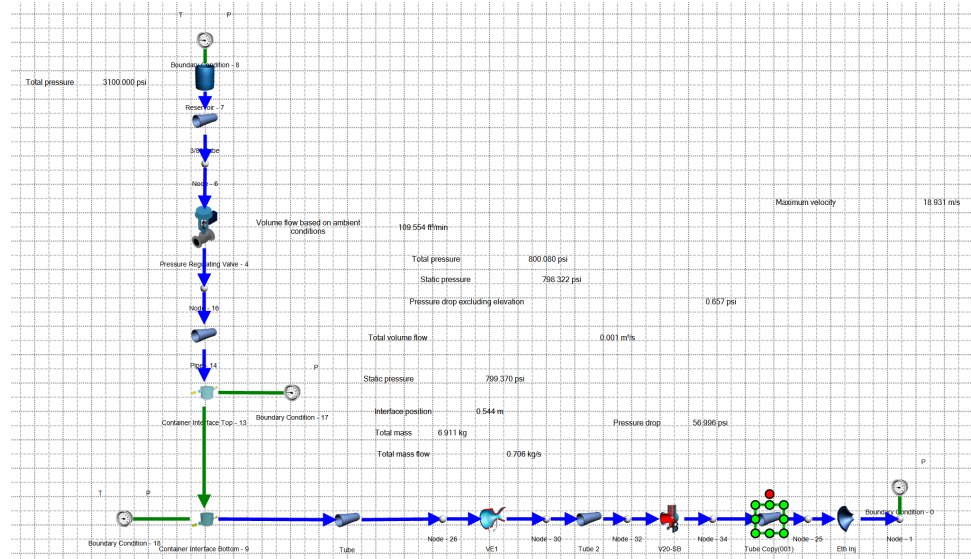


Figure A.2.1: Flownex model constrained for initial steady-state solution

To determine the transient pressure and volumetric flow rate, the boundary conditions placed on the tank were removed to remove the initial constraints on the tank pressures and temperatures. The results of the transient simulation have been provided in Figure 5.1.2.1.1 and 5.1.2.1.2, demonstrating that the system maintains adequate pressure and that the regulator is sufficiently sized per the current analytical predictions.

These results were compared to the custom MATLAB script results described above. These results can be observed in Figure A.4.2 and A.4.3.

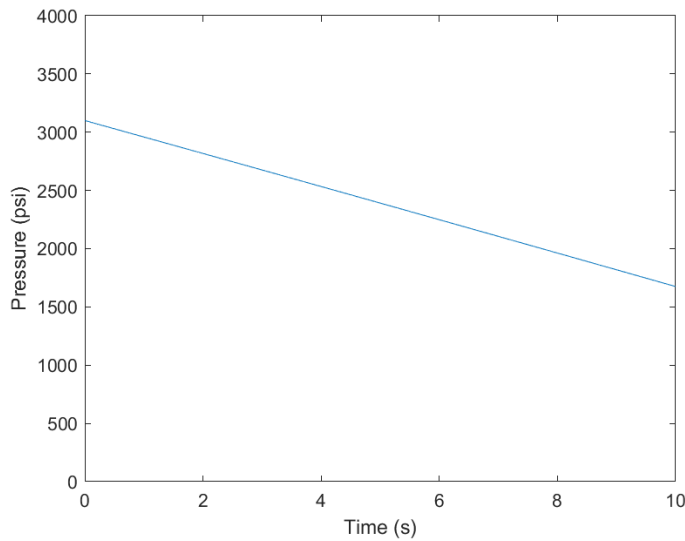


Figure A.2.2: Predicted pressurant tank pressure vs. time (Custom MATLAB model)

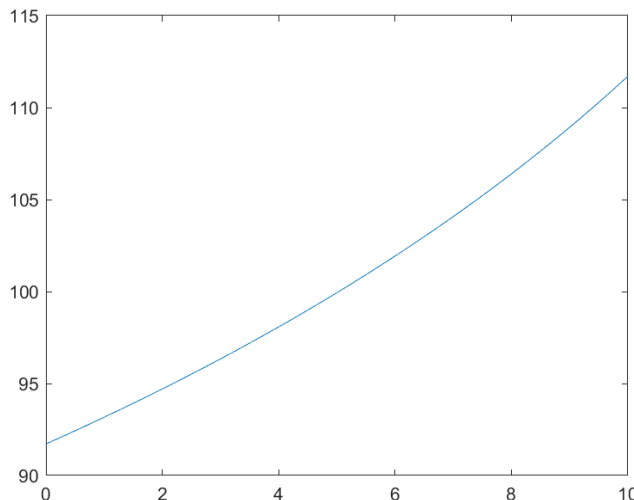


Figure A.2.3: Predicted regulator volumetric flow rate vs. time (Custom MATLAB model)

Comparison to the flownex results revealed that the standard adiabatic expansion model tended to predict a higher final pressure and lower transient volumetric flow rate increase. A possible source for this deviation could be the use of CoolProp for the fluid properties in the MATLAB script. From previous experience with the plugin, while generally reliable, it can provide erroneous results at times, often deviating significantly from what is provided by superior sources like well-established equations of state or RefProp. It is also important to note that the assumption of adiabatic expansion, while likely valid due to the relatively short burn duration, represents an idealized scenario and therefore acts as a source of error. Since the Flownex results were much more conservative and likely more accurate due to the solution method that the software used, it was used for the sizing process presented in the preceding sections of the report.

## APPENDIX A.3 TANK SIZING

The nominal burn duration is 9.2 seconds and assumed operating temperature is 21°C. At the assumed operating temperature, the density of ethanol is 789.6 kg/m<sup>3</sup>. Thus, the ethanol volume can be calculated as follows.

$$V_{EtOH} = \frac{(\dot{m} * \Delta t)}{\rho^{0.95}} = 7L \quad (A.5.1)$$

To compute the ethanol tank size, an assumed ullage volume of 2.5% was used based on previous design experience of systems using ethanol as fuel. Accounting for the ullage volume results in the required pressure vessel volume. The computation can be performed as follows.

$$V_{EtOH, req} = 1.025 * V_{EtOH} = 7.2L \quad (A.5.2)$$

As mentioned in Section 5.1.2.2.1, the casing was cut slightly longer than required during manufacturing. This resulted in a final tank volume of 7.4L.

According to AIGA safe practices for handling of nitrous oxide, pressure vessel sizing should be done according to the appropriate filling ratio of the tank. The blowdown simulations highlighted in A1.1 yielded a required initial total nitrous mass of 23kg. According to AIGA safe practices for handling of nitrous oxide, local regulations in North America permit an admissible filling ratio of 0.68 kg/L [3]. Therefore, the required tank volume can be computed as follows.

$$V_{N2O, tank} = \frac{23}{0.68} \quad (A.5.3)$$

$$V_{N2O, tank} = 34L \quad (A.5.4)$$

## APPENDIX A.4 TANK STRESS ANALYSIS

Contrary to the SRAD tank design in last year's design report, the tank stress analysis was conducted entirely by hand. The proceeding process was selected over Finite Element Analysis as it was found that reliance on FEA resulted in significant oversizing of the retention pins for the tank bulkheads. This is caused by the ambiguity associated with bearing stress, a phenomenon that is commonly approximated with basic hand calculations among many amateur rocketry teams. Per the relief valve sizing, the MEOP of the ethanol tank was determined to be 1030 psi. This was the higher of the two, and served as the baseline MEOP for the design process. Four failure modes were considered for the stress analysis: pin shear, pin tearout, tensile failure at the minimum cross-section, and bearing failure.

Due to the extensive amount of time and effort required to tap bolt holes, the team decided to use 24 18-8 steel clevis pins as the retention mechanism for the bulkheads. The tensile strength of the pins per the manufacturer was 72000 psi. To approximate the shear strength, this value was multiplied by 0.6 to yield a shear strength of 43200 psi. The OD of the pin is 0.25". The shear stress per pin was calculated as follows:

$$\tau = \frac{PA_{bulkhead}}{nA_{shear}} \quad (\text{A.6.1})$$

Where,

P: Pressure on bulkhead (MEOP)

$A_{bulkhead}$ : Internal bulkhead area

n: Number of pins

A: Shear area of pin

Substitution of the preceding values yields a shear stress of 21727 psi per clevis pin. Dividing the shear strength by the shear stress per pin yields a FOS for pin shear of 1.988. Per the HalfCat pressure design guide The area on which this shear stress acts can be found by multiplying the distance between the edge of the fastener hole and the edge of the casing by the thickness of the casing, then multiplying by two for each bolt [17]. The center of each pin is located 1" from the edge of the casing. Thus, the tear-out stress can be calculated as follows:

$$\sigma_{tear} = \frac{PA_{bulkhead}}{2tn(E - \frac{d_{pin}}{2})} \quad (\text{A.6.2})$$

Where,

t: Tank thickness

E: Distance from center of pin to tank edge

Application of (A.6.2) yields a tear out stress of 3250 psi. Considering that the shear strength of 6061-T6 aluminum is 30000 psi, the FOS for tear-out was calculated to be 9.2. Tensile failure at the minimum cross-section is considered to occur at the location of the pin midpoints. The cross sectional area at this point is approximated by subtracting the pin diameter from the circumference of the casing, and multiplying the difference by the casing thickness to determine the cross-sectional area. The tensile stress was therefore calculated as follows:

$$\sigma_{tensile} = \frac{PA_{bulkhead}}{nt[(D_{o,casing}-t)\pi - n^*d_{pin}]} \quad (\text{A.6.3})$$

The FOS for yield is defined with respect to the yield strength of the casing material. Per consultation of the supplier's MTR report, this was determined to be 35000 psi. Application of A.6.3 therefore resulted in a yield FOS of 3.1. Bearing stress was approximated by assuming that the pin force applied to the corresponding projected area. This value was then compared to the bearing yield strength to determine the corresponding FOS. The bearing stress was therefore calculated as follows:

$$\sigma_{bearing} = \frac{PA_{bulkhead}}{nd_{pin}t} \quad (\text{A.6.4})$$

The bearing yield strength of 6061-T6 aluminum was determined to be 56000 psi per consultation with [17]. The FOS for bearing yield was therefore calculated to be 2.5. FEA of this configuration indicated that yielding would occur. However, slight yielding of the material subjected to bearing stress is not entirely unexpected nor is it something that would be considered as failure of the tank. The localized yielding of material surrounding the pin is likely to be in such a way that reduces the bearing stress on the casing to a level that is sufficient to achieve an equilibrium position. To accurately capture this phenomenon, additional computational effort into more complex FEA would have been required. It is for this reason that the preceding method is commonly used to approximate the safety factors associated with bearing failure, resulting in an acceptable result that is more consistent with tank configurations used by other amateur rocketry teams.

## APPENDIX A.5 CAVITATING VENTURI SIZING

The assumed inlet pressures of the venturis are equivalent to the theoretical tank pressures. The initial throat area of each cavitating venturi is to be calculated according to the following [18]:

$$A_{th} = \frac{\dot{m}}{0.83 * \sqrt{2 * \rho * (P_{inlet} - P_{throat})}} \quad (\text{A.7.1})$$

With an assumed circular throat profile, application of the previous equation yields a throat diameter of 3mm for the ethanol venturi. This throat diameter was inputted into the Flownex model presented in Appendix A.4, which allowed for the pressure drop between the tank and venturi to be accounted for. This resulted in a final throat diameter of 3.2mm.

## APPENDIX B - THRUST VECTOR CONTROL ACTUATOR SIZING

### APPENDIX B.1 - ANALYSIS METHODOLOGY

All calculations for TVC are done using information from “Considerations for Thrust Vector Control In-Flight Load Prediction” by Nathaniel A. Stepp from NASA MSFC. When choosing what parameters to take into consideration when calculating actuator strength the main actuator load considerations include:

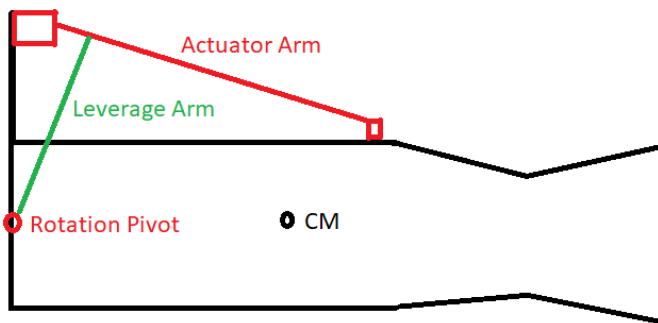
1. Translational vehicle acceleration acting on engine CM (typically LARGE contribution)
2. Radial Thrust vector offset (typically LARGE contribution)
3. Propellant feedline duct displacement from centre axis (typically MEDIUM contribution)
4. Momentum change in propellant feedline flow (typically SMALL contribution)
5. Gimbal bearing coulomb friction (typically SMALL contribution)
6. Angular vehicle velocity about the vehicle CM acting on the engine CM (typically SMALL contribution)
7. Anglue vehicle acceleration about the vehicle CM acting on CM (typically SMALL contribution)
8. Gravitational acceleration acting on engine CM (typically SMALL contribution)

Fortunately for static fire, there is no vehicle acceleration therefore (1), (6) and (7) are negligible in the analysis. As well our nitrous feed line is being run down the centre line of the engine so there is negligible resistance from propellant feedline therefore (3) and (4) and negligible in our analysis as well. Lastly the gimbal bearing friction would be a contributing factor (5), however

our design utilizes bearing with suitable static and dynamic strength so the friction is also negligible. Lastly the torque from the thrust (2) is also negligible because the thrust is transferred through the centre of the combustion chamber and basically having 0 torque on the whole system. Therefore maximum load on the TVC would come from the engine being perfectly horizontal and moving opposite to the actuator's pulling direction.

## APPENDIX B.2 - GRAVITATIONAL FORCE ACTING ON TVC

The maximum gravitational force acting on the TVC is when the engine is horizontal to the rotational pivot.



$$T_g = d * g * m$$

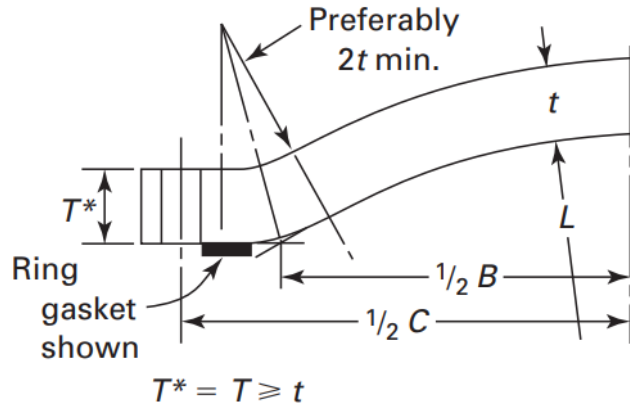
*d = the distance from engine CM to the pivot point*

The determined force needed was found to be about 50 lbf.

## APPENDIX C - INJECTOR STRESS ANALYSIS

### APPENDIX C.1 - INJECTOR LID DIMENSIONS

Table [A] presents a summary of each variable and its associated meaning. Values are given for pre-selected dimensions in the CAD model. All dimensions are in inches, and all stresses are in psi.



(c)

Figure C.1: Cutaway from Figure 1-6 in [A] (page 239) showing the desired lid geometry

Table 2-6 in [A] provides formulas for each moment arm for lap-type flanges. These are employed below.

$$h_D = \frac{C-B}{2} \quad (\text{D.1})$$

$$h_T = h_G = \frac{C-G}{2} \quad (\text{D.2})$$

Table C.1.1: Variables for rule-of-thumb head calculations according to [A]

Variable	Description	Value (in)
A	outside diameter of flange	7.5
B	inside diameter of flange	5.875
C	bolt-circle diameter	6.9
G	diameter at location of gasket load reaction. In this case, G = mean diameter of gasket contact face	6.057
S	Maximum allowable stress	45,000 psi
P	Operating pressure = MEOP * 2 x FOS	2030

$h_D$	radial distance from bolt circle to the circle on which $H_D$ (moment on D) acts	0.6875
$h_T$	radial distance from bold circle to the circle on which $H_T$ (moment on T) acts	0.5965
$h_G$	radial distance from gasket load reaction to the bolt circle	0.5965
$W_{m1}$	minimum required bolt load for the operating conditions	59,326.95 lbf
$M_0$	total moment acting upon the flange for the operating conditions	80,417.68 lbf*in

Minimum required bolt load  $W_{m1}$  is calculated according to Mandatory Appendix 2: 2-5 eq.

(1):

$$W_{m1} = 0.785G^2P + (2b \times 3.14GmP) \quad (D.3)$$

where  $m$  is the gasket factor according to Table 2-5.1. For self energizing types such as o-rings,  $m = 0$  and  $W_{m1}$  simplifies to:

$$W_{m1} = 0.785G^2P = 59,326.95 \text{ lbf}$$

$$M_0 = W_{m1}(h_D + h_T + h_G) = 80,417.68 \text{ lbf}$$

The head thickness is calculated below, applying Mandatory Appendix 1: 1-6 eq. (4):

$$t = \frac{5PL}{6S} = 0.248 \text{ in}$$

Flange thickness is calculated from Mandatory Appendix 1: 1-6 eq. (5):

$$T = Q + \sqrt{\frac{1.875M_0(C+B)}{SB(7C-5B)}}$$

Where

$$Q = \frac{PL}{4S} \left( \frac{C+B}{7C-5B} \right) = 0.0502$$

Thus,

$$T = 0.6707 \text{ in}$$

From these values it was determined that a head thickness of 0.250" and a flange thickness of 0.67" would be sufficient.

#### APPENDIX C.2 - INJECTOR FLANGE BOLT COUNT

Taking the normal force given dimension B in Table D.1.1 at 2 x MEOP,

$$F = PA = 2060 \text{ psi} \times \frac{\pi}{4} (5.875)^2 = 55,843.53 \text{ lbf}$$

This is in slight disagreement with the ASME Code results calculated in Appendix A for maximum bolt load  $W_{m1}$ , which gave 59,326.95 lbf. As such, the higher of the two values is used below.

From McMaster-Carr, the ultimate tensile strength of a high strength grade 8 steel hex  $\frac{1}{4}$ -20" bolt is 150,000 psi.

Hence the total number of bolts required N is:

$$N = \frac{F}{UTS \times \frac{\pi}{4}(d_{min})^2} = \frac{59,326.95}{150,000 \times \frac{\pi}{4}(0.1905)^2} = 13.87$$

Where  $d_{min}$  is the minor diameter of the bolt.

## APPENDIX D - THRUST CHAMBER NOZZLE

$$L = \lambda \cdot \frac{(\varepsilon^{\frac{1}{3}} - 1) \cdot R_t}{\tan(\theta_e)} \quad \varepsilon = \frac{\text{exit area}}{\text{throat area}} \quad \lambda = \text{linear scaling factor}$$

$$L = 0.8 \cdot \frac{(\varepsilon^{\frac{1}{3}} - 1) \cdot R_t}{\tan(\theta_e)} \quad \varepsilon = \frac{10.9859}{2.7759} \quad \lambda = 0.8$$

$$L = 0.8 \cdot \frac{(3.9576^{\frac{1}{3}} - 1) \cdot 0.94}{\tan(15^\circ)}$$

$$L = 2.77"$$

## APPENDIX E - THRUST CHAMBER SIZING

Chamber sizing was performed using a combination of CEA and Microsoft Excel. Several iterations were performed with various O/F ratios. These iterations will be presented in the LCR, however, a final O/F ratio of 4.7 was chosen. An initial pass in RPA was used to obtain ballpark flow rates during the initial design process. The provided flow rates were 2.8 kg/s and 0.6 k/gs respectively. A chamber pressure of 350 psi after several iterations of the propellant system and engine. Running a CEA calculation with the selected chamber pressure, O/F ratio and a  $P_{\text{chamber}}/P_{\text{exit}}$  pressure ratio of 28.3, the following results were obtained.

Table E.1: CEA Results

Parameter	Result
Ae/A*	4.2304
Gamma	1.146
Molar Mass	25.59
TO (K)	3141.58
C*	1583.6

The throat area was determined using the corrected C\*. The C\* was corrected by multiplying the C\* by the 83% to determine the corrected C\* coefficient. This yielded a value of 1314.38. From the corrected C\*, the throat area was calculated using E.1.

$$A^* = \frac{\dot{m}C^*}{P_{t2}} \quad (\text{E.1})$$

Substitution of the known values results in a  $0.00185\text{m}^2$ . From Table E.1, the area ratio of the exit is 4.2304. Multiplying the throat area by the expansion ratio yields an exit area of  $0.00783\text{m}^2$ . The throat area was used for subsequent sizing of the remaining portions of the chamber with an assumed contraction ratio of 7 and  $L^*$  of 2.2m. Multiplying the throat area by the expansion ratio yielded a chamber area of  $0.0126\text{m}^2$ . As the  $L^*$  is the ratio of the chamber volume and throat diameter, use of the preceding values yielded a chamber length 0.314m. The relevant chamber dimensions have been summarized in Table E.2.

Table E.2: Summary of Chamber Dimensions

Parameter	Result
Throat Diameter	1.9 inches
Exit Diameter	3.93 inches
Chamber Diameter	5.286 inches
Chamber Length	12.4 inches